Journal of Materials Chemistry A

Design, Synthesis, and Performance of Adsorbents for Heavy Metal Removal from Wastewater: A Review

Journal:	*Journal of Materials Chemistry A*
Manuscript ID	TA-REV-08-2021-006612.R1
Article Type:	Review Article
Date Submitted by the Author:	07-Nov-2021
Complete List of Authors:	Fei, Yuhuan; Michigan Technological University, Materials Science and Engineering Hu, Yun Hang; Michigan Technological University, Materials Science and Engineering

Design, Synthesis, and Performance of Adsorbents for Heavy Metal Removal from Wastewater: A Review

Yuhuan Fei, Yun Hang Hu *

Department of Materials Science and Engineering, Michigan Technological University, Houghton, MI 49931-1295, USA

*Corresponding author. Tel: +1 906 487 2261.

E-mail address: yunhangh@mtu.edu

Abstract

Heavy metal contamination has caused serious impacts on the environments and risks towards human health, promoting intensive R&D efforts for removal of heavy metals from their primary sources (industrial and agricultural wastewaters). Among all developed techniques, the adsorption removing approach has attracted the most attention. This article reviews the recent developments of adsorbents for removing heavy metal ions from wastewaters in the past decade (2011-2020). It starts with design principles, followed by the evaluation of adsorbents and their performances for removing various heavy metals. Mainly developed adsorbents include carbon materials (activated carbon, nanotubes, and graphene), polymers, metal compounds (nanoparticles, MXenes, metal-organic frameworks, and magnetic materials), boron and carbon nitrides, and zeolites. The challenges are also discussed as the perspectives.

KEYWORDS

Heavy metals, wastewater treatment, adsorption, adsorbents

1 Introduction

The term "heavy metals" was used as early as 1817, when Gmelin categorized all inorganic compounds into 10 nonmetals, 11 light metals (with densities of 0.86-5.00 g cm^{-3}), and 25 heavy metals (with densities of 5.31-22.00 g cm^{-3}).[1] Over the past century, this term has been increasingly used in multidisciplinary studies and legislations, with its definition continuously extended. Generally, heavy metals refer to metals (and metalloids) with relatively high densities, large atomic mass (or atomic weights), or big atomic numbers. Considering the environmental hazards, the most commonly recognized and intensively investigated "heavy metals" include arsenic (As), cadmium (Cd), chromium (Cr), cobalt (Co), copper (Cu), iron (Fe), lead (Pb), manganese (Mn), mercury (Hg), nickel (Ni), silver (Ag), and zinc (Zn).[2]

Heavy metal contamination receives attention due to their potential toxicity, resistance to biodegradation, and ability to enrich through food chain and accumulate in human organs.[3] Heavy metal intake occurs mainly through inhalation exposure, dermal absorption, and dietary ingestion. When the accumulation amounts surpass the tolerance levels, the tissues and organs may be damaged, resulting in varied symptoms including dizziness, headache, insomnia, amnesia, and even cancers. In response to this, the levels of heavy metals in drinking water are under strict regulation by influential organizations, such as World Health Organization (WHO) and the United States Environmental Protection Agency (USEPA). The heavy metal-bearing wastewater produced through industrial and agricultural activities is a primary contamination source. Hence, efforts have been devoted to researches on aqueous heavy metal contaminations with regard to their toxicity and risk assessment,[2,3] source and distribution,[4] as well as detection and removal technologies.[5,6]

The past half century has witnessed astonishing evolution in heavy metal treatment, including modification of the traditional methods and development of the innovative ones. Commonly applied methods include adsorption, precipitation, membrane filtration, ion exchange, etc.[5,6] Evidenced by the surprisingly increased number of the published articles (Figure 1), adsorption has attracted the most attention due to simple procedure, easy operation, and low cost. Numerous excellent review articles have evaluated the development of specific novel adsorbents (such as chitosan,[7] nanomaterials,[8] and one-dimensional carbon nanotubes[9]) and integration of adsorption with other technologies (like biosorption[10] and membrane capacitive deionization[11]). However, a comprehensive assessment on recent progress of adsorption removing technique is necessary. This has encouraged us to write this review article on the developments of various adsorbents in the last decade (2011-2020) with emphasis on their design, synthesis, and performances for removing heavy metals from wastewater.

2 Design principles of adsorbents

In adsorption, heavy metal ions are transported from the aqueous solution to the absorbent surface and subsequently bound to the surface via physical or chemical interactions. Hence, ideal adsorbents should have these features: (1) large accessible surface area, (2) strong interaction between the active sites and the heavy metals, (3) selectivity towards the target heavy metal species, and (4) easy regeneration.

Adsorbents are expected to have large accessible surface area that provides adequate sites for adsorption of heavy metal ions. Two types of strategies have been developed to generate large surface areas:

- ***Generating rich pores:*** A porous structure can increase surface area, thus enhancing adsorption. Porous materials are typically obtained via bottom-up and top-down approaches. The former assembles simple units (like atoms and molecules) into larger porous architectures, while the latter generates or tunes pores within the bulk materials. Bottom-up methods are often employed to synthesize porous crystal materials. For example, zeolites are synthesized by crystallization of silicate and aluminate anions in alkali solution via hydrothermal approach.[12] In contrast, the top-down approach allows facile regulation on the microstructures of materials. For example, the carbonized polyacrylonitrile (PAN) fabrics can be converted into activated carbon fabrics after heat-treatment under 900~1100℃ with CO_2 or steam.[13] Although both gases can react with the irregular carbon and/or the crystalline carbon edges to form CO, CO_2 mainly attacks the fiber surface to generate open pores, whereas the gaseous water molecules can permeate into the inner structure to develop internal pores. The ultrasonic activation was also demonstrated to open the blocked pores and create new pores in biochar to promote the removal of Ni(II) and Pb(II).[14] Compared to the physical activation approaches discussed above, chemical activation can modify the microstructure and functionality of materials with lower activation temperatures (400~900℃), shorter activation time, and higher yields, though it might cause structural damages.[15] As a common activating reagent, KOH is widely used for the heat treatment of carbonaceous materials to produce a series of intermediate products that facilitate chemical activation (with potassium compounds), physical activation (with CO_2 and gaseous water), and carbon lattice expansion (with metallic K), resulting in activated carbons with highly porous networks.[15] The accessible surface area is also dependent on pore size, as micropores are usually too small to be accessed by heavy metal ions. For example, $ZnCl_2$-impregnted carbon activated at 600℃ for 1 hour resulted in large surface area (2431 m^2 g^{-1}) with high microporosity (60.9%), while KOH-impregnation generated activated carbon with relatively smaller surface area (1506 m^2 g^{-1}) but wider pore size distribution (microporosity of 44.2%).[16] As a result, KOH-activated carbon showed better adsorption performance (1.06 mmoles g^{-1} for Cd^{2+} and 1.61 mmoles g^{-1} for Ni^{2+}) compared to $ZnCl_2$-activated carbon (0.23 mmoles g^{-1} for Cd^{2+} and 0.33 mmoles g^{-1} for Ni^{2+}).
- ***Decreasing particle sizes:*** Surface area can be enlarged by decreasing particle sizes, and thus nanoparticles

generally provide large surface areas. For example, the ascorbic acid-coated Fe_3O_4 nanoparticles with a diameter of less than 10 nm were successfully synthesized, leading to large specific surface area (179 m^2 g^{-1}) and high adsorption capacities of 16.6 mg g^{-1} for As(V) and 46.1 mg g^{-1} for As(III).[17] However, nanoparticles are prone to aggregation in aqueous environment, causing a loss in surface area. Fortunately, nanoparticles can be immobilized on polymer matrix.[18] Besides, surface modification can also improve the dispersibility of nanoparticles. For example, the citrate-immobilized Fe_3O_4 nanoparticles displayed perfect water-solubility (28 mg mL^{-1}) and stability (over one month), contributing to excellent removal performance for Pb^{2+} and Cr^{6+}.[19]

The adsorption capacity of an adsorbent is dependent on not only its accessible surface area, but also the interaction between its active sites and heavy metal ions. The adsorption strength of heavy metal ions could be enhanced via surface modification and optimization of operation conditions:

- ***Surface modification:*** The affinity of the adsorbents towards the heavy metals can be enhanced by doping with atoms (such as -N and -P) and functionalization with metal-binding groups (like -COOH, $-NH_2$, -SH, etc.). This explains why the amino-functionalized silica nano hollow spheres (NH_2-SNHSs) displayed better adsorption performance for Cd(II), Ni(II), and Pb(II) compared to the non-functionalized SNHSs.[20] Besides, surface modification can be accomplished through integration with polymers, which act as both the source of functional groups and the template for construction of desired structures.[21,22] Notably, the gold-decorated copolymer nanofibers with abundant nitrogen binding sites (from functional groups such as imine, amido, and amino) exhibited high activity and selectivity for Hg^{2+} despite the coexistence of As, Cd, Cu, Pb, and Zn ions.[23]
- ***Optimization of operation conditions:*** Operating conditions (like pH, temperature, and coexistence of other substances) have great impacts on the interaction between the adsorbent surface and the metal ions. In the case of polymers, the acidic environment not only provides more protons that compete with heavy metal ions for adsorption sites, but also generates more protonated-functional groups that are positively charged, resulting in retarded adsorption of metal cations.[24] On the other hand, basic condition might cause the precipitation of metal hydroxides, and thus interfere with the interactions between the heavy metal ions and the adsorbents. Therefore, polymer adsorbents are often used under neutral or weakly acidic environment.[25,26]

The selectivity to heavy metals also needs to be considered in the design of adsorbents. To achieve efficient adsorption, the active sites are supposed to have higher affinity towards the target metal species than other components. Engineering of the features and the nanostructures of adsorbents have been exploited to increase their adsorption selectivity:

- ***Engineering the features*** of an adsorbent is a promising approach to tune selective adsorption. For example, the pine gasification biochar (PG) provided higher adsorption capacity for Cr(III) with negligible adsorption for Cr(VI), whereas the pine biomass modified with TiO_2 (Pine/TiO_2) exhibited better adsorption for Cr(VI) than for Cr(III).[27] It was also observed that the N-biochar-supported MgO could preferentially eliminate heavy metals in the presence of natural organic matter (humic acid) and other cations (Na^+).[28]
- ***Nanostructured materials*** have been developed for efficient and selective detoxification of heavy metals from wastewater. For example, polyacrylonitrile (PAN) nanofibers with stably and homogeneously grafted functional groups were fabricated via electrospinning process.[29] These nanofibers could devour over 99% heavy metals (copper, lead, and zinc) and selectively capture Pb(II) with extremely high adsorption capacity of 1250 mg g^{-1} from multicomponent solution that also contained Cu(II) and Zn(II) (with the adsorption capacities of 33 and 769 mg g^{-1}, respectively).

It is also crucial that the adsorbents are separated from the aqueous systems and regenerated without significant performance degradation. This has prompted intensive efforts to explore the following techniques:

- ***Separation of adsorbents*** is a challenge for batch processes. To achieve high adsorption efficiency, adsorbents are often hydrophilic nanomaterials that cannot be easily separated by sedimentation or filtration. Inefficient recycling of the heavy metal-laden adsorbents can cause regeneration efficiency loss and potential environmental hazard. One solution is magnetization, namely, the adsorbents are incorporated with magnetite (Fe_3O_4) nanoparticles to obtain magnetic natures that allow easy magnetic separation. For example, the Fe_3O_4/biochar nanoparticles saturated with Ni(II) and Pb(II) could be easily separated from water with an external magnetic field.[14] Separation can also be promoted by immobilization of the nanomaterials. For example, the metal-organic frameworks (MOFs) immobilized on alginate beads with the size of ~1000 μm could be easily separated from water after exhaustion without sacrificing Cr(VI) removal efficiency (98%) and regeneration efficiency (82%).[30]
- ***Desorption of heavy metal ions*** determines both regeneration of the used adsorbents and recovery of the collected heavy metals. Nonetheless, a high adsorption capacity requires a stronger attraction between the adsorbent and the heavy metal ions, whereas the desorption of heavy metal ions prefers a weaker interaction with the absorbent. Hence, adsorbent regeneration is often realized under the help of additional eluents such as acids, alkalis, or chelating agents. It was reported that the ion-imprinted polymers could maintain stable adsorption performance within three cycles of regeneration with HNO_3 via H^+ ions exchanging with the absorbed metal cations.[31] In another case, the copper-laden magnetic composite microspheres was repeatedly

regenerated with NaOH for six times without obvious decrease in removal capacity.[32] In addition, a magnetic organodisulfide polymer adsorbent could be regenerated with ethylenediaminetetraacetic salt due to its strong attraction to heavy metals and no significant capacity loss was observed within five regeneration cycles.[33] The conditions (like pH, temperature, agitation speed, etc.) should also be optimized for satisfactory regeneration performance.[34]

3 Adsorbents for heavy metal removal

According to the chemical components and material structures, adsorbents are classified as carbon materials, polymers, metallic and metal compounds, and others in this section. Their synthesis, properties, and heavy metal removal performances are deeply discussed as follows.

3.1 Carbon adsorbents

Carbon-based materials are recognized as ideal adsorbents for heavy metals with diverse adsorption mechanisms (Figure 2). Their inherently large surface area and highly porous structure are beneficial for physisorption. Besides, carbon adsorbents usually contain abundant oxygen-containing groups that can trigger electrostatic attraction, complexation, and ion exchange with metal ions. It should be noted that these hydrophilic groups can also enhance their ability to disperse in aqueous solution and contact with the ions. In addition, carbon materials can be facilely modified with metal-binding agents that allow surface precipitation (e.g., thiol for lead[35]) and redox (e.g., reductive iron nanoparticles for pentavalent arsenic[36]) or enhance the aforementioned mechanisms. Common carbon adsorbents include activated carbon, carbon nanotubes, graphene, and biochar (Table 1).

3.1.1 Activated carbon

Activated carbon (AC) is a carbon-rich pyrolysis product of biomass or other carbonaceous materials. During the pyrolysis process, the carbon source materials are physically activated by hot gases via carbonization/oxidation or chemically activated by acids, strong bases, or salts, as discussed in the previous section. Chemical activation is preferred since it can generate quality-consistent porous products under lower pyrolysis temperature within shorter activation duration. It was reported that KOH-activation improved the adsorption performance of natural biomass-derived AC by increasing the surface area from 1.5 to 3106 $m^2 g^{-1}$ and the pore volume from 0.001 to 1.62 $cm^3 g^{-1}$.[37]

The large surface area and porous structure make AC a promising adsorbent. AC was used to purify copper electrolytes as early as 1929, but did not attract special attention in metal removal and recovery until the 1970s.[38] In 1971, Smith demonstrated effective mercury removal by AC adsorption, and explored its applications for removal of other trace metals (such as As, Cr, Co, Hg, and Ag) with Sigworth.[39] Since large portion of the specific surface area of

AC comprises from micropores that are inaccessible for heavy metal ions, it is necessary to enlarge the pores, and chemical activation (e.g., KOH activation; Figure 3a)[16] is an effective method as discussed in the previous section. Besides, large pores can also be constructed using other porous materials as the precursors or the templates. For example, carbon foam produced from phenolic resins showed an open cell structure with abundant mesopores (Figure 3b) and large surface area of 458 m^2 g^{-1}.[40] Interestingly, the as-obtained carbon foam was observed to contain certain amount of calcium sulfide formed during the foaming process, and this by-product could facilitate metal adsorption through surface precipitation. As a result, the carbon foam achieved high adsorption capacities of 491 mg g^{-1} for Pb(II) and 247 mg g^{-1} for Cu(II).

Another strategy is to enhance the affinity of the active sites on the adsorbent surface towards the heavy metal ions. Since van der Waals interactions with the metal ions are the dominant mechanism of AC adsorption, doping/functionalization with metal-binding atoms/groups can improve both adsorption efficiency and selectivity towards the target heavy metal species. For example, the amine-functionalized nanoporous carbon, compared to the unmodified one, achieved significantly improved adsorption capacity and removal efficiency for nickel (from 5.4 to 47.2 mg g^{-1}, from 12% to 99%), lead (from 18.1 to 161.4 mg g^{-1}, from 14% to 97%), cadmium (from 11.3 to 85.6 mg g^{-1}, from 12% to 94%), and copper (from 4.9 to 46.9 mg g^{-1}, from 15% to 93%).[41] It should be noted that this adsorbent exhibited impressive regeneration efficiency of 100% since the captured metal ions could be readily released from the protonated amine groups in acidic eluent solution (namely HCl), and no significant loss in removal efficiency was observed within nine regeneration cycles. This adsorbent outperformed pristine AC that suffered decreased adsorption efficiency of 50% after six cycles of nitric acid treatment.[42] Additionally, heavy metals generally display the strongest adsorption behavior at the optimal pH, whereas the lower pH tends to increase the repulsion between the metal cations and the protonated groups on carbon surface, and the higher pH leads to metal precipitation. Hence, AC adsorbents are usually used in neutral or weakly acid solution.[16,40,41] Nonetheless, a hierarchically porous N-doped carbon (Figure 3c) could effectively eliminate Pb(II) and Cd(II) under a wide pH range from 2 to 6.[43]

3.1.2 Carbon nanotubes

Carbon nanotubes (CNTs) are cylindrical tubes of one layer (single-walled carbon nanotubes, or SWCNTs) or multiple layers (multi-walled carbon nanotubes, or MWCNTs) of graphene. CNTs can be synthesized through chemical vapor deposition (CVD), namely, decomposition of hydrocarbon gases and subsequent growth of nanotubes on the metal catalysts. Despite the merits such as low operational temperatures (usually 300~1200℃), high-quality products with tunable microstructure, and potential for large-scale production, CVD products usually require purification with etchants like K_2MnO_4/NaOH to remove the metal particles and carbonaceous impurities (such as carbon nanoparticles and amorphous carbon).[44] Although impurities are rapidly and efficiently devoured at the expense of weight loss and

structural damages (such as opening of the caps, cutting of the length, introduction of defects and functional groups, etc.),[45] some of the structural changes may increase hydrophilicity and solubility of the CNTs and thus facilitate their dispersion in water and contact with heavy metal ions.

Since the first report by Iijima in 1991,[46] CNTs have been expected to provide satisfactory adsorption performance because of the large surface area from the vast external surface of the tubes (compared to AC where the interior surface provides the main sites for adsorption), and the porous structure primarily originating from the inner hollow cavities of the tubes with open ends and the aggregated pores of the entangled tubes. As early as 2002, Li and coworkers fabricated CNTs via nickel-catalyzed pyrolysis of propylene and hydrogen followed with nitric acid purification.[47] The purified CNTs showed markedly increased Pb(II) adsorption capacity of 15.6 mg g^{-1} compared to the unpurified ones (1.0 mg g^{-1}) since the concentrated nitric acid removed the catalysts, introduced of metal-binding groups (such as hydroxyl, carboxyl, and carbonyl), and also enlarged the surface area of the CNTs from 134 to 145 m^2 g^{-1}. It was also declared that the Pb(II) removal efficiency increased with pH due to either the inhibited protonation of the functional groups (under acidic condition) or the cooperative precipitation of the plumbous hydroxide (under neutral condition). Nitric acid purification is widely used as it introduces metal-binding functional groups without causing serious structural damages to the CNTs.

Raw CNTs with insufficient functional groups suffer easy aggregation, poor water-dispersion, and low metal adsorption capacity and selectivity. However, the adsorption performance of CNTs can be improved by functionalizing them with functional groups such as hydroxyl, carboxyl, amine, and amino, which have strong chemical and/or electrostatic interactions with heavy metal ions. The aforementioned purification methods can introduce oxygen-containing groups, but they may generate structural damages and thus reduce the stability of the CNTs. O_2-plasma oxidization was proved to be an effective, efficient, and environmentally friendly alternative approach to introduce hydrophilic carbonyl and carboxyl groups without obvious structural damages.[48] Furthermore, it was found that -COOH could promote Pb(II) adsorption through ion exchange and surface precipitation, achieving the removal of 93% Pb(II) at the pH of 2. Plasma techniques were also applied for grafting of polyacrylic acid (PAA) on MWCNTs to fabricate the MWCNTs-g-PAA composite adsorbent.[25] This composite exhibited the enhanced hydrophilicity and metal uptake, since the grafted PAA introduced abundant carboxyl groups that could form stable complexes with Co(II). The integration of other appropriate polymers such as polyaniline (PANI), polypyrrole (PPy), and polyhydroxylbutyrate (PHB), are also beneficial to the adsorptive surface properties of CNTs.[49,50] The PHB/CNTs adsorbent (Figure 4a-c) with a mesoporous structure (the pore radius of 3.3 nm) and a large surface area of 253 m^2 g^{-1} was synthesized by the catalytic chemical vapor deposition (CCVD) for detoxifying the industrial electroplating wastewater bearing As, Cd, Cr, Cu, Fe, Ni, Pb, and Zn.[50] It achieved high removal efficiencies above 85% for all heavy metal species within 10 min. Furthermore, the

PHB/CNTs could eliminate 100% As(III) and 99% Cr(VI) despite their high initial concentrations of 58.0 and 72.3 mg L^{-1}, respectively. Such high metal affinity was attributed to the carboxyl and carbonyl groups on the external surface that could capture heavy metal ions via electrostatic attraction (with protonated groups under acidic environment) and coordination (Figure 4d). In addition, PHB is a biocompatible, non-toxic, and insoluble polymer that sinks in water, thus the PHB/CNTs should have lower environmental risks than CNTs.

Like AC adsorbents, the CNTs display better adsorption performance under neutral and weakly acid conditions.[25,48,50] Furthermore, the regeneration of CNTs generally causes a lower decrease in adsorption capacity, compared to the AC adsorbents that suffer regeneration issues. For example, the Pb(II)-laden activated carbon suffered from decreased adsorption efficiency of 50% after six cycles of nitric acid treatment.[42] In contrast, the Zn(II)-laden CNTs maintained above 75% of adsorption capacity even after 10 cycles of nitric acid regeneration, slightly decreasing the Zn(II) adsorption capacity from 26.8 to 20.6 mg g^{-1}.[51]

3.1.3 Graphene

Graphene, with the extraordinary thermal and electrical conductivities, stiffness and elasticity, mechanical strength, and chemical inertness originating from the unique two-dimensional honeycomb lattice composed of carbon atoms, has attracted great attention since its first successful exfoliation by Novoselov and Geim in 2004.[52] For large-scale production of stable graphene products, the Hummers' method is often adopted to rapidly transform bulk graphite into high-yield graphite oxide that can be readily exfoliated by sonication in aqueous solution.[53] Although the exfoliated graphene oxide (GO) suffers loss of conductivity, the subsequent thermal or chemical reduction and functionalization can effectively recover the reduced conductivity, and the as-prepared reduced graphene oxide (rGO) and functionalized graphene with acquired defects and functional groups have rippled or crumpled structures that protect them from restacking or agglomeration.[54] Besides, epitaxial growth through chemical vapor deposition was also reported to produce large-scale patterned graphene films with outstanding electrical conductivity, mechanical strength, and optical transparency, indicating macroscopic application as electrodes for foldable, stretchable, and flexible electronics.[55]

With the large theoretical surface area of ~2630 m^2 g^{-1}, graphene is also a superior adsorbent for antibiotics, dyes, aromatic pollutants, as well as heavy metals.[56] As early as 2009, graphene was exploited as platforms for heavy metal sensors due to the exceptionally high sensitivity with low signal to noise ratio, high electrical conductivity, and tremendous surface area to volume ratio.[57] The electrochemical sensors using the Nafion-graphene/bismuth film electrodes performed ultrasensitive determination for Pb^{2+} and Cd^{2+} with the detection limit of 0.02 μg L^{-1}, where bismuth acted as the nontoxic metal-sensitive electrode coating material, Nafion as the solubilizing agent and antifouling coating with cationic exchange capacity, and graphene as the conductive agent with high adsorptive capacity due to its large surface area. Wang and coworkers evaluated GO with carboxyl groups for the adsorption of copper ions.[58] They

found that the coordination between Cu^{2+} and -COOH induced the folding/aggregation of GO sheets, achieving the larger copper adsorption capacity of 46.6 mg g^{-1} than those of CNTs (28.5 mg g^{-1}) and AC (5 mg g^{-1}). Furthermore, the few-layered graphene oxide (FLGO) nanosheets (Figure 5a), which were prepared from graphite via the modified Hummers method, exhibited the maximum adsorption capacities of 106.3 mg g^{-1} for Cd(II) and 68.2 mg g^{-1} for 30 mg L^{-1} Co(II) at the optimal pH of 6.[59] However, chemically and thermally reduced GO materials showed lower Cd(II) adsorption capacities of 6.3 and 0.5 mg g^{-1}, respectively, compared with GO (35.7 mg g^{-1}), even though their surface areas of 378 and 276 m^2 g^{-1} are larger than that of GO (39 m^2 g^{-1}).[60] This was due to the dramatic loss of oxygen-containing groups in the reduced GO, revealing the dominant role of the functionality. For this reason, reduced graphene oxide (rGO) materials are rarely used alone as adsorbents for the removal of heavy metals.

Functionalization with other metal-binding groups/agents can also improve the adsorption performance of graphene for heavy metals. It was found that ethylenediamine triacetic acid (EDTA)-functionalized GO (EDTA-GO) devoured Pb(II) ions from wastewater to the concentration below 0.5 ppb, achieving the adsorption capacity of 479.0 mg g^{-1} due to the large surface area of 623 m^2 g^{-1} and the enormous amount of chelating groups (-OH and -COOH) of GO and EDTA.[61] The 2,2′-dipyridylamine (DPA)-modified GO (DPA-GO) could simultaneously diminish Cd(II), Cu(II), Ni(II), and Pb(II) with high efficiency because of the strong complexation between the heavy metal ions and DPA (containing C-N and C=N).[62] Sulfur-functionalized GO coated with mesoporous TiO_2 shell (sulfur-GO/TiO_2) effectively scavenged Pb(II), Cd(II), Ni(II), and Zn(II) with higher efficiency than sulfur-GO and sulfur-GO/SiO_2 because of increased surface area and enhanced binding activity (Figure 5b-e).[63]

Integration with other materials is another strategy to improve the adsorption performance of graphene and its derivatives. Earlier works mainly applied graphene as a matrix for other adsorbents due to its large surface area. For example, iron oxide (IO) was grown on the robust rGO surface in the form of needlelike nanoparticles.[64] The obtained IO/rGO composites (Figure 6a and b) reached a larger surface area of 1460 m^2 g^{-1} compared with rGO (375 m^2 g^{-1}) since the IO particles and graphene sheets acted as the reciprocal spacers that protected each other from aggregation or restacking. With the large accessible surface area of the IO nanoparticles, the composites attained high adsorption capacities of 218 mg g^{-1} for As(V) and 190 mg g^{-1} for Cr(VI) within 20 min. IO also endowed the composites with magnetic properties that facilitated easy recycling with an external magnetic field. Furthermore, graphene possesses its own ability for adsorptive removal of heavy metals. To inhibit restacking and aggregation, graphene and its derivatives were often combined with porous materials such as SiO_2 (Figure 6c and d),[65] chitosan,[66] alginate,[67,68] and polymers[22] for removal of As, Cd, Cr, Cu, Hg, Pb, etc. GO/chitosan also showed strong ability to capture Au(III), indicating its potential for recovery of noble metals.[66] With the introduction of stable and non-toxic polypyrrole (PPy), rGO selectively captured Hg(II) with high adsorption capacity of 980 mg g^{-1} despite the coexistence of Cu(II), Cd(II), Pb(II),

and Zn(II) (Figure 6e and f).[22]

Three-dimensional graphene (3DG) materials, which possess abundant meso- and macropores and large accessible surface area, are promising adsorbents for removal of heavy metal ions. 3DG materials can be fabricated via direct chemical reaction between alkali metals (or their derivatives) and CO/CO_2,[69-72] or integration with other materials as composite hydrogels/aerogels.[67] Yi and coworkers synthesized a GO/alginate/polyvinylalcohol (PVA) hydrogel microspheres (through crosslinking of the linear biopolymer sodium alginate by Ca^{2+}) for heavy metal removal.[21] The homogeneous hydrogel microspheres exhibited the maximum adsorption capacities of 247.2 and 403.8 mg g^{-1} for Cu(II) and radionuclide uranium (UO_2^{2+}). Zhang and coworkers fabricated the novel 3DG/δ-MnO_2 aerogels with an interconnected 3D network homogenously deposited with ultrathin birnessite nanosheets (Figure 7a).[73] The 3DG/δ-MnO_2 aerogels (Figure 7b and c) rapidly (within 30 min) attained large saturated adsorption capacities of 643.6, 250.3, and 228.5 mg g^{-1} for Pb(II), Cd(II), and Cu(II), respectively. The aerogels remained the original shape and exhibited slightly degraded performance after eight operation-regeneration cycles. Furthermore, the aerogels can be easily separated without the risks of secondary contamination.

With the large specific surface area, hierarchically porous microstructure, high electrical conductivity, and stable electrochemical properties, 3DG is a promising electrode material for capacitive deionization. Capacitive deionization (CDI), also denoted as electrosorption and electrochemical demineralization, is an energy-efficient, cost-effective, and environment-friendly technology for water purification.[74,75] The electrodes can capture heavy metal ions from water under an external electrical potential and readily release the ions by reversing the electrode polarity for regeneration. Conventional electrode materials (including carbon aerogels, mesoporous carbon, activated carbon, and CNTs as well as their derivatives and composites) have shown the ability to remove heavy metals, such as Cr(VI), Cr(III), Cu(II), and As(V), with the maximum adsorption capacity ranging from 24.6 to 100 mg g^{-1}.[76-79] 3DG has been explored as a novel electrode material, and the functionality and microstructure of the 3DG materials are often tailored for further improved electrochemical properties and adsorption performance by introduction of foreign atoms, functional groups, and other materials.[80] Therefore, increase attention has been paid to CDI removal of heavy metals with graphene electrodes (Table 2). In 2017, S-doped, N-doped, and S, N-codoped 3DG aerogels were exploited for electrosorption of Cu(II), Cd(II), Hg(II), and Pb(II) in a three-electrode cell using a home-made paper working electrode coated with 3DG aerogels on both sides.[81] To fabricate an asymmetric two-electrode CDI unit, 3DG was synthesized from the aqueous suspension of graphene oxide and polystyrene (PS) microspheres via a replication and deposition method and subsequently grafted with ethylenediaminetetraacetic acid (EDTA) and 3-aminopropyltriethoxysilane (APTES) to obtain 3DEGR (Figure 8a and b) and 3DNGR as the cathode and the anode materials, respectively.[82] In the asymmetric two-electrode unit (Figure 8c), the 3DEGR-based cathode could capture lead and sodium cations by chelation and electrostatic attraction, whereas

the 3DNGR-based anode could decrease the anion concentration in the aqueous solution to minimize the co-ion effects. After saturation, Na^+ and the anions were released upon voltage reversing and short circuit, while stably bound Pb^{2+} were subsequently eluted from EDTA with HNO_3 solution. Consequently, 97.2% Na^+ and 99.6% Pb^{2+} could be separately collected and recovered, and the electrodes could be efficiently regenerated without significant efficiency loss for eight cycles. With this CDI unit, above 98% heavy metals (Pb, Hg, Cd, Ni) were separated and recovered from the bimetal solution with the coexistence of Na^+. Furthermore, thiol-functionalized GO/AC-based working electrode could preferentially devour 99% Pb^{2+} despite the coexistence of Ca^{2+} and Mg^{2+}, demonstrating efficient detoxification without sacrificing the healthy cations from the tap water.[35] The native phosphate ions in tap water were accumulated on the counter electrode in the charge process. The concentrated phosphate ions could form precipitates with Pb^{2+} in the discharging and thus facilitate electrode regeneration despite the strong affinity between the thiol groups and Pb^{2+}. This electrode also showed excellent removal performance for other heavy metals such as Cu, Cd, and Ni, suggesting its promising application in drinking water treatment. Doping atoms that can bind metals into the graphene matrix can lead to distinguished decontamination properties. Hu and coworkers observed that the pyridinic N-dominated graphene preferentially captured Na^+, while the pyrrolic N-dominated graphene were prone to formation of stable complexes with Pb^{2+}.[83] Based on the Lewis theory, Na^+ is a harder Lewis acid than Pb^{2+} featuring the lower polarizability and weaker reducibility, while the pyridinic N is a harder Lewis base than the pyrrolic N. For this reason, hard acids (Na^+) tend to interact with hard bases (pyridinic N), whereas soft acids (Pb^{2+}) favorably bind with soft bases (pyrrolic N), which is consistent with the observed results. Similarly, the GO/polypyrrole composite electrode material showed good ability to remove Cu(II) from water.[84]. Highly porous N-doped graphene electrodes were also utilized for membrane capacitive deionization (MCDI).[85] The MCDI unit devoured over 90% heavy metals from the multi-metal system (Pb, Cd, Cu, Fe, etc.) with wide range of initial concentrations (0.05~200 mg L^{-1}) within 30 min and remained stable regeneration performance for ten cycles without significant degradation. This was attributed to the crumpled networks, mesoporous structure, large surface area (695 m^2 g^{-1}), and abundant defective sites of the N-doped graphene nanosheets. In addition, the combination between graphene and metal compounds was also explored for removing heavy metals via a CDI process. For example, the Fe-rGO/AC composite was employed for capacitive detoxification of the carcinogenic As(V).[86] The composite exhibited improved adsorption capacity and accelerated adsorption rate, since Fe-rGO allowed effective chemisorption while AC contributed to mesoporous structure for boosting ion transfer and uniform dispersion of Fe-rGO. Fe_3O_4 nanoparticles were also distributed on porous graphene to form a magnetic nanocomposite, achieving large electrosorption capacities of 40.0~49.0 mg g^{-1} for Pb(II), Cu(II), and Cd(II).[87] TiO_2 nanotubes was also exploited to modify graphene.[88] The TiO_2 nanotube/rGO composite acquired large surface area of 511 m^2 g^{-1} with mesoporous structure and strong electrical double layer behavior, leading to the electrosorption capacities of 253.2 mg g^{-1} for Cu(II)

and 241.6 mg g^{-1} for Pb(II). The MoS_2/graphene composite also exhibited good performance for the CDI, which could eliminate 92.3% Cu(II) and 91.3% Pb(II) from the low concentration solutions (17.9 mg L^{-1} copper and 99.4 mg L^{-1} lead, respectively).[89] It showed an excellent stability for 50 regeneration cycles.

3.1.4 Biochar

Biochar, which is the carbon-rich pyrolysis product of biomass under inert atmosphere, has been widely evaluated for removal of Cu, Zn, Mn, Cr, Fe, Pb, Cd, Ni, and Co with wide range of initial concentration (1~1000 mg L^{-1}) due to its large surface area, abundant functional groups, rich source materials, etc.[90-92] For example, biochar derived from rice and corn husk showed its ability to remove 65% Cr(VI), 90% Fe(III), and 90% Pb(II) from aqueous solution,[90] while the sesame straw-derived biochar was demonstrated to treat Pb, Cd, Cu, Cr, and Zn with high concentration of 320 mg L^{-1}.[91] To improve its metal adsorption capacity and selectivity, biochar is often modified. As reported,[92] Mg-loaded biochar exhibited excellent performance for the treatment of Cd(II), Cu(II), and Pb(II) with concentrations as high as 1000 mg L^{-1} due to its enhanced mineral precipitation and ion exchange. N-doped biochar embedded with MgO nanoparticles (NPs) (MgO/N-biochar) exhibited very large Pb(II) adsorption capacity of 893.0 mg g^{-1} and short equilibrium time (within 10 min), which was attributed to its enhanced surface coordination (with the abundant C=O or O=C-O, pyrrolic, pyridonic, and pyridinic N) and ion exchange.[28]

Notably, the biochar can be applied under both acidic and basic environment, which broadens its application for the treatment of contaminant real-water. Biochar also showed its efficiency for remediation of soil irrigated with heavy metal-bearing wastewater, demonstrating another strategy for heavy metal removal from wastewater through biochar-enhanced soil amendment.[93]

3.2 Polymer adsorbents

Polymers are natural or synthetic macromolecules composed of repeating units, which are formed via polymerization of small molecules (known as monomers). There are various classification criteria for polymers. In terms of the types of repeating units (or monomer residues), polymers are categorized as homopolymers (containing only one type of repeating units) and copolymers (containing two or more types of repeating units). Based on the components, polymers are sorted into organic (with the backbone composed of carbon atoms) and inorganic (with the backbone composed of non-carbon atoms; e.g., silicones featuring the -Si-O-Si-O- backbone) polymers. According to the architectures, polymers are considered as linear polymers (featuring long-chain backbones), grafted polymers (featuring oligomers as side chains), star polymers (featuring several chains emanating from a common center; e.g., dendrimers featuring a core moiety with hyperbranched interior repeat units and numerous surface groups), and crosslinked polymers (featuring three-dimensional network of crosslinked chains).[94,95] Polymers are widely used in adsorption

processes because of their chemical stability, mechanical strength, biocompatibility, large surface area, and porous feature. Furthermore, the abundant functional groups on the polymers can act as active sites for adsorption of pollutants or modification of other target functional groups. Therefore, polymer materials are widely used for heavy metal removal (Table 3), including natural (e.g., chitosan, alginate, starch, etc.) and synthetic polymers with functional groups (including -NH_2, -COOH, -OH, etc.).

3.2.1 Natural polymers

Natural polymers, especially polysaccharides and their derivatives, have been reported as low-cost and effective adsorbents for heavy metal removal. Chitosan is the most widely used biopolymer adsorbent due to its wide availability, hydrophilicity, biodegradability, remarkable adsorption properties, and simple preparation (by boiling chitin in KOH solution). It is a deacytylated form of chitin, which is the second most abundant polysaccharide on the earth that can be found in the shells of shrimp and crab as well as the cell walls of yeast and fungi. Chitosan can capture heavy metals through chelation (with the available electron pairs of the nitrogen and oxygen atoms) and electrostatic attraction (with the protonated amino and hydroxyl groups under acidic environment), but raw chitosan suffers from high crystallinity, low mechanical strength, solubility in acidic media, and chemical instability. Therefore, chitosan derivatives and composites are more common for practical applications. As reported,[7] chitosan immobilized on SiO_2 (GO, biochar, or others) showed improved mechanical strength, intensified thermal stability, porous structure with increased surface area, and water-insolubility in acidic environment, thus resulting in enhanced adsorption performance for removal of Cd(II), Co(II), Cr(III), Cu(II), Mn(II), Ni(II), Pb(II), Zn(II), etc. Besides, the linear chains of chitosan can also crosslink with polymers (e.g., polyethyleneimine[96] and polyacrylic acid[97]) to form a three-dimensional network for the improvements in mechanical strength, chemical stability, and insolubility in acidic/alkaline media or organic solvents. Furthermore, chitosan and its composites can be grafted to increase adsorption strength (with increased density of the adsorption sites) and selectivity (with altered adsorption sites and uptake mechanisms). Repo and coworkers explored EDTA-functionalized chitosan/silica hybrid adsorbent, removing 96.5% Cd(II), 99.2% Cd(II), 93.5% Co(II), and 95.2% Ni(II) ions from single-metal solutions.[98] The hybrid adsorbent preferentially collected Ni(II) and Pb(II) ions when used in multi-metal solutions, indicating a potential method for selective separation of metal ions from multi-component systems. This would be due to its rigid structure, large surface area, high porosity, and surface functionality.

Alginate, a polysaccharide derived from grown seaweed, shows high affinity to heavy metals. For example, it was found that the alginate gels rapidly (within 10 min) reached saturated Pb(II) adsorption capacity of 435.3 mg g^{-1} in wastewater with its initial concentration as high as 800 mg L^{-1}.[99] Because of the unique gelation behavior, alginate is often utilized to fabricate aerogel, hydrogel, and gel beads with other adsorbent materials (e.g., GO, carboxymethyl cellulose, and polyvinyl alcohol).[21,67,68,100] These porous hybrid adsorbents showed strong ability to devour Cd(II),

Cu(II), Pb(II), etc. with the initial concentration up to 635 mg L^{-1}. Other biopolymers, such as cellulose,[100,101] lignin,[102] starch,[103] and soy protein,[104] were also demonstrated to eliminate heavy metals (such as cadmium, copper, and lead) with an initial concentration ranging from 5 to 500 mg L^{-1}.

Geopolymers, which are the amorphous aluminosilicate materials with unique three-dimensional network, high strength, and environmentally friendly features, have also been exploited as a potential adsorbent. As an example, the highly porous hollow gangue microsphere/geopolymer captured ~90% Cd(II), Cu(II), and Pb(II), as well as ~70% Zn(II) from wastewater via ion exchange, electrostatic attraction, physisorption, and chemisorption.[105]

It is noteworthy that most of the natural polymers mentioned above achieve the best adsorption performance at weakly acidic conditions (generally pH 4~6), where the protonated functional groups can contribute to uptake of heavy metal ions via electrostatic attraction.

3.2.2 Synthetic porous polymers

Synthetic polymers have attractive advantages such as easy synthetic routes, tunable surface functionality, adjustable nanostructures, non-toxicity, and low cost, but the low adsorption capacity and poor selectivity restrict their application as adsorbents for the removal of heavy metals. For this reason, polymeric adsorbents are usually synthesized from monomers with functional groups that have metal-binding abilities. So far, it has been reported that heavy metals (such as Cd, Cr, Cu, Hg, Ni, Pb, Zn, etc.) can be removed by polyaniline (PANI) (amine and imine),[49] polypyrrole (PPy) (amine),[49] polyhydroxybutyrate (PHB) (ester),[50] polyvinyl alcohol (PVA) (hydroxyl),[21,106] polyacrylamine (PAM) (carbonyl and amine),[101] polyethylenimine (PEI) (amine),[96] polyethylene glycol (PEG) (oxygen),[107] polyacrylic acid (PAA) (carboxyl),[25,26] and polyacrylonitrile (PAN) (-C≡N).[29] Generally, these macromolecules tend to bend and twist for maximized intermolecular interactions and thus form non-porous structures with space-efficiently packed chains that give small accessible surface area and insufficient binding sites. Furthermore, these ordinary polymers are prone to dissolve in acidic/basic solutions or organic solvents, leading to the swelling and diffusion limitation. To solve these issues, the development of porous polymers is necessary.

Porous polymers are broadly defined as the micro-/meso-/macroporous materials comprised predominantly of light, non-metal elements (C, H, O, N, B, etc.).[108] Compared to other common porous materials (e.g., activated carbon, silicas, and zeolites), porous polymers provide new opportunities for catalysis, gas separation, energy storage, etc. due to diverse synthetic chemistries (both synthetic routes and post-modification approaches), tunable porosity and functionality, physical and chemical stability, as well as low-cost and scalability.[108,109] Porous polymers are generally categorized as the amorphous porous organic polymers (POPs) and the crystalline covalent organic frameworks (COFs). Furthermore, POPs can be sub-divided into hypercrosslinked polymers (HCPs), polymers of intrinsic microporosity (PIMs), and conjugated microporous polymers (CMPs).[108-110]

Davankov and coworkers first introduced hypercrosslinked polystyrene in 1970s.[111] Mostly based on Friedel-Crafts chemistry, HCPs can be synthesized via either inter- or intramolecular crosslinking of preformed chains at the swollen state or direct polymerization and polycondensation of monomers.[111,112] The extensive chemical crosslinks lead to rich pores, while the rigid bridges protect the porous networks from collapse upon solvent removal, resulting in permanent porosity and large surface area. Recently, a class of layered 2D HCP materials was reported to reach the surface area of 3002 m^2 g^{-1}.[113] With prudent selection of precursors and crosslinkers combined with optimal synthesis conditions (solvents, catalysts, temperatures, etc.), the porosity and functionality of HCPs can be tailored for water detoxification. Surface-modified HCPs could be synthesized via Friedel-Crafts reaction followed by sulfonation.[114] With large surface area of 1025 m^2 g^{-1}, rich micropores (average pore size of 1.1 nm), and abundant hydrophilic sulfonic acid groups, the obtained HCPs could remove over 90% heavy metals (Cu^{2+}, Ni^{2+}, Pb^{2+}, and Cr^{3+}) within 30 min. Similarly, a $FeCl_3$ catalyzed Friedel-Crafts reaction was employed to synthesize a dimethyl iminodiacetate-contained HCP whose methyl groups were subsequently hydrolyzed to afford a iminodiacetic acid-functionalized HCP.[115] Via coordination with amino active sites and carboxyl groups, this HCP achieved outstanding Pb(II) uptake capacity of 1138 mg g^{-1}. Besides, this adsorbent exhibited excellent selectivity with the capture efficiency trend of Pb(II)≈Co(II)>Cd(II)>Hg(II)>Zn(II)>Fe(III)≫Mg(II)>Na(I) and chemical stability over a wide range of pH (1~12). A thiourea-modified hypercrosslinked polystyrene resin reached the adsorption capacity of 689.8 mg g^{-1} for Pb^{2+}, 430.6 mg g^{-1} for Cd^{2+}, and 289.7 mg g^{-1} for Cu^{2+}.[116] Heavy metal ions could be captured by the plentiful metal-binding groups (-NH_2 and -SH) to form complexes. Recently, a series of hypercrosslinked imidazolium-based poly(ionic liquid)s (PILs) were designed and synthesized via free-radical polymerization (Figure 9).[117] The mesoporous structure of these PILs allowed sufficient exposure of the ample exchangeable Br^- anions and fast mass transfer during their ion exchange with Cr(VI). As a result, the PILs displayed selective adsorption for Cr(VI) against other competing anions (Cl^-, NO_3^-, $H_2PO_4^-$, SO_4^{2-}) and stable performance under a wide pH range of 2~6. Interestingly, the lightly crosslinked polymers, also denoted as polymer hydrogels, have also shown extraordinary ability to capture heavy metals from wastewater. In contrast to the HCPs with non-swelling rigid networks, polymer hydrogels exhibit superior water retention ability such as high swelling ratio (fractional increase in weight due to water absorption) and hydrophilicity. Therefore, polymer hydrogels have been used to remove heavy metals, such as Cd(II), Co(II), Cr(III), Cu(II), Ni(II), Hg(II), Pb(II), and Zn(II) with their sponge-like structures with large accessible surface areas and abundant metal-binding groups, the extraordinary swelling and diffusion properties without sacrificed mechanical stability, and water-insolubility.[26,118,119] In a work inspired by ethylenediaminetetraacetic acid (EDTA), a biocompatible and cost-effective polydentate hydrogel was synthesized via a one-pot transamidation reaction between hydrolyzed polyacrylamide (HPAM) and branched polyethylenimine (BPEI) (Figure 10a-c).[119] Attributed to the numerous EDTA-mimicking coordinating groups (carboxyl

and amides), the hydrogel manifested the maximum adsorption capacities of 340.6, 436.5, 439.3, 210.7, 285.1, and 395.1 mg g^{-1} for Cr^{3+}, Cu^{2+}, Zn^{2+}, Cd^{2+}, Hg^{2+}, and Pb^{2+}, respectively, and 482.2 mg g^{-1} in a multicomponent system containing all the metal species above (Figure 10d-e).

PIMs were first reported by McKeown and coworkers in 2004.[120] The permanent porosity of PIMs arises from the space-inefficient packing of the rigid and contorted backbones. In contrast to most porous materials, PIMs are generally soluble and thus solution processable like ordinary polymers, namely, PIMs can be cast from solution to membranes for separation applications. PIM-1, one of the best-known PIMs, can be synthesized via an efficient dibenzodioxane-forming reaction.[120] PIM-1 could hardly adsorb heavy metal ions from aqueous solutions due to their hydrophobicity, while hydrolyzed PIM-1 electrospun fibers with hydrophilic carboxyl groups conversed from nitrile groups were capable of coordinating Pb^{2+} and Cu^{2+},[121] and further thiol-functionalization would endow the modified PIM-1 with ability of fluorescent sensing and selective adsorption for Hg^{2+} (regardless of coexisted Cu^{2+}, Cr^{3+}, Cd^{2+}, and Ni^{2+}) (Figure 11).[122] Recently, porous poly(arylene ether)s synthesized via Pd-catalyzed C-O polycondensation displayed incredibly high Hg(II) uptake of 775 mg g^{-1} and specific Hg^{2+} detection over other common cations.[123]

CMPs are π-conjugated porous networks comprising rigid aromatic building units. Control over pore sizes remained difficult during synthesis of amorphous porous polymers until Cooper and coworkers synthesized the first CMPs using a Sonogashira-Hagihara coupling chemistry in 2007.[124] The pore size of CMPs can be tailored by the monomer strut length.[124,125] A porous organic polymer (CBAP-1) synthesized via the Friedel-Crafts reaction between terephthaloyl chloride and 1,3,5-triphenylbenzene could be further grafted with either 2-aminoethanethiol (AET) or ethylenediamine (EDA) for Hg(II) removal (Figure 12a).[126] Despite the similar surface areas (422 and 450 m^2 g^{-1}, respectively), microporosities (both ~88%), and pore diameters (both 0.65 nm), CBAP-1 (AET) showed higher adsorption capacity (232 mg g^{-1}) than CBAP-1 (EDA) (181 mg g^{-1}), which was attributed to different adsorption mechanisms. The amine groups from the grafted EDA and AET chains could capture Hg(II) through coordination bonding, whereas the thiol groups from AET could form stronger covalent bonds with Hg(II) (Figure 12b and c). As a result, CBAP-1 (AET) displayed adsorption efficiency (>96% Hg^{2+} removal efficiency within 2 min), selectivity (for Hg^{2+} and Pb^{2+} over Fe^{3+}, Ca^{2+}, Mg^{2+}, and Na^{+}), recyclability (100% desorption with 2 M HCl and 0.5 M thiourea), and reusability (unnoticeable adsorption capacity loss within 10 cycles). Friedel-Crafts reactions could also be employed to synthesize a series of ketone-based HCPs which were post-functionalized with melamine (MA) through the Schiff-based reaction.[127] The triazine rings of MA offered rigid skeletons and plentiful nitrogen, affording various MA-based CMPs with large surface area (up to 555 m^2 g^{-1}) and high Hg(II) uptake (up to 372 mg g^{-1}). Similarly, another triazine-based CMP (synthesized from MA and phthalate) obtained ample carboxyl and amino groups and thus displayed strong selectivity for Hg(II) over Fe(III), Cd(II), Ni(II), Zn(II), Ca(II), Mg(II), Na(I), and K(I).[128] However, when triazine rings

were used as tritopic nodes to connect dimethylpyrazole neighbors, the resultant CMP showed remarkable selectivity for Ag(I) over Cu(II), Cd(II), Co(II), Ni(II), Pb(II), and Zn(II).[129] Zhao et al. constructed mesoporous POPs (FC-POP) through Friedel-Crafts alkylation of triptycene and subsequently grafted either hooped or extended amino chains in these networks (Figure 12d).[130] The hooped chains had stronger interactions with Pb(II) through chelation and coordination, and the as-obtained POPs exhibited extremely high Pb(II) uptake of 1134 mg g^{-1}, ultrafast adsorption rate (reaching equilibrium within 5 min), insensitivity to pH (from 2~8), recycling stability, and multifunctionality (>90% removal of Cr^{3+}, Fe^{3+}, Co^{2+}, Cu^{2+}, Ni^{2+}, and Zn^{2+}).

COFs are crystalline networks comprising covalently bonded nodes and struts. Formation of strong covalent bonds tends to generate disordered, amorphous materials such as the aforementioned subclasses of POPs. To construct crystalline extended organic structures, Yaghi and coworkers employed reversible solvothermal condensation reactions where the judiciously selected building blocks could be linked by strong covalent bonds to crystallize the first 2D COFs (COF-1 and COF-5) in 2005.[131] Mild conditions (diluted solvents and low heating temperature of 120℃) were adopted to control the diffusion and reaction rates, forming the most thermodynamically stable structures. The obtained COFs exhibited either staggered or eclipsed hexagonal structures and achieved high thermal stability (up to 500~600℃), permanent porosity (pore size of 0.7~2.7 nm), and large surface area (711 and 1590 m^2 g^{-1}, respectively). Furthermore, they synthesized 3D COFs with improved surface area (3472 m^2 g^{-1} for COF-102 and 4210 m^2 g^{-1} for COF-103) via self-condensation or co-condensation reactions of triangular and tetrahedral nodes.[132] Based on reticular chemistry, the structural topology and functionality of COFs can be advisably designed and facilely tuned via different synthesis routes (such as boron condensation, triazine-based trimerization, and imine condensation), producing boron-containing, triazine-based, and imine-based COFs.[133] Since boron-containing COFs generally suffer from framework degradation and loss of porosity upon exposure to moist air or water, triazine-based and imine-based COFs are usually applied for water purification. Triazine-based COFs, also known as covalent triazine frameworks (CTFs), can be synthesized by ionothermal nitrile cyclotrimerization in molten $ZnCl_2$, as firstly reported by Thomas and coworkers.[134] CTF-1 prepared from dicyanobenzene achieved the highest Pd(II) adsorption capacity of 29.3 mg g^{-1},[135] while novel thioether-based CTF nanospheres synthesized from premade thioether ligand displayed large surface area (1459 m^2 g^{-1}), quick capture (within 5 min) of both Hg(II) ions (1253 mg g^{-1}) and Hg(0) vapor (813 mg g^{-1}), selectivity (over Na^+, K^+, Mg^{2+}, Co^{2+}, Cr^{2+}, and Zn^{2+}), and cyclability (retaining 95% Hg^{2+} removal efficiency) (Figure 13a and b).[136] Recently, a novel CTF synthesized from a scalable one-pot hydrothermal method displayed outstanding capture ability (with the adsorption capacity of 1826 mg g^{-1}) and sensitivity (with the detection limit of 63 ppb) towards Hg(II) (Figure 13c and d).[137] The irregularly aligned nanoneedles of CTF offered mesoporous cavities, while the numerous double bonds and N and O atoms could capture Hg(II) via cation-π interactions, soft-soft interactions, and electrostatic attraction. Notably, the high reaction

temperature and harsh reaction environment may influence the structural regularity of resultant CTFs. Imine-based COFs, which could be produced from co-condensation of aldehydes and amines/hydrazides, exhibited comparable crystallinity with boron-containing COFs and superior stability in water and most organic solvents.[138,139] Employing a bottom-up strategy, Wang and coworkers designed and synthesized COF-LZU8 from trimesaldehyde (as the tritopic nodes) and pre-synthesized thioether monomers (as the tailored struts) (Figure 14a).[140] Thioether groups were densely distributed in a straight channel (with a diameter of ~1.3 nm) originated from the 2D eclipsed structure, which facilitated the access of Hg^{2+} to S atoms. Hence, COF-LZU8 is an effective Hg(II) scavenger (removal efficiency of 98%) and promising Hg(II) sensor with excellent sensitivity (detection limit of 25 ppb) and selectivity (over Li^{+}, Na^{+}, K^{+}, Mg^{2+}, Ca^{2+}, Sr^{2+}, Ba^{2+}, Al^{3+}, Ag^{+}, Cd^{2+}, Co^{2+}, Cu^{2+}, Fe^{2+}, Fe^{3+}, Ni^{2+}, Pb^{2+}, and Zn^{2+}). When the thioether monomer is replaced by diaminoguanidine hydrochloride, a guanidinium-based ionic COF could be obtained (Figure 14b).[141] The positively charged guanidinium could attract Cr(VI) oxoanions via hydrogen bonding and electrostatic interactions, while the weakly bound Cl^{-} could exchange with these oxoanions. As a result, this ionic COF eliminated Cr(VI) effectively (from 1 ppm to 10 ppb), rapidly (within 1 min), and selectively (regardless of coexisted MoO_4^{2-}, $HAsO_4^{2-}$, SeO_4^{2-}, and SO_4^{2-}). As shown in Figure 15, the straight channels of COFs can be enlarged (with a diameter of 2.8~3.3 nm)[142,143] using 1,3,5-tris(4-aminophenyl)benzene as the tritopic nodes, and the obtained COFs can be post-functionalized through simple click reactions, thus affording large surface area (1934 $m^2\ g^{-1}$),[143] extremely high adsorption capacities (e.g., 4395 mg g^{-1} for Hg^{2+} ions[144] and 863 mg g^{-1} for Hg^0 vapor[142]), fast adsorption kinetics (removing 99% Hg^{2+} within 5 min),[143] chemical stability (over a pH range of 0~14),[143] selectivity (over Na^{+}, K^{+}, Mg^{2+}, Ca^{2+}, As^{3+}, Fe^{3+}, Cd^{2+}, Zn^{2+}, etc.), and recyclability (with invisible capacity loss within 20 regeneration cycles).[145] Generally speaking, the irreversible bond formation enables rapid production of a wide range of POPs with decent chemical stability even in aggressive media (high acidity or basicity), but the ill-defined and ununiformly sized pores of POPs discourage selective removal of heavy metals. In contrast, COFs possess tailored porous structure and customized functionality, though the reversible bond formation generally time-consuming (multiday procedures)[142] and require specific reaction conditions.

3.2.3 Polymer composites

It is promising to develop organic-inorganic composites that combine the merits of both organic polymers and inorganic adsorbents. The polymers could be linked with metallic clusters to form metal-organic frameworks (MOFs) with three-dimensional network structure, which will be discussed in Section 3.3.2. Other structurally engineered polymer materials, such as ion-imprinted crown ether,[31] core-shell microgel particles,[146] and nanofibers,[29,106] have also been demonstrated for the extraordinary adsorption capacity with excellent metal affinity and selectivity, superior stability with wide pH window, and easy separation with satisfactory recyclability and reusability. Furthermore, the excellent mechanical strength and the adjustable surface functionality of polymers make them suitable to be supports for

inorganic nanomaterials, such as CNTs,[25,49,50] GO,[21,22] SiO_2,[147] and Fe_3O_4.[148] These inorganic/polymer hybrid adsorbents showed good dispersion and easy recycling of the incorporated nanoparticles without sacrificing their inherent properties, achieving enhanced performance in detoxification of As(III), Co(II), Cr(III), Cr(VI), Cu(II), Fe(II), Fe(III), Ni(II), Hg(II), Pb(II), Zn(II), etc.

3.3 Metallic and metal compound adsorbents

The past decade has witnessed the emerging of the metallic and metal compound adsorbents for the removal of heavy metals due to their unique properties, such as large surface area and highly tunable microstructures. These adsorbents can be categorized as metallic and metal compound nanoparticles, structurally engineered metal compound adsorbents, and magnetic adsorbents (Table 4).

3.3.1 Metallic and metal compound nanoparticles

Metallic materials with extremely small particle size have been intensively explored for removing heavy metals because of their large surface area, high permeability, excellent reactivity, non-toxicity, etc. For example, nanoscale zero valent iron (NZVI) possesses very large surface area and significant reduction capacity, exhibiting its capability to devour As(III), As(V), Cr(VI), Pb(II), etc. with the initial concentration ranging from 10 to 1000 mg L^{-1}.[36,149,150] However, bare NZVI nanoparticles (NPs) suffered from agglomeration and unselective oxidation in aqueous solution, which sharply deteriorated their efficiency and durability. Hence, NZVI NPs are often stabilized onto support materials that are porous, inexpensive, and environmentally friendly. For example, reduced graphite oxide (RGO) was used as a support for the NZVI NPs, capturing 35.8 mg g^{-1} As(III) at the optimal pH of 4~10 via surface complexation (in the form of H_3AsO_3 for pH<9.1) and electrostatic attraction (in the form of $H_2AsO_3^-$ for pH>9.1), and 29.0 mg g^{-1} As(V) at the optimized pH of 2 via electrostatic attraction (in the form of $H_2AsO_4^-$).[36] As a low-cost material, the Syzygium Jambos Alston (SJA) leaf extract was used to support the biogenic iron NPs (in the form of Fe^0 and Fe^{2+}).[149] The obtained Fe/SJA composites showed the adsorption capacity as high as 983.2 mg Cr(VI)/g Fe even in the coexistence of organic matters (humic acid) and other ions (Na^+, Ca^{2+}, Mg^{2+}, Cu^{2+}, Zn^{2+}, Cl^-, NO_3^-, etc.). This was attributed to the reduction of Cr(VI) to Cr(III) by Fe^0 and Fe^{2+} and then its coprecipitation with the as-produced Fe(III). Furthermore, it was found that the dispersion of NZVI NPs on the flower-like $Mg(OH)_2$ (Figure 16a-d) increased its surface area from 12 to 40 m^2 g^{-1}, leading to the enhancement of its Pb(II) adsorption capacity from 1718.4 to 1986.6 mg g^{-1}.[150] The Pb(II) attracted onto the surface of the NZVI/$Mg(OH)_2$ composites was partly reduced to bulk Pb^0 by NZVI and partly captured via ion exchange with $Mg(OH)_2$, followed by subsequent hydroxide precipitation. This demonstrates a synergistic effect between NZVI and $Mg(OH)_2$.

Compared to metallic NPs, metal compound NPs have the advantages in hydrophilicity, chemical stability, and

distinctive microstructure. As reported,[151] the CuO NPs could be used alone for adsorptive decontamination of Cr(VI) even at the pH of 3, but its small surface area of 84 m^2 g^{-1} and inevitable agglomeration resulted in the limited adsorption capacity of 15.6 mg g^{-1}. To improve the adsorption performance of metal oxides, Razzaz et al. attempted to stabilize TiO_2 NPs with the electrospun chitosan nanofibers via coating and entrapping methods (Figure 16e and f), leading to the increases in surface area (from 237 to 281 m^2 g^{-1}), pore volume (from 0.465 to 0.512 cm^3 g^{-1}), and average pore diameter (from 4.32 to 5.12 nm).[152] This entrapping method allowed uniform and stable dispersion of the TiO_2 NPs within the chitosan matrix, which could capture 715.7 mg g^{-1} Cu(II) and 579.1 mg g^{-1} Pb(II) and experienced negligible performance deterioration after five regeneration cycles with HNO_3. In contrast, the TiO_2 coated chitosan nanofibers showed lower adsorption capacities of 526.5 mg g^{-1} Cu(II) and 475.5 mg g^{-1} Pb(II), which dropped by 40% after five regeneration cycles due to the loss of the TiO_2 coating layer. Metal sulfides were also explored to remove heavy metals. For example, Qu and coworkers utilized the cation exchange properties of the ZnS nanocrystals (16 m^2 g^{-1}) to realize sequential precipitation and separation of 99.9% Hg(II), 99.9% Cu(II), 90.8% Pb(II), and 66.3% Cd(II) within 5 min.[153] Although the ZnS nanocrystals performed stably at pH above 3, it could produce hazardous H_2S under stronger acidic conditions. Interestingly, mechanically activated $CaCO_3$ selectively recovered 99.3% Cu(II) in the presence of Mn(II), Zn(II), and Ni(II) with the mineral phase conversion to posnjakite.[154]

3.3.2 Structurally engineered metal compound adsorbents

Nanoparticles are generally suffering easy agglomeration, chemical instability in acid solutions, and difficult separation after use. Therefore, metal-based materials with high structural tunability have been constructed into a variety of two- and three-dimensional architectures.

MXenes, a family of layered transition metal carbides and nitrides, are efficient adsorbents due to the large surface area, hydrophilicity, and chemical stability. Peng et al. chemically exfoliated the layered titanium carbide with NaOH to prepare the alk-MXene, $Ti_3C_2(OH/ONa)_xF_{2-x}$, in which the titanium surface terminated by -F, -OH, and -ONa not only has higher spatial accessibility to the heavy metal ions (due to promoted hydrophilicity and hindered restacking of the nanosheets), but also provides rich ion exchange sites, leading to the enhanced adsorption.[155] As a result, the alk-MXene preferentially scavenged Pb(II) from contaminated water in the presence of high level of competing cations such as Mg(II) and Ca(II), achieving the effluent Pb(II) concentration below 2 μg L^{-1} that meets the WHO drinking water standard (10 μg L^{-1}). Xu and coworkers reported the integrated films of the negatively charged $Ti_3C_2T_x$ (T-surface functionalities) MXene nanosheets inserted with positively charged rGO for pressure-free water filtration (Figure 17a and b).[156] The integrated films exhibited extraordinary adsorption performance to multifarious metal species including $HCrO_4^-$, $AuCl_4^-$, $PdCl_4^{2-}$, and Ag^+, reaching the high removal capacities of 84 mg g^{-1} Cr(VI), 890 mg g^{-1} Pd(II), 1241 mg g^{-1} Au(III), and 1172 mg g^{-1} Ag(I). The films are superior to the other two-dimensional materials that could only

selectively detoxify limited metal species through coordination chemistry or electrostatic attractions. This was attributed to the introduction of rGO that significantly increased the surface area of the MXene film from 20 to 126 $m^2 g^{-1}$, thus enhancing the solid-liquid interactions and mass transfer. Furthermore, the integrated films not only allowed efficient diffusion and intercalation of the metal ions, but also showed the ability to reduce the metal species from Cr(VI) to Cr(III) and from Pd(II), Au(III), and Ag(I) to their metallic phases (Figure 17c). The post-hydroxylation of the MXene surface further promoted the wettability of the integrated films and favored the reduction processes. Layered double hydroxides (LDHs), a class of layered clay minerals, are also exploited as adsorbents due to their simple preparation, large surface areas, adjustable interlayer spaces, and tunable adsorption sites. For example, the FeMgAl-LDHs (Fe-LDHs) with different intercalated anions (MoS_4^{2-}, S_5^{2-}, NO_3^-, and CO_3^{2-}) exhibited different abilities for uptake of heavy metals with distinct adsorption mechanisms (Figure 17d and e).[157] The Fe-MoS_4 LDH achieved the highest adsorption capacities of 582 mg g^{-1} for Hg(II) and 565 mg g^{-1} for Ag(I), which were slightly influenced by the presence of Na^+, Mg^{2+}, Ca^{2+}, Cl^-, NO_3^-, and SO_4^{2-}, through the dominant complexation mechanism inside the LDH layers. Similarly, the Fe-S_5 LDH could also selectively capture 279 mg g^{-1} Hg(II) and 341 mg g^{-1} Ag(I) with negligible efficiency loss in the coexistence of competing cations/anions. Meanwhile, the Fe-MoS_4 and Fe-S_5 LDHs could provide excellent adsorption performance within a wide pH range of 3~8. In contrast, the Fe-NO_3 and Fe-CO_3 LDHs showed poor adsorption capacities and low selectivity due to the dominant precipitation mechanism.

Metal-organic frameworks (MOFs), a class of compounds with metal ions/clusters connected to organic ligands via coordination, are efficient adsorbents due to their large surface area, high porosity, and intelligent architecture. However, most of MOFs are unstable in aqueous conditions. Therefore, only stable MOFs can be employed for the heavy metal removal from wastewater. For example, MOF-808, which is a stable MOF with 6-connected Zr6 nodes and a large surface area of 2424 $m^2 g^{-1}$, was functionalized as MOF-808-EDTA absorbent by submerging MOF-808 powders in ethylenediaminetetraacetic acid disodium salt (EDTA-2Na) aqueous solution (Figure 18a).[158] The MOF-808-EDTA composite was proved to be a broad-spectrum metal ion trap for 22 metal species including soft (Hg^{2+}, Pd^{2+}, Cd^{2+}, etc.), hard (Fe^{3+}, Mn^{2+}, etc.), and borderline (Pb^{2+}, Zn^{2+}, Cu^{2+}, Co^{2+}, Ni^{2+}, etc.) Lewis metal ions. EDTA provided strong chelating groups with non-specific affinity to various metals, while MOF-808 acted as a robust porous support that allowed well-distributed high-density binding sites (Figure 18b). Hence, the EDTA-incorporated MOF-808 adsorbent eliminated all heavy metal species with excellent removal efficiencies above 99% from both single- and multi-metal systems (Figure 18c). Unlike EDTA that always forms water soluble complexes with metals, the exhausted adsorbent could be readily separated from water and regenerated by EDTA-2Na solution without apparent decrease in metal uptake capacity. Therefore, the EDTA-incorporated MOF-808 is a promising candidate for the treatment of real wastewater containing multifarious or unpredictable heavy metal species. Zeolitic imidazolate frameworks (ZIFs) are a sub-family

of MOFs that have zeolite-like network with nitrogen-rich imidazolate ligands. Numerous ZIFs possess excellent thermal and chemical stability. By varying the precursor and the reaction condition, ZIF adsorbents with different morphologies, features and adsorption performance could be synthesized via the solvothermal reaction.[159] As a presentative, wafer-like ZIF-67 with abundant micro- and mesopores as well as large surface area of 1289 m^2 g^{-1} was demonstrated to devour 1348.4 mg g^{-1} Pb(II) and 617.5 mg g^{-1} Cu(II). In contrast, the flaky hexahedron ZIF-8 with only micropores and lower surface area of 937 m^2 g^{-1} showed worse detoxification performance for Pb(II) (1119.8 mg g^{-1}) and Cu(II) (454.7 mg g^{-1}).

Metal compound adsorbents with 3D hierarchical architectures have also been explored for heavy metal removal. For example, the 3D hierarchical urchin-like hollow spheres of goethite (α-FeOOH) were fabricated through the one-pot synthesis of Fe(II) ions and glycerol without templates, surfactants, and toxic organic solvents (Figure 19a-c).[160] The void interior sizes of the obtained α-FeOOH spheres could be tailored by changing glycerol concentration. Despite the relatively small surface area of 97 m^2 g^{-1}, the well-defined α-FeOOH hollow spheres with a hierarchical shell allowed effective electrostatic attraction and ion exchange with heavy metal ions, thus achieving the adsorption capacities of 58 mg g^{-1} for As(V) and 80 mg g^{-1} for Pb(II). Furthermore, a modified nuclei-assisted hydrothermal (NAH) method was used to synthesize a stable trilayer titanate architecture where a film of titanate microflowers was immobilized on the titanium foil substrate (bottom layer) and subsequently coated with a top layer of titanium nanowires (Figure 19d and e).[161] Na^+ and hydroxyls on the titanate microflowers allowed the capture of Pb^{2+} via ion exchange and surface precipitation, and the highly ordered architectures of the titanate further facilitated the adsorption. As the result, with the large surface area of 2157 m^2 g^{-1}, the as-prepared hierarchical titanate reached the large adsorption capacity of 1013 mg g^{-1} for Pb.

3.3.3 Magnetic adsorbents

Adsorbents are often modified for improved hydrophilicity and wettability to facilitate stable dispersion in water, full contact with heavy metal ions, and efficient ion transfer. However, it remains a challenge to separate the exhausted adsorbents since the traditional separation methods (e.g., centrifugation and filtration) generally suffer from increased cost, high energy consumption, and unsatisfactory efficiency. Therefore, magnetic nanomaterials receive increased attention with remarkable advantages, such as excellent heavy metal adsorption and easy magnetic separation. For example, a one-pot hydrothermal method was developed to synthesize citrate-immobilized magnetite nanoparticles, where the negatively charged carboxyl groups from the citrate ions provided repulsive forces among the nanoparticles, and the hydrophilic surface further facilitated the dispersion of these nanoparticles.[19] The as-prepared Fe_3O_4 nanoparticles showed high solubility and stability (beyond a month) in water, and could be effectively recycled via magnetic separation. Despite the relatively small surface area of 59 m^2 g^{-1}, these water-soluble Fe_3O_4 nanoparticles fully

dissolved in water and thus efficiently eliminated 90% Pb(II) within 2 min through the strong electrostatic attraction between the negatively charged magnetite surface and the metal ions.

However, the lack of selectivity to heavy metals may impair the performance of the magnetic adsorbents in complex wastewater that contains other cations (Na^+, Ca^{2+}, Mg^{2+}, ect.). To solve this issue, an organodisulfide polymer (PTMT) was coated on the magnetite nanoparticles to fabricate the porous core-shell magnetic microspheres, where the PTMT shell with rough and rugged surface provided abundant thiol groups as the primary binding sites for heavy metals (Figure 20a).[33] With the small surface area of 64 m^2 g^{-1}, these magnetic microspheres reached the high adsorption capacities of 603 mg g^{-1} for Hg(II), 533 mg g^{-1} for Pb(II), and 216 mg g^{-1} for Cd(II). The adsorption capacity changed with heavy metal species due to different complexation strength between the metal ions and the surface functional groups, whereas it remained stable in coexistence with high concentration inorganic salts (NaCl and Na_2SO_4), indicating the excellent selectivity to heavy metals. Furthermore, the metal-laden microspheres could be magnetically separated within 20s and subsequently regenerated with EDTA-2Na solution, leading to slightly decreased adsorption performance. Notably, the selectivity of adsorbents can be further improved for specific heavy metal species. As mentioned in Section 3.2.2, ion imprinted polymers are able to recognize target ions with extraordinary selectivity and affinity. With this design, the Fe_3O_4 nanoparticles was coated with Ag^+-imprinted thiourea-chitosan polymer to acquire selective Ag(I) capture ability (Figure 20b).[162] Although its surface area is 6 m^2 g^{-1}, the ion imprinted magnetic polymers scavenged 90% Ag(I) from the wastewater with the initial silver concentration up to 2157 mg L^{-1} as the amine groups from the thiourea moieties offered strong metal binding sites via coordination. Hence, these adsorbents achieved the maximized Ag(I) adsorption capacity of 532 mg g^{-1} at pH 5, since the protonated amine groups generated in acidic environment could suppress Ag(I) uptake via electrostatic repulsion, whereas the hydroxide precipitation of Ag(I) in the basic media could inhibit the formation of metal-resin complex. The adsorbent also showed about 10 times larger adsorption capacity for Ag(I) than for other heavy metals such as Cd(II), Zn(II), Pb(II), and Cu(II), indicating its selectivity for capturing Ag(I) from multi-metal-ion solutions. Furthermore, the exhausted adsorbents reached high desorption efficiency of 95% when using HNO_3 as the eluent, and the adsorption capacity remained 90% after five regeneration cycles. Therefore, the Ag(I) ion imprinted magnetic polymers are promising adsorbents for removal, recovery, and preconcentration of Ag(I) from wastewater.

3.4 Other adsorbents

Besides the above discussed types of adsorbents, other materials were also explored for heavy metal removal, including minerals, boron/carbon nitrides, and industrial and agricultural wastes (Table 5). These are discussed in this section.

3.4.1 Minerals

As a simple mineral material, silica is often used as an adsorbent due to its large surface area, definite pore size, rich hydroxyl groups, high chemical stability, and non-toxicity. It was observed that the silica nano hollow spheres (SNHSs) with the surface area of 919 m^2 g^{-1} and rich hydroxyls could capture 8.4 mg g^{-1} Ni(II), 20.8 mg g^{-1} Cd(II), and 26.8 mg g^{-1} Pb(II).[20] It was interesting that functionalization with amino and thiol groups reduced the pore size of SNHSs and thus decreased the surface area of the obtained NH_2-SNHSs to 370 m^2 g^{-1}, but this did not retard the adsorption of heavy metals. On the contrary, NH_2-SNHSs could scavenge 31.3 mg g^{-1} Ni(II), 40.7 mg g^{-1} Cd(II), and 96.8 mg g^{-1} Pb(II). The enhanced adsorption capacity and selectivity revealed the impacts of surface functionality. Therefore, it has attracted the increased attention to decorate silica spheres with functional groups such as poly(acrylic acid) (PAA) to achieve higher adsorption capacity (e.g., 178.6 mg g^{-1} for trivalent chromium).[147]

Zeolites are microporous aluminosilicate minerals with a general formula of $M_{2/n}O \cdot Al_2O_3 \cdot xSiO_2 \cdot yH_2O$, where n denotes the valence of the charge-balancing cation M (usually Na, K, Mg, Ca, etc.), x the molecular ratio of SiO_2 over Al_2O_3 (usually above 2), and y the moles of water in the zeolite structure. The charge-balancing cations, which are loosely held within the three-dimensional framework composed of alumina and silica tetrahedral units and the linking oxygen atoms, can be easily replaced by heavy metal ions. Furthermore, different from MOFs with relative low stability due to their inorganic/organic coordination structures, zeolites are inorganic crystal porous materials with very high thermal and chemical stability. These endow zeolites with capability of capturing heavy metal ions from wastewater. Common mineral zeolites include chabazite, clinoptilolite, analcime, heulandite, and stilbite. It was found that the synthesized zeolite exhibited an adsorption capacity ~10 times higher than that of the natural clinoptilolite.[163] Meng et al. fabricated high quality zeolite A from natural halloysite mineral and observed high adsorption capacities of 123.0 and 227.7 mg g^{-1} for Ag^+ and Pb^{2+}, respectively.[164] In addition, zeolite A exhibited the highest selectivity for silver and lead ions, moderate selectivity for chromium, copper, and zinc ions, and the lowest selectivity for manganese, nickel, and iron ions. Furthermore, zeolite A preferentially adsorbed heavy metal ions than innocuous cations in their coexistence. Another attractive merit of zeolites is their ability to stabilize the captured heavy metal ions via simple thermal treatment.[165] At 900-1000℃, the lead- and copper-laden zeolites were calcined into $PbAl_2Si_2O_8$ and $CuAl_2O_4$, respectively, exhibiting the significantly inhibited ion leaching behavior compared with the untreated ones. Therefore, the heavy metal ions loosely accommodated within the porous framework of zeolites can be easily stabilized without bringing potential risk of secondary contamination.

Clays, the fine-grained particles (with a diameter below 2.0 μm) mainly composed of tetrahedral (Si^{4+}) sheets and octahedral (Al^{3+}, Fe^{3+}, Fe^{2+}, or Mg^{2+}) sheets, are regarded as low-cost and effective adsorbents for heavy metals due to their large surface area, high cation exchange capacity, and ubiquitous occurrence in natural. Clays have both amorphous

and crystalline forms, and the latter possesses various lamellar structures such as 1:1 tube type (halloysite), 1:1 layer type (kaolinite), 2:1 layer type (montmorillonite, vermiculite), and 2:1 layer-chain type (attapulgite, sepiolite).[166] Compared to zeolites that feature the regular microporous structures, clays provide relatively flexible pore structures with expandable interlayer space that facilitate the accommodation of heavy metal ions. Natural raw clays such as kaolinite, bentonite, and montmorillonite can adsorb heavy metals (such as Cd, Cu, Hg, Mn, Ni, Pb, and Zn) from aqueous solutions, but the uncontrollable removal rates (from 45% to 99%), the relatively low metal adsorption capacities (generally below 100 mg g^{-1}), and the narrow pH range (generally 6~8) suggest the demand for modified clay adsorbents.[167,168] Thermal treatment can induce dehydration and dihydroxylation of clays, increasing the porosity and the exposed surface area. It was observed that calcination at over 700℃ transformed serpentine from layered structure to amorphous form with increased surface area (from 6 to 14 m^2 g^{-1}) and enhanced Cd(II) adsorption (from 8.7 to 15.2 mg g^{-1}) through the facilitated surface precipitation mechanisms.[169] It should be noted that and an over-high calcination temperature can destroy the clay structure and hence deteriorate the functionality. Acid treatment can open the edges and pore spaces to significantly increase surface area for heavy metal ions. As reported, montmorillonite and vermiculate treated with HNO_3 and subsequently saturated with $NaNO_3$ showed significantly increased surface area and improved removal rates (above 60%) for various heavy metal species including Cu(II), Cd(II), Co(II), Ni(II), Pb(II), Zn(II), etc.[170] Both clay adsorbents could be efficiently regenerated with a single extraction of HCl or HNO_3. Nevertheless, inappropriate acid treatment may cause the decreases in surface area and adsorption capacity due to structural collapse and loss of octahedral cations.

3.4.2 Boron and carbon nitrides

Boron nitride (BN), an analogue of graphite, is a promising adsorbent due to its large specific surface area, chemical durability, oxidation resistance, and abundant structural defects. Li et al. synthesized the activated BN with tunable structural and surficial characteristics through a simple structure-directed method.[171] The as-obtained BN has large surface area of 2078 m^2 g^{-1} and big pore volume of 1.66 cm^3 g^{-1} with abundant micro-/mesopores, attaining high adsorption capacities of 352, 215, 235, and 225 mg g^{-1} for Cr (III), Co (II), Ni (II), and Pb (II) ions, respectively, and excellent reusability. A similar micro-/mesoporous BN adsorbent was also demonstrated to have high removal capacities for methyl orange and Cu (II) ions.[172] Furthermore, structural engineering (e.g., hexagonal nanosheets and spheres) and chemical modification (such as oxygen-doping and fluorination) were employed to further improve the adsorption performance of BN materials.[173-175]

As the most stable allotrope of carbon nitride, graphitic carbon nitride (g-C_3N_4) has attracted intensive concern. Its intrinsic functional groups, which are -NH_2, -NH-, and =N-, show a superior adsorption capacity for heavy metal ions through complexation.[176-178] Hu et al. synthesized g-C_3N_4 with urea for removing Pb(II) from aqueous solutions.[176] They

revealed the great effect of pH values on Pb(II) adsorption, namely, the main contributor to the adsorption was the outer-sphere surface complexation (or ion exchange) of g-C_3N_4 at pH<7, but the inner-sphere surface complexation at pH>7. Furthermore, the g-C_3N_4 could be regenerated through the desorption of Pb(II) by 1.0 M HCl solution. The important role of the inner-sphere surface complexation was also demonstrated by Shen et al. for the adsorption of heavy metal ions over g-C_3N_4, achieving adsorption capacities of 1.36 mmol/g for Pb(II), 2.09 mmol/g for Cu(II), 1.00 mmol/g for Cd(II), and 0.64 mmol/g for Ni(II).[179] The excellent performance of g-C_3N_4 nanosheets for removing Cd(II) or Cr (VI) from water was further demonstrated by Cai et al.[177] and Xiao et al.[180]

3.4.3 Industrial and agricultural wastes

Various industrial wastes, which are potentially low-cost adsorbents, were demonstrated for the treatment of heavy metal-bearing water. For easy recycles, they are often made into pellets or granular forms. In some cases, they are combined with zeolites or activated carbon to obtain large surface area and porosity, high mechanical and chemical stability, and rich functional groups. For example, the pellets of fired coal fly ash could reduce the concentration of Cu(II) and Cd(II) from water,[181] while the fly-ash-derived zeolite showed excellent adsorption performance of removing Cu^{2+}, Co^{2+}, Cr^{3+}, Cd^{2+}, Ni^{2+}, Zn^{2+}, and Pb^{2+} via ion exchange.[182,183] The granular blast furnace slag was used to selectively remove Pb(II) from water containing Cu(II), Cd(II), Ni(II), and Na(I) via physical adsorption, ion exchange, and precipitation.[184] The clarified sludge from the steel industry achieved the adsorption capacity of 25 mg g^{-1} for Zn(II) with an equilibrium time of 1 hour, compared to those for rice husk ash (3 hours) and activated alumina and neem bark (4 hours).[185] The red mud, a bauxite processing residue comprising fine particles of silica and metal (Al, Fe, Ca, Ti, etc.) oxides and hydroxides, could scavenge 96.5% As(V) and 87.5% As(III) from aqueous solution within 60 min because of the high surface reactivity.[186] The sawdust could eliminate 94.8% Cu(II) at pH 7 mainly via ion exchange mechanism,[187] whereas the organic sewage sludge was transformed to activated carbon through chemical activation (with H_2SO_4, H_3PO_4, and $ZnCl_2$) for removal of Hg(II).[188] Notably, the non-metallic powder derived from waste printed circuit boards from electronic industry was demonstrated to remove Cd(II) via physisorption and ion exchange (with K^+) with equivalent performance to the commercial products.[189]

Since the 1990s, the adsorption of heavy metals by agricultural wastes has been explored for their merits, such as strong affinity and selectivity to heavy metals due to various binding groups, low-cost due to abundant availability and easy processing, low sludge production, and high regeneration capability.[190] Commonly used agricultural waste adsorbents include the straws, husks, barks, shells, leaves, roots, and peels of the plants (Table 5). They are mainly composed of cellulose, lignin, starch, lipids, sugars, proteins, and others, which provide rich functional groups (such as amido, amino, sulfhydryl, carbonyl, alcoholic, phenolic, and acetamido groups) and thus ensure high adsorption capacity of heavy metal ions via various mechanisms including physisorption, complexation and chelation, surface precipitation,

and ion exchange. The adsorption of metal ions is also influenced by conditions, such as adsorbent dose, contact time, agitation speed, and pH values. For example, the raw rice straw showed the adsorption capacity of 13.9 mg g^{-1} for Cd(II) in the pH range of 2~6, and its mechanism involved ion exchange with cations (e.g., Na^+, K^+, Mg^{2+}, and Ca^{2+}) and chelation with binding groups (e.g., C=C, C=O, -OH, and -COOH).[191] Furthermore, after the introduction of polymers with various functional groups that could improve hydrophilicity and metal affinity, the rice straw composites achieved surprisingly high adsorption capacities of 662.9 mg g^{-1} for Pb(II), 248.8 mg g^{-1} for Cu(II), 110.1 mg g^{-1} for Zn(II), and 94.9 mg g^{-1} for Ni(II).[192] Similarly, the introduction of grafted copolymer with abundant hydroxyl and carboxyl groups into orange peel increased its adsorption capacities for Ni^{2+}, Cd^{2+}, and Pb^{2+} by 16.5, 4.6, and 4.2 times, respectively.[193] Acid modification through hydrothermal treatment could also increase the carboxyl functionality of Bougainvillea spectabilis, achieving the removal of 99.5% Pb(II) from aqueous solution through ion exchange and electrostatic interactions.[194] Furthermore, plant biomass can be utilized for the production of activated charcoal or biochar to eliminate heavy metals such as Co(II), Ni(II), and Zn(II).[195,196] Therefore, these wastes are expected to offer significant advantages over the expensive commercial adsorbents.[197]

3.4.4 Functionalized mesoporous adsorbents

Mesoporous materials, which possess pore diameters in the range of 2~50 nm, typically include mesoporous silica (e.g., Folded Sheet Materials/FSM-16,[198] Mobile Composition of Matter/MCM-41,[199] MCM-48,[200] Santa Barbara Amorphous/SBA-15[201]), mesoporous carbon (e.g., CMK-1,[202] Seoul National University/SNU-2,[203] Fudan University/FDU-14,[204] 3DG[69-72]), mesoporous polymers (e.g., mesoporous CMPs[130] and mesoporous COFs[131]), and mesoporous metal compounds (e.g., ZIF-67[159] and α-FeOOH hollow spheres[160]). These materials are mainly produced via the (soft or hard) template-direct synthesis and the self-assembly, generating the ordered mesopores and the disordered ones, respectively. For instance, the best known hexagonal mesoporous silica (MCM-41) was synthesized by calcination of cooperatively assembled aluminosilicate gels (as the silica precursor) and surfactants (as the soft template),[199] while the first highly mesoporous carbon (CMK-1) with uniform pore size distribution (3 nm) was synthesized by infiltration of sucrose (as the carbon source) in the mesopores silica molecular sieve (MCM-48, as the hard template), carbonization, and finally template removal in NaOH solution.[202] When a template-free self-assembly strategy is applied, however, the resulting materials can display either disordered structures (e.g., mesoporous CMPs[130] and ZIF-67[159]) or well-ordered ones (e.g., mesoporous COFs[131] and uniform α-FeOOH hollow spheres[160]).

Pristine mesoporous polymers and metal compounds have the ability to capture heavy metals via inherently rich metal-binding components (such as the N and S atoms in polymer chains and the reductive/exchangeable constituents in metal compounds), and the adsorption performance can be further improved via post-functionalization (see detailed discussion in Sections 3.2.2 and 3.3.2). In contrast, pristine mesoporous silica and carbon have unsatisfactory ability of

heavy metal removal due to limited metal-binding groups.[205] Therefore, development of functionalized mesoporous silica and carbon has attracted burgeoning attention. There are two major synthesis routes, namely, post-synthesis and one-pot synthesis. The post-synthesis approach can allow to graft various functional groups to the surface of the pristine mesoporous materials, while the one-pot synthesis can achieve uniform distribution of functional groups though at the risk of disordered mesopores.[205,206] For example, ordered mesoporous carbon CMK-3 could be synthesized with SBA-15 as the hard template and post-functionalized with 3-aminopropyltrimethoxysilane, leading to a modified mesoporous carbon adsorbent.[207] This adsorbent achieved high adsorption capacities of 8.6 mmol g^{-1} for Cu(II) and 3.5 mmol g^{-1} for Pb(II) through ligand formation with amine groups as well as cation exchange and electrostatic attraction with carboxylic moieties. In contrast, highly disordered mesoporous structure was observed in PEI-functionalized mesocellular silica foam obtained via co-condensation of tetraethoxyorthosilicate (TEOS, as the precursor), propyl-PEI (pPEI, as the modifier), trimethylbenzene (TMB, as the swelling agent), and P123 (as the directing agent) followed by removal of the swelling and directing agents.[208] With plentiful imine moieties and ample disordered mesopores (some narrowly distributed around 3 nm and others widely distributed around 8 nm), this silica foam reached a high Cd(II) uptake of 625 mg g^{-1}. Recently, a highly ordered periodic mesoporous organosilica material was synthesized via template-assisted one-pot hydrothermal polymerization of pre-functionalized monomers (Figure 21).[209] This material showed large surface area (971 m^2 g^{-1}), abundant micropores (1.5 nm) and mesopores (3.0 nm), as well as rich thiadiazole and thiol moieties. Attributed to the large accessible surface area and strong metal affinity (from the plentiful N and S atoms), this novel material presented fast Hg(II) uptake (from 2 ppm to 2 ppb within 5 min), excellent adsorption capacity (2081 mg g^{-1}), and chemical stability (over the pH range of 1~8).

4 Conclusions and prospects

The past decade has witnessed great progress in adsorbents for the removal of heavy metals, which was comprehensively reviewed in this article. As the first part, we discussed the design principle for efficient adsorbents with emphasis on four technical requirements: large accessible surface area, strong interaction between the active sites and the heavy metals, selectivity towards the target heavy metal species, and easy regeneration. In the second part, the synthesis and performance of advanced adsorbents were evaluated for heavy metal removal, including (1) carbon-based materials (activated carbons, nanotubes, graphene, and biochar), (2) polymers, (3) metal-based materials (nanoparticles, MXenes, metal-organic frameworks, and magnetic materials), (4) boron/carbon nitrides, (5) zeolites, and (6) industrial and agricultural wastes. Many of these adsorbent materials exhibited excellent capacities for various heavy metal ions from water solutions. Nevertheless, there are the following limitations and challenges in the heavy metal removal from

wastewater via adsorption processes:

First, the performances of most adsorbents were tested for heavy metal removal at a laboratory scale in a simple aqueous system, which is far from practical application conditions. More efforts should be devoted to the application of the adsorbents in treatment of real industrial wastewater at larger scales.

Second, the high selectivity of adsorbents to target metal ions is still a challenge. This would encourage more efforts to functionalize adsorbent surfaces with desired chemical groups that can selectively bind specific metal ions.

Third, used adsorbents have to be recycled in case of secondary pollution, which needs efficient separation at low cost. Incorporation of adsorbents into porous supports is widely employed to solve the problem, but it suffers from the decrease in the exposed surface area and the inevitable releasing of the adsorbents. Magnetic adsorbents can be easily recycled with a magnetic field, but their relatively high sensitivity to pH restricts their application within neutral environment. To solve these issues, intensive R & D efforts for more efficient adsorbents and processes are necessary.

Finally, current research is mostly focused on removal of heavy metals without concerning their recovery. With appropriate eluents, the absorbed heavy metals (especially the precious metals like silver) can be released for further purification. This not only produces high-quality metals, but also reduces the toxicity of the sludge in case of secondary pollution. As a promising technique, CDI can simultaneously recovery absorbed heavy metals (for the production of high-quality metals) and regenerate adsorbents. Therefore, the development of more efficient CDI electrode materials would become important research.

Author contributions

Yuhuan Fei: writing - original draft. Yun Hang Hu: conceptualization, funding acquisition, supervision, and writing - review & editing.

Notes

There are no conflicts to declare.

Acknowledgements

We are grateful for support from the National Science Foundation (CMMI-1661699).

References

1. F. Habashi, *Bull. Hist. Chem.*, 2009, **34**, 30-31.
2. J. O. Duruibe, M. O. C. Ogwuegbu and J. N. Egwurugwu, *Int. J. Phys. Sci.*, 2007, **2**, 112-118.
3. L. Jarup, *Br. Med. Bull.*, 2003, **68**, 167-182.

4. N. Abdu, A. Abdulkadir, J. O. Agbenin and A. Buerkert, *2D Mater.*, 2011, **89**, 387-397.
5. M. A. Barakat, *Arabian J. Chem.*, 2011, **4**, 361-377.
6. F. L. Fu and Q. Wang, *J. Environ. Manage.*, 2011, **92**, 407-418.
7. U. Upadhyay, I. Sreedhar, S. A. Singh, C. M. Patel and K. L. Anitha, *Carbohydr. Polym.*, 2021, **251**.
8. V. Kumar, D. Katyal and S. Nayak, *Environ. Sci. Pollut. Res.*, 2020, **27**, 41199-41224.
9. B. Verma and C. Balomajumder, *Environ. Technol. Innov.*, 2020, **17**.
10. H. Q. Qin, T. J. Hu, Y. B. Zhai, N. Q. Lu and J. Aliyeva, *Environ. Pollut.* , 2020, **258**.
11. J. L. Yang, Y. Bu, F. Y. Liu, W. Q. Zhang, D. D. Cai, A. D. Sun, Y. Q. Wu, R. Zhou and C. P. Zhang, *Int. J. Electrochem. Sci.*, 2020, **15**, 7848-7859.
12. N. Murayama, H. Yamamoto and J. Shibata, *Int. J. Miner. Process.*, 2002, **64**, 1-17.
13. T.-H. Ko, W.-S. Kuo and C.-H. Hu, 2001, **81**, 1090-1099.
14. B. Sajjadi, R. M. Shrestha, W.-Y. Chen, D. L. Mattern, N. Hammer, V. Raman and A. Dorris, *J. Water Process. Eng.*, 2021, **39**, 101677.
15. J. Wang and S. Kaskel, *J. Mater. Chem.*, 2012, **22**, 23710-23725.
16. A. Nayak, B. Bhushan, V. Gupta and P. Sharma, *J. Colloid Interf. Sci.*, 2017, **493**, 228-240.
17. L. Feng, M. Cao, X. Ma, Y. Zhu and C. Hu, *J. Hazard. Mater.*, 2012, **217-218**, 439-446.
18. Y. Fu, Y. Sun, Y. Zheng, J. Jiang, C. Yang, J. Wang and J. Hu, *Sep. Purif. Technol.*, 2021, **259**, 118112.
19. L. X. Wang, J. C. Li, Q. Jiang and L. J. Zhao, *Dalton Trans.*, 2012, **41**, 4544-4551.
20. M. Najafi, Y. Yousefi and A. A. Rafati, *Sep. Purif. Technol.*, 2012, **85**, 193-205.
21. X. Yi, F. Sun, Z. Han, F. Han, J. He, M. Ou, J. Gu and X. Xu, *Ecotoxicol. Environ. Saf.*, 2018, **158**, 309-318.
22. V. Chandra and K. S. Kim, *Chem. Commun.*, 2011, **47**, 3942-3944.
23. F. H. Narouei, L. Livernois, D. Andreescu and S. Andreescu, *Sens. Actuators B Chem.*, 2021, **329**, 129267.
24. N. Prakash, S. A. Vendan, P. N. Sudha and N. G. Renganathan, *Inorg. Nano-Met. Chem.*, 2016, **46**, 1664-1674.
25. H. Chen, J. Li, D. Shao, X. Ren and X. Wang, *Chem. Eng. J.*, 2012, **210**, 475-481.
26. Q. Meng, B. Peng and C. Shen, *Colloids Surf. B*, 2018, **167**, 176-182.
27. J. Zhao, R. Boada, G. Cibin and C. Palet, *Sci. Total Environ.*, 2021, **756**, 143816.
28. L.-L. Ling, W.-J. Liu, S. Zhang and H. Jiang, *Environ. Sci. Technol.*, 2017, **51**, 10081-10089.
29. D. Morillo Martin, M. Faccini, M. A. Garcia and D. Amantia, *J. Environ. Chem. Eng.*, 2018, **6**, 236-245.
30. S. Daradmare, M. Xia, V. N. Le, J. Kim and B. J. Park, *Chemosphere*, 2021, **270**, 129487.
31. X. Luo, L. Liu, F. Deng and S. Luo, *J. Mater. Chem. A*, 2013, **1**, 8280-8286.
32. C. Xiao, X. Liu, S. Mao, L. Zhang and J. Lu, *Appl. Surf. Sci.*, 2017, **394**, 378-385.
33. X. Huang, J. Y. Yang, J. K. Wang, J. T. Bi, C. Xie and H. X. Hao, *Chemosphere*, 2018, **206**, 513-521.
34. L. Ulloa, M. Martinez-Minchero, E. Bringas, A. Cobo and M. F. San-Roman, *Sep. Purif. Technol.*, 2020, **253**, 117516.
35. X. K. Huang, X. R. Guo, Q. Q. Dong, L. J. Liu, R. Tallon and J. H. Chen, *Environ. Sci. Nano*, 2019, **6**, 3225-3231.
36. C. Wang, H. Luo, Z. Zhang, Y. Wu, J. Zhang and S. Chen, *J. Hazard. Mater.*, 2014, **268**, 124-131.
37. G. Singh, R. Bahadur, J. Mee Lee, I. Young Kim, A. M. Ruban, J. M. Davidraj, D. Semit, A. Karakoti, A. a. H. Al Muhtaseb and A. Vinu, *Chem. Eng. J.*, 2021, **406**, 126787.
38. T. Watanabe and K. Ogawa, *Journal*, 1929, **24**, 10376.
39. E. A. Sigworth and S. B. Smith, *J. Am. Water Work. Assoc.*, 1972, **64**, 386-391.
40. C.-G. Lee, J.-W. Jeon, M.-J. Hwang, K.-H. Ahn, C. Park, J.-W. Choi and S.-H. Lee, *Chemosphere*, 2015, **130**, 59-65.
41. O. Sayar, M. M. Amini, H. Moghadamzadeh, O. Sadeghi and S. J. Khan, *Microchim. Acta* 2013, **180**, 227-233.
42. V. K. Gupta, S. K. Srivastava, D. Mohan and S. Sharma, *Waste Manage. (Oxford)* 1998, **17**, 517-522.
43. X. Yuan, N. An, Z. Zhu, H. Sun, J. Zheng, M. Jia, C. Lu, W. Zhang and N. Liu, *Process Saf. Environ. Prot.*, 2018, **119**, 320-329.
44. J. Zhang, H. Zou, Q. Qing, Y. Yang, Q. Li, Z. Liu, X. Guo and Z. Du, *J. Phys. Chem. B*, 2003, **107**, 3712-3718.

45. P.-X. Hou, C. Liu and H.-M. Cheng, *Carbon*, 2008, **46**, 2003-2025.
46. S. Iijima, *Nature*, 1991, **354**, 56-58.
47. Y.-H. Li, S. Wang, J. Wei, X. Zhang, C. Xu, Z. Luan, D. Wu and B. Wei, *Chem. Phys. Lett.*, 2002, **357**, 263-266.
48. X.-Y. Yu, T. Luo, Y.-X. Zhang, Y. Jia, B.-J. Zhu, X.-C. Fu, J.-H. Liu and X.-J. Huang, *ACS Appl. Mater. Interfaces* 2011, **3**, 2585-2593.
49. M. Ghorbani and H. Eisazadeh, *J. Vinyl Addit. Technol.*, 2013, **19**, 213-218.
50. M. T. Bankole, A. S. Abdulkareem, I. A. Mohammed, S. S. Ochigbo, J. O. Tijani, O. K. Abubakre and W. D. Roos, *Sci. Rep.*, 2019, **9**.
51. C. Lu, H. Chiu and C. Liu, *Ind. Eng. Chem. Res.*, 2006, **45**, 2850-2855.
52. K. S. Novoselov, A. K. Geim, S. V. Morozov, D. Jiang, Y. Zhang, S. V. Dubonos, I. V. Grigorieva and A. A. Firsov, 2004, **306**, 666-669.
53. W. S. Hummers and R. E. Offeman, *J. Am. Chem. Soc.*, 1958, **80**, 1339-1339.
54. M. J. McAllister, J.-L. Li, D. H. Adamson, H. C. Schniepp, A. A. Abdala, J. Liu, M. Herrera-Alonso, D. L. Milius, R. Car, R. K. Prud'homme and I. A. Aksay, *Chem. Mater.*, 2007, **19**, 4396-4404.
55. K. S. Kim, Y. Zhao, H. Jang, S. Y. Lee, J. M. Kim, K. S. Kim, J.-H. Ahn, P. Kim, J.-Y. Choi and B. H. Hong, *Nature*, 2009, **457**, 706-710.
56. Q. Zhang, Q. X. Hou, G. X. Huang and Q. Fan, *Environ. Sci. Pollut. Res.*, 2020, **27**, 190-209.
57. J. Li, S. Guo, Y. Zhai and E. Wang, *Anal. Chim. Acta* 2009, **649**, 196-201.
58. S.-T. Yang, Y. Chang, H. Wang, G. Liu, S. Chen, Y. Wang, Y. Liu and A. Cao, *J. Colloid Interf. Sci.*, 2010, **351**, 122-127.
59. G. Zhao, J. Li, X. Ren, C. Chen and X. Wang, *Environ. Sci. Technol.*, 2011, **45**, 10454-10462.
60. J. Wang and B. Chen, *Chem. Eng. J.*, 2015, **281**, 379-388.
61. C. J. Madadrang, H. Y. Kim, G. Gao, N. Wang, J. Zhu, H. Feng, M. Gorring, M. L. Kasner and S. Hou, *ACS Appl. Mater. Interfaces* 2012, **4**, 1186-1193.
62. R. Zare-Dorabei, S. M. Ferdowsi, A. Barzin and A. Tadjarodi, *Ultrason. Sonochem.*, 2016, **32**, 265-276.
63. M. Pirveysian and M. Ghiaci, *Appl. Surf. Sci.*, 2018, **428**, 98-109.
64. H. Y. Koo, H.-J. Lee, H.-A. Go, Y. B. Lee, T. S. Bae, J. K. Kim and W. S. Choi, *Chem. Eur. J.*, 2011, **17**, 1214-1219.
65. X. M. Wang, Y. F. Pei, M. X. Lu, X. Q. Lu and X. Z. Du, *J. Mater. Sci.*, 2015, **50**, 2113-2121.
66. L. Liu, C. Li, C. Bao, Q. Jia, P. Xiao, X. Liu and Q. Zhang, *Talanta*, 2012, **93**, 350-357.
67. C. Jiao, J. Xiong, J. Tao, S. Xu, D. Zhang, H. Lin and Y. Chen, *Int. J. Biol. Macromol.*, 2016, **83**, 133-141.
68. W. M. Algothmi, N. M. Bandaru, Y. Yu, J. G. Shapter and A. V. Ellis, *J. Colloid Interf. Sci.*, 2013, **397**, 32-38.
69. H. Wang, K. Sun, F. Tao, D. J. Stacchiola and Y. H. Hu, *Angew. Chem. Int. Ed.*, 2013, **52**, 9210-9214.
70. L. Chang, W. Wei, K. Sun and Y. H. Hu, *J. Mater. Chem. A*, 2015, **3**, 10183-10187.
71. L. Chang, D. J. Stacchiola and Y. H. Hu, *ACS Appl. Mater. Interfaces* 2017, **9**, 24655-24661.
72. Z. Sun and Y. H. Hu, *Acc. Mater. Res.*, 2021, **2**, 48-58.
73. J. Liu, X. Ge, X. Ye, G. Wang, H. Zhang, H. Zhou, Y. Zhang and H. Zhao, *J. Mater. Chem. A*, 2016, **4**, 1970-1979.
74. L. Chang, Y. Fei and Y. H. Hu, *J. Mater. Chem. A*, 2021, **9**, 1429-1455.
75. L. Chang and Y. Hang Hu, *J. Colloid Interf. Sci.*, 2019, **538**, 420-425.
76. P. Rana, N. Mohan and C. Rajagopal, *Water Res.*, 2004, **38**, 2811-2820.
77. C.-C. Huang and J.-C. He, *Chem. Eng. J.*, 2013, **221**, 469-475.
78. S.-Y. Huang, C.-S. Fan and C.-H. Hou, *J. Hazard. Mater.*, 2014, **278**, 8-15.
79. X. Su, A. Kushima, C. Halliday, J. Zhou, J. Li and T. A. Hatton, *Nat. Comm.*, 2018, **9**, 4701.
80. Y. Zhou, Q. Ji, H. Liu and J. Qu, *Environ. Sci. Technol.*, 2018, **52**, 7477-7485.
81. Y. Wei, L. Xu, K. Yang, Y. Wang, Z. Wang, Y. Kong and H. Xue, *J. Electrochem. Soc.* , 2017, **164**, E17-E22.
82. P. Y. Liu, T. T. Yan, J. P. Zhang, L. Y. Shi and D. S. Zhang, *J. Mater. Chem. A*, 2017, **5**, 14748-14757.
83. Q. H. Ji, C. Z. Hu, H. J. Liu and J. H. Qu, *Chem. Eng. J.* , 2018, **350**, 608-615.

84. J. Xue, Q. Sun, Y. Zhang, W. Mao, F. Li and C. Yin, *ACS Omega*, 2020, **5**, 10995-11004.
85. L. Liu, X. Guo, R. Tallon, X. Huang and J. Chen, *Chem. Commun.* , 2017, **53**, 881-884.
86. M. Dai, M. Zhang, L. Xia, Y. Li, Y. Liu and S. Song, *ACS Sustain. Chem. Eng.*, 2017, **5**, 6532-6538.
87. G. Bharath, E. Alhseinat, N. Ponpandian, M. A. Khan, M. R. Siddiqui, F. Ahmed and E. H. Alsharaeh, *Sep. Purif. Technol.* , 2017, **188**, 206-218.
88. L. Bautista-Patacsil, J. P. L. Lazarte, R. C. Dipasupil, G. Y. Pasco, R. C. Eusebio, A. Orbecido and R. Doong, *J. Environ. Chem. Eng.*, 2020, **8**.
89. J. Han, T. Yan, J. Shen, L. Shi, J. Zhang and D. Zhang, *Environ. Sci. Technol.* , 2019, **53**, 12668-12676.
90. P. M. Sanka, M. J. Rwiza and K. M. Mtei, *Water Air Soil Pollut.*, 2020, **231**.
91. J.-H. Park, Y. S. Ok, S.-H. Kim, J.-S. Cho, J.-S. Heo, R. D. Delaune and D.-C. Seo, *Chemosphere*, 2016, **142**, 77-83.
92. A. Y. Li, H. Deng, Y. H. Jiang, C. H. Ye, B. G. Yu, X. L. Zhou and A. Y. Ma, *Langmuir*, 2020, **36**, 9160-9174.
93. A. H. A. Khan, I. Nawaz, S. Yousaf, A. S. Cheema and M. Iqbal, *J. Environ. Manage.* , 2019, **242**, 46-55.
94. G. R. Strobl, *The physics of polymers*, Springer, 3 edn., 1997.
95. E. Vunain, A. K. Mishra and B. B. Mamba, *Int. J. Biol. Macromol.* , 2016, **86**, 570-586.
96. B. J. Wang, Y. Zhu, Z. S. Bai, R. Luque and J. Xuan, *Chem. Eng. J.* , 2017, **325**, 350-359.
97. L. X. Zhang, S. Y. Tang, F. X. He, Y. Liu, W. Mao and Y. T. Guan, *Chem. Eng. J.* , 2019, **378**.
98. E. Repo, J. K. Warchol, A. Bhatnagar and M. Sillanpaa, *J. Colloid Interf. Sci.*, 2011, **358**, 261-267.
99. F. Wang, X. Lu and X. Y. Li, *J. Hazard. Mater.* , 2016, **308**, 75-83.
100. H. Ren, Z. Gao, D. Wu, J. Jiang, Y. Sun and C. Luo, *Carbohydr. Polym.* , 2016, **137**, 402-409.
101. C. B. Godiya, X. Cheng, D. W. Li, Z. Chen and X. L. Lu, *J. Hazard. Mater.* , 2019, **364**, 28-38.
102. Z. Li, D. Xiao, Y. Ge and S. Koehler, *ACS Appl. Mater. Interfaces* 2015, **7**, 15000-15009.
103. G. Y. Zhou, C. B. Liu, L. Chu, Y. H. Tang and S. L. Luo, *Bioresour. Technol.* , 2016, **219**, 451-457.
104. J. Liu, D. Su, J. Yao, Y. Huang, Z. Shao and X. Chen, *J. Mater. Chem. A*, 2017, **5**, 4163-4171.
105. S. Yan, F. Y. Zhang, L. Wang, Y. D. Rong, P. G. He, D. C. Jia and J. L. Yang, *J. Environ. Manage.* , 2019, **246**, 174-183.
106. L. R. Rad, A. Momeni, B. F. Ghazani, M. Irani, M. Mahmoudi and B. Noghreh, *Chem. Eng. J.* , 2014, **256**, 119-127.
107. R. M. Hassan, S. M. Ibrahim, S. A. Sayed and I. A. Zaafarany, *ACS Omega*, 2020, **5**, 4424-4432.
108. J.-X. Jiang and A. I. Cooper, in *Functional Metal-Organic Frameworks: Gas Storage, Separation and Catalysis*, ed. M. Schröder, Springer Berlin Heidelberg, Berlin, Heidelberg, 2010, DOI: 10.1007/128_2009_5, pp. 1-33.
109. D. Wu, F. Xu, B. Sun, R. Fu, H. He and K. Matyjaszewski, *Chem. Rev.* , 2012, **112**, 3959-4015.
110. J.-S. M. Lee and A. I. Cooper, *Chem. Rev.* , 2020, **120**, 2171-2214.
111. V. A. Davankov and M. P. Tsyurupa, *React. Polym.* , 1990, **13**, 27-42.
112. M. P. Tsyurupa and V. A. Davankov, *React. Funct. Polym.* , 2002, **53**, 193-203.
113. S. Wang, C. Zhang, Y. Shu, S. Jiang, Q. Xia, L. Chen, S. Jin, I. Hussain, A. I. Cooper and B. Tan, *Science Advances*, 2017, **3**, e1602610.
114. B. Li, F. Su, H.-K. Luo, L. Liang and B. Tan, *Micropor Mesopor Mat*, 2011, **138**, 207-214.
115. D. A. Anito, T.-X. Wang, Z.-W. Liu, X. Ding and B.-H. Han, *J. Hazard. Mater.* , 2020, **400**, 123188.
116. Z. Yang, X. Huang, X. Yao and H. Ji, *J. Appl. Polym. Sci.* , 2018, **135**, 45568.
117. Y. Xie, J. Lin, J. Liang, M. Li, Y. Fu, H. Wang, S. Tu and J. Li, *Chem. Eng. J.* , 2019, **378**, 122107.
118. L. A. Shah, M. Khan, R. Javed, M. Sayed, M. S. Khan, A. Khan and M. Ullah, *J. Clean. Prod.*, 2018, **201**, 78-87.
119. S. Panja, S. Hanson and C. Wang, *ACS Appl. Mater. Interfaces* 2020, **12**, 25276-25285.
120. P. M. Budd, B. S. Ghanem, S. Makhseed, N. B. McKeown, K. J. Msayib and C. E. Tattershall, *Chem. Commun.* , 2004, DOI: 10.1039/B311764B, 230-231.
121. C. Zhang, P. Li, W. Huang and B. Cao, *Chem. Eng. Res. Des.* , 2016, **109**, 76-85.
122. J. Xu, S. Ma, Y. Li, X. Li, J. Ou and M. Ye, *J. Environ. Chem. Eng.*, 2020, **8**, 104545.
123. S. Guo and T. M. Swager, *J. Am. Chem. Soc.* , 2021, **143**, 11828-11835.

124. J.-X. Jiang, F. Su, A. Trewin, C. D. Wood, N. L. Campbell, H. Niu, C. Dickinson, A. Y. Ganin, M. J. Rosseinsky, Y. Z. Khimyak and A. I. Cooper, *Angew. Chem. Int. Ed.*, 2007, **46**, 8574-8578.
125. J.-X. Jiang, F. Su, A. Trewin, C. D. Wood, H. Niu, J. T. A. Jones, Y. Z. Khimyak and A. I. Cooper, *J. Am. Chem. Soc.* , 2008, **130**, 7710-7720.
126. S. Ravi, P. Puthiaraj, K. H. Row, D.-W. Park and W.-S. Ahn, *Ind. Eng. Chem. Res.*, 2017, **56**, 10174-10182.
127. L. Wang, Q. Xiao, D. Zhang, W. Kuang, J. Huang and Y.-N. Liu, *ACS Appl. Mater. Interfaces* 2020, **12**, 36652-36659.
128. R. Peng, G. Chen, F. Zhou, R. Man and J. Huang, *Chem. Eng. J.* , 2019, **371**, 260-266.
129. J. Liu, K.-K. Yee, K. K.-W. Lo, K. Y. Zhang, W.-P. To, C.-M. Che and Z. Xu, *J. Am. Chem. Soc.* , 2014, **136**, 2818-2824.
130. K. Zhao, L. Kong, W. Yang, Y. Huang, H. Li, S. Ma, W. Lv, J. Hu, H. Wang and H. Liu, *ACS Appl. Mater. Interfaces* 2019, **11**, 44751-44757.
131. A. P. Côté, A. I. Benin, N. W. Ockwig, M. O'Keeffe, A. J. Matzger and O. M. Yaghi, *Science*, 2005, **310**, 1166-1170.
132. H. M. El-Kaderi, J. R. Hunt, J. L. Mendoza-Cortés, A. P. Côté, R. E. Taylor, M. O'Keeffe and O. M. Yaghi, *Science*, 2007, **316**, 268-272.
133. Z. Ni and R. I. Masel, *J. Am. Chem. Soc.* , 2006, **128**, 12394-12395.
134. P. Kuhn, M. Antonietti and A. Thomas, *Angew. Chem. Int. Ed.*, 2008, **47**, 3450-3453.
135. Z. A. Ghazi, A. M. Khattak, R. Iqbal, R. Ahmad, A. A. Khan, M. Usman, F. Nawaz, W. Ali, Z. Felegari, S. U. Jan, A. Iqbal and A. Ahmad, *New J. Chem.* , 2018, **42**, 10234-10242.
136. S. Mondal, S. Chatterjee, S. Mondal and A. Bhaumik, *ACS Sustain. Chem. Eng.*, 2019, **7**, 7353-7361.
137. M. Afshari, M. Dinari, K. Zargoosh and H. Moradi, *Ind. Eng. Chem. Res.*, 2020, **59**, 9116-9126.
138. F. J. Uribe-Romo, J. R. Hunt, H. Furukawa, C. Klöck, M. O'Keeffe and O. M. Yaghi, *J. Am. Chem. Soc.* , 2009, **131**, 4570-4571.
139. F. J. Uribe-Romo, C. J. Doonan, H. Furukawa, K. Oisaki and O. M. Yaghi, *J. Am. Chem. Soc.* , 2011, **133**, 11478-11481.
140. S.-Y. Ding, M. Dong, Y.-W. Wang, Y.-T. Chen, H.-Z. Wang, C.-Y. Su and W. Wang, *J. Am. Chem. Soc.* , 2016, **138**, 3031-3037.
141. S. Jansone-Popova, A. Moinel, J. A. Schott, S. M. Mahurin, I. Popovs, G. M. Veith and B. A. Moyer, *Environ. Sci. Technol.* , 2019, **53**, 878-883.
142. Q. Sun, B. Aguila, J. Perman, L. D. Earl, C. W. Abney, Y. Cheng, H. Wei, N. Nguyen, L. Wojtas and S. Ma, *J. Am. Chem. Soc.* , 2017, **139**, 2786-2793.
143. N. Huang, L. Zhai, H. Xu and D. Jiang, *J. Am. Chem. Soc.* , 2017, **139**, 2428-2434.
144. L. Merí-Bofí, S. Royuela, F. Zamora, M. L. Ruiz-González, J. L. Segura, R. Muñoz-Olivas and M. J. Mancheño, *J. Mater. Chem. A*, 2017, **5**, 17973-17981.
145. X.-F. Lu, W.-H. Ji, L. Yuan, S. Yu and D.-S. Guo, *Ind. Eng. Chem. Res.*, 2019, **58**, 17660-17667.
146. K. Naseem, R. Begum, W. Wu, M. Usman, A. Irfan, A. G. Al-Sehemi and Z. H. Farooqi, *J. Mol. Liq.* , 2019, **277**, 522-531.
147. Y. L. Tang, Y. Q. Li, Y. J. Zhang, C. H. Mu, J. F. Zhou, W. H. Zhang and B. Shi, *Ind. Eng. Chem. Res.*, 2020, **59**, 3383-3393.
148. H. Shen, S. Pan, Y. Zhang, X. Huang and H. Gong, *Chem. Eng. J.* , 2012, **183**, 180-191.
149. Z. Xiao, H. Zhang, Y. Xu, M. Yuan, X. Jing, J. Huang, Q. Li and D. Sun, *Sep. Purif. Technol.* , 2017, **174**, 466-473.
150. M. Liu, Y. Wang, L. Chen, Y. Zhang and Z. Lin, *ACS Appl. Mater. Interfaces* 2015, **7**, 7961-7969.
151. V. K. Gupta, R. Chandra, I. Tyagi and M. Verma, *J. Colloid Interf. Sci.*, 2016, **478**, 54-62.
152. A. Razzaz, S. Ghorban, L. Hosayni, M. Irani and M. Aliabadi, *J. Taiwan Inst. Chem. Eng.* , 2016, **58**, 333-343.
153. L. Fang, L. Li, Z. Qu, H. M. Xu, J. F. Xu and N. Q. Yan, *J. Hazard. Mater.* , 2018, **342**, 617-624.
154. T. Wen, Y. L. Zhao, T. T. Zhang, B. W. Xiong, H. M. Hu, Q. W. Zhang and S. X. Song, *Chemosphere*, 2020, **246**.

155. Q. Peng, J. Guo, Q. Zhang, J. Xiang, B. Liu, A. Zhou, R. Liu and Y. Tian, *J. Am. Chem. Soc.* , 2014, **136**, 4113-4116.
156. X. Xie, C. Chen, N. Zhang, Z.-R. Tang, J. Jiang and Y.-J. Xu, *Nat. Sustain.*, 2019, **2**, 856-862.
157. A. Jawad, L. Peng, Z. W. Liao, Z. H. Zhou, A. Shahzad, J. Ifthikar, M. M. Zhao, Z. L. Chen and Z. Q. Chen, *J. Clean. Prod.*, 2019, **211**, 1112-1126.
158. Y. Peng, H. Huang, Y. Zhang, C. Kang, S. Chen, L. Song, D. Liu and C. Zhong, *Nat. Comm.*, 2018, **9**, 187.
159. Y. Huang, X. F. Zeng, L. L. Guo, J. H. Lan, L. L. Zhang and D. P. Cao, *Sep. Purif. Technol.* , 2018, **194**, 462-469.
160. B. Wang, H. Wu, L. Yu, R. Xu, T.-T. Lim and X. W. Lou, *Adv. Mater.* , 2012, **24**, 1111-1116.
161. J. T. Bi, X. Huang, J. K. Wang, Q. Q. Tao, H. J. Lu, L. Luo, G. P. Li and H. X. Hao, *Chem. Eng. J.* , 2020, **380**.
162. L. Fan, C. Luo, Z. Lv, F. Lu and H. Qiu, *J. Hazard. Mater.* , 2011, **194**, 193-201.
163. T. A. Kurniawan, G. Y. S. Chan, W. H. Lo and S. Babel, *Chem. Eng. J.* , 2006, **118**, 83-98.
164. Q. P. Meng, H. Chen, J. Z. Lin, Z. Lin and J. L. Sun, *J. Environ. Sci.*, 2017, **56**, 254-262.
165. X. Lu, F. Wang, X.-y. Li, K. Shih and E. Y. Zeng, *Ind. Eng. Chem. Res.*, 2016, **55**, 8767-8773.
166. S. Gu, X. Kang, L. Wang, E. Lichtfouse and C. Wang, *Environ. Chem. Lett.* , 2019, **17**, 629-654.
167. B. O. Otunola and O. O. Ololade, *Environ. Technol. Innov.*, 2020, **18**, 100692.
168. N. Tahari, H. Nefzi, A. Labidi, S. Ayadi, M. Abderrabba and J. Labidi, in *Water Pollution and Remediation: Heavy Metals*, eds. Inamuddin, M. I. Ahamed and E. Lichtfouse, Springer International Publishing, Cham, 2021, DOI: 10.1007/978-3-030-52421-0_16, pp. 539-569.
169. C.-Y. Cao, C.-H. Liang, Y. Yin and L.-Y. Du, *J. Hazard. Mater.* , 2017, **329**, 222-229.
170. V. E. dos Anjos, J. R. Rohwedder, S. Cadore, G. Abate and M. T. Grassi, *Appl. Clay Sci.* , 2014, **99**, 289-296.
171. J. Li, X. Xiao, X. Xu, J. Lin, Y. Huang, Y. Xue, P. Jin, J. Zou and C. Tang, *Sci. Rep.*, 2013, **3**, 3208.
172. J. Li, J. Lin, X. Xu, X. Zhang, Y. Xue, J. Mi, Z. Mo, Y. Fan, L. Hu, X. Yang, J. Zhang, F. Meng, S. Yuan and C. Tang, *Nanotechnology*, 2013, **24**, 155603.
173. J. Zhang, H.-l. Zhang, P. Zhou, P.-h. Qing, H.-b. Xu and Y. Zhang, *Mater. Lett.* , 2018, **213**, 211-213.
174. F. Liu, J. Yu, X. Ji and M. Qian, *ACS Appl. Mater. Interfaces* 2015, **7**, 1824-1832.
175. F. Liu, S. Li, D. F. Yu, Y. P. Su, N. N. Shao and Z. T. Zhang, *ACS Sustain. Chem. Eng.*, 2018, **6**, 16011-16020.
176. R. Hu, X. Wang, S. Dai, D. Shao, T. Hayat and A. Alsaedi, *Chem. Eng. J.* , 2015, **260**, 469-477.
177. X. Cai, J. He, L. Chen, K. Chen, Y. Li, K. Zhang, Z. Jin, J. Liu, C. Wang, X. Wang, L. Kong and J. Liu, *Chemosphere*, 2017, **171**, 192-201.
178. W. Xiangxue, L. Xing, W. Jiaqi and Z. Hongtao, *J. Inorg. Mater.*, 2021, **35**, 260-270.
179. C. Shen, C. Chen, T. Wen, Z. Zhao, X. Wang and A. Xu, *J. Colloid Interf. Sci.*, 2015, **456**, 7-14.
180. G. Xiao, Y. Q. Wang, S. N. Xu, P. F. Li, C. Yang, Y. Jin, Q. F. Sun and H. J. Su, *Chin. J. Chem. Eng.* , 2019, **27**, 305-313.
181. A. Papandreou, C. J. Stournaras and D. Panias, *J. Hazard. Mater.* , 2007, **148**, 538-547.
182. K. S. Hui, C. Y. H. Chao and S. C. Kot, *J. Hazard. Mater.* , 2005, **127**, 89-101.
183. R. Apiratikul and P. Pavasant, *Chem. Eng. J.* , 2008, **144**, 245-258.
184. S. V. Dimitrova, *Water Res.* , 2002, **36**, 4001-4008.
185. A. K. Bhattacharya, S. N. Mandal and S. K. Das, *Chem. Eng. J.* , 2006, **123**, 43-51.
186. H. S. Altundoğan, S. Altundoğan, F. Tümen and M. Bildik, *Waste Manage. (Oxford)* 2002, **22**, 357-363.
187. B. Yu, Y. Zhang, A. Shukla, S. S. Shukla and K. L. Dorris, *J. Hazard. Mater.* , 2000, **80**, 33-42.
188. F.-S. Zhang, J. O. Nriagu and H. Itoh, *Water Res.* , 2005, **39**, 389-395.
189. M. Xu, P. Hadi, G. Chen and G. McKay, *J. Hazard. Mater.* , 2014, **273**, 118-123.
190. T. A. H. Nguyen, H. H. Ngo, W. S. Guo, J. Zhang, S. Liang, Q. Y. Yue, Q. Li and T. V. Nguyen, *Bioresour. Technol.* , 2013, **148**, 574-585.
191. Y. Ding, D. Jing, H. Gong, L. Zhou and X. Yang, *Bioresour. Technol.* , 2012, **114**, 20-25.
192. P. X. Yu, X. Wang, K. M. Zhang, M. Y. Wu, Q. Y. Wu, J. Y. Liu, J. J. Yang and J. N. Zhang, *Cellulose*, 2020, **27**, 5223-5239.

193. N. Feng, X. Guo, S. Liang, Y. Zhu and J. Liu, *J. Hazard. Mater.* , 2011, **185**, 49-54.
194. H. Nazir, M. Salman, M. Athar, U. Farooq, A. Wahab and M. Akram, *Water Air Soil Pollut.*, 2019, **230**.
195. H. Lalhruaitluanga, M. N. V. Prasad and K. Radha, *Desalination*, 2011, **271**, 301-308.
196. M. Kilic, C. Kirbiyik, O. Cepeliogullar and A. E. Putun, *Appl. Surf. Sci.* , 2013, **283**, 856-862.
197. M. Ahmaruzzaman, *Adv. Colloid Interface Sci.* , 2011, **166**, 36-59.
198. Y. Tsuneo, S. Toshio, K. Kazuyuki and K. Chuzo, *B Chem Soc Jpn*, 1990, **63**, 988-992.
199. C. T. Kresge, M. E. Leonowicz, W. J. Roth, J. C. Vartuli and J. S. Beck, *Nature*, 1992, **359**, 710-712.
200. J. S. Beck, J. C. Vartuli, W. J. Roth, M. E. Leonowicz, C. T. Kresge, K. D. Schmitt, C. T. W. Chu, D. H. Olson, E. W. Sheppard, S. B. McCullen, J. B. Higgins and J. L. Schlenker, *J. Am. Chem. Soc.* , 1992, **114**, 10834-10843.
201. D. Zhao, J. Feng, Q. Huo, N. Melosh, G. H. Fredrickson, B. F. Chmelka and G. D. Stucky, *Science*, 1998, **279**, 548-552.
202. R. Ryoo, S. H. Joo and S. Jun, *J. Phys. Chem. B*, 1999, **103**, 7743-7746.
203. J. Lee, S. Yoon, S. M. Oh, C.-H. Shin and T. Hyeon, *Adv. Mater.* , 2000, **12**, 359-362.
204. Y. Meng, D. Gu, F. Zhang, Y. Shi, L. Cheng, D. Feng, Z. Wu, Z. Chen, Y. Wan, A. Stein and D. Zhao, *Chem. Mater.* , 2006, **18**, 4447-4464.
205. E. Da'na, *Micropor Mesopor Mat*, 2017, **247**, 145-157.
206. C. Liang, Z. Li and S. Dai, *Angew. Chem. Int. Ed.* , 2008, **47**, 3696-3717.
207. H. Hamad, Z. Ezzeddine, F. Lakis, H. Rammal, M. Srour and A. Hijazi, *Mater. Chem. Phys.*, 2016, **178**, 57-64.
208. Y. Snoussi, M. Abderrabba and A. Sayari, *J. Taiwan Inst. Chem. Eng.* , 2016, **66**, 372-378.
209. S. Das, S. Chatterjee, S. Mondal, A. Modak, B. K. Chandra, S. Das, G. D. Nessim, A. Majee and A. Bhaumik, *Chem. Commun.* , 2020, **56**, 3963-3966.
210. C. M. Futalan, C.-C. Kan, M. L. Dalida, K.-J. Hsien, C. Pascua and M.-W. Wan, *Carbohydr. Polym.* , 2011, **83**, 528-536.

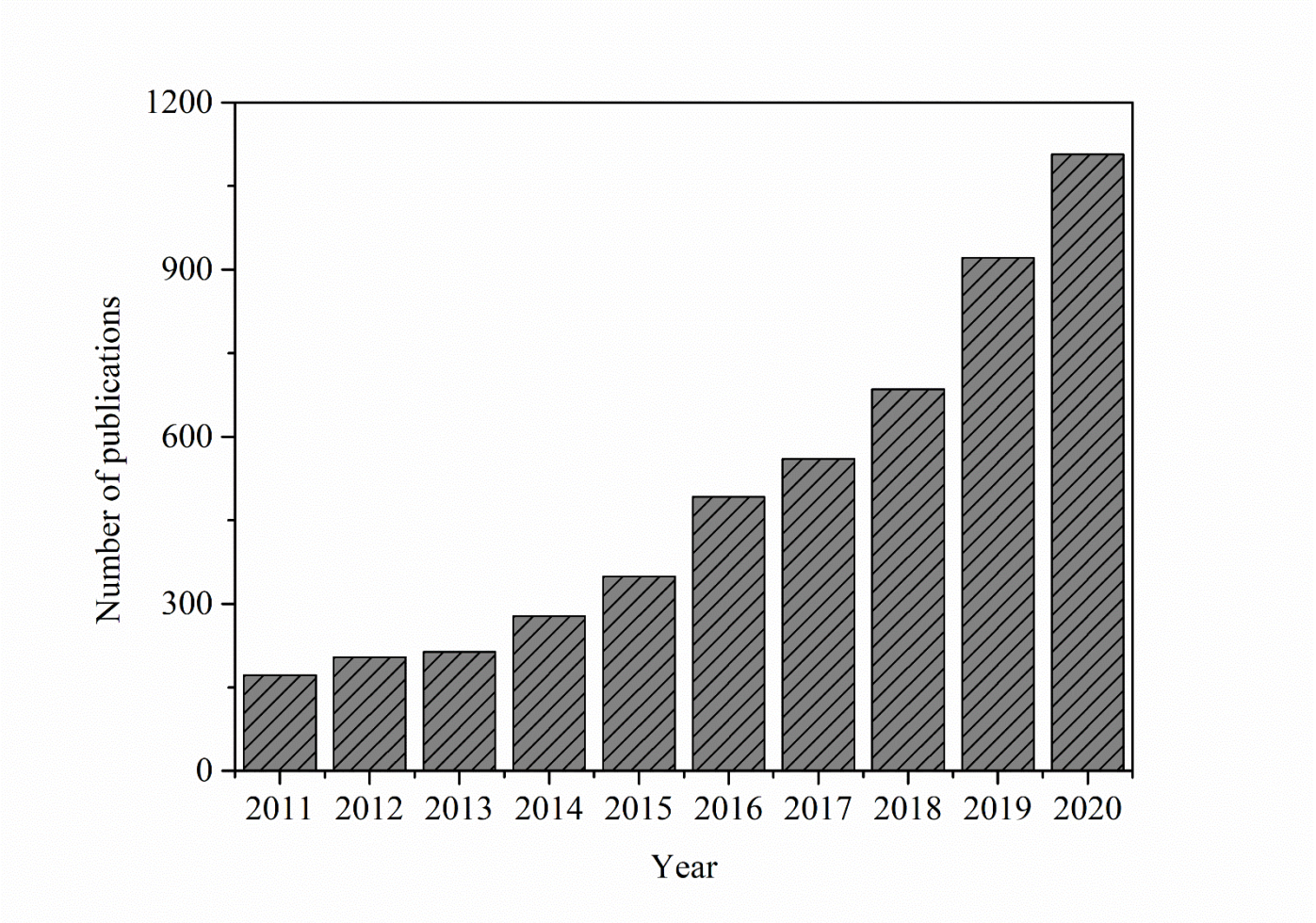

Figure 1. The number of annual publications in the field of "heavy metals & wastewater & adsorption" in the past decade (2011-2020) from Web of Science.

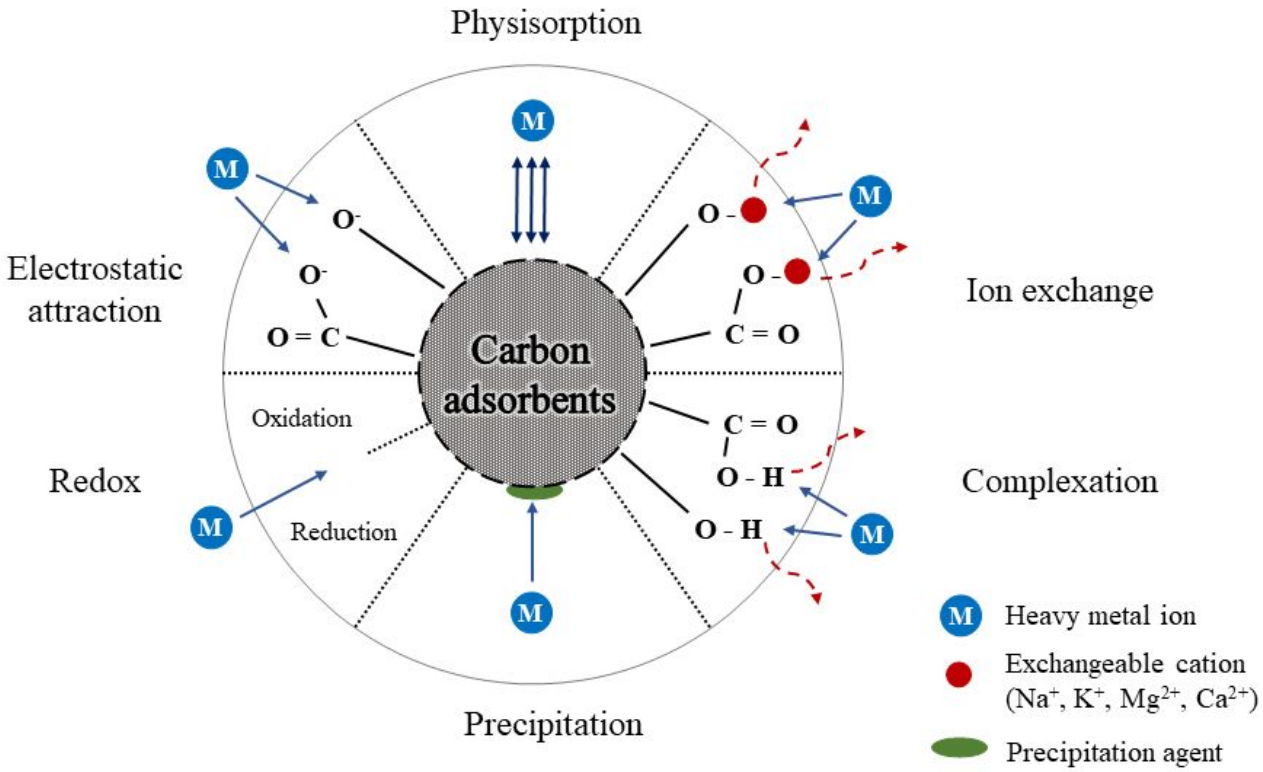

Figure 2. Schematic diagram for metal adsorption over carbon materials.

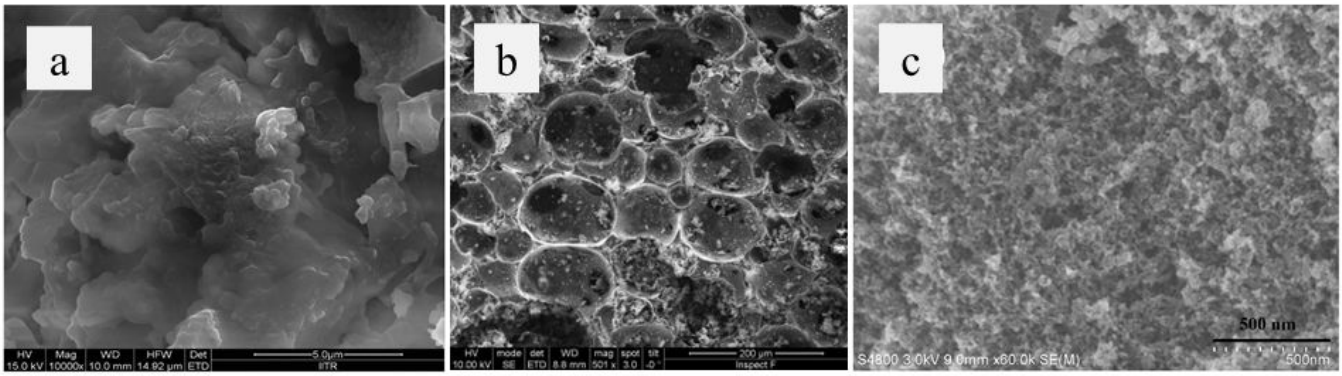

Figure 3. SEM images of (a) KOH-activated carbon,[16] reproduced with permission. Copyright 2017, Elsevier; (b) phenolic resin-derived mesoporous carbon foam,[40] reproduced with permission. Copyright 2015, Elsevier; and (c) hierarchically porous N-doped carbon,[43] reproduced with permission. Copyright 2018, Elsevier.

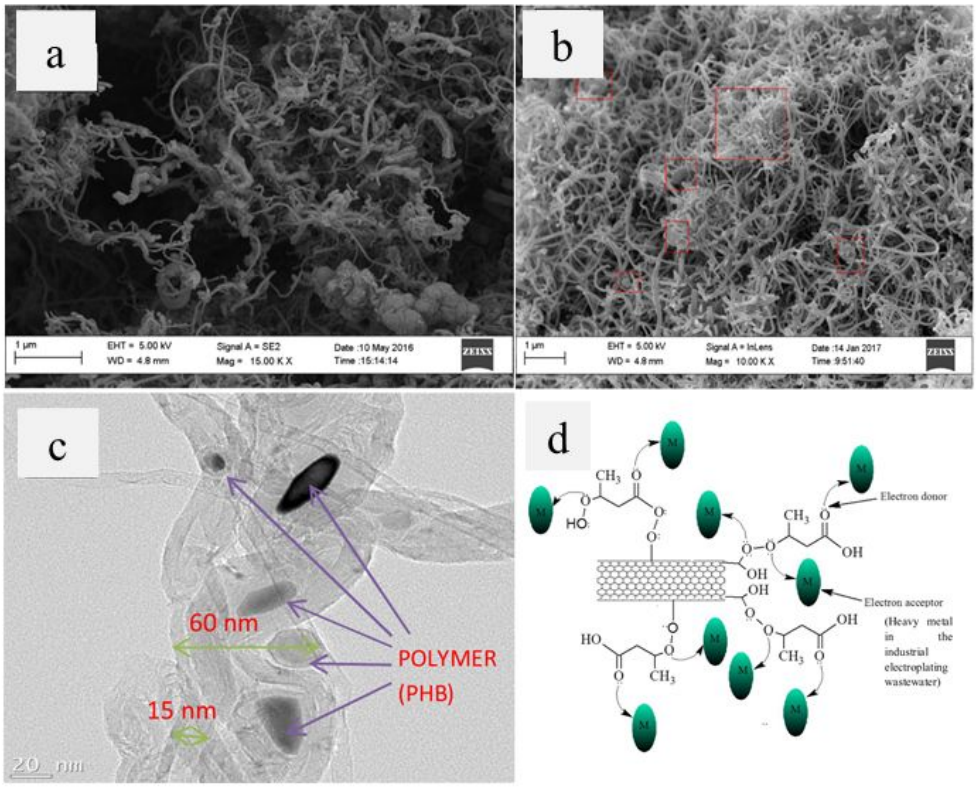

Figure 4. SEM images of PHB/CNTs (a) before and (b) after utilizing for electroplating wastewater treatment; (c) TEM image of PHB/CNTs; (d) Chemical mechanism pathway for the adsorption of heavy metals from the electroplating wastewater using PHB/CNTs.[50] Reproduced with permission. Copyright 2019, The authors (Mercy Temitope Bankole et al.).

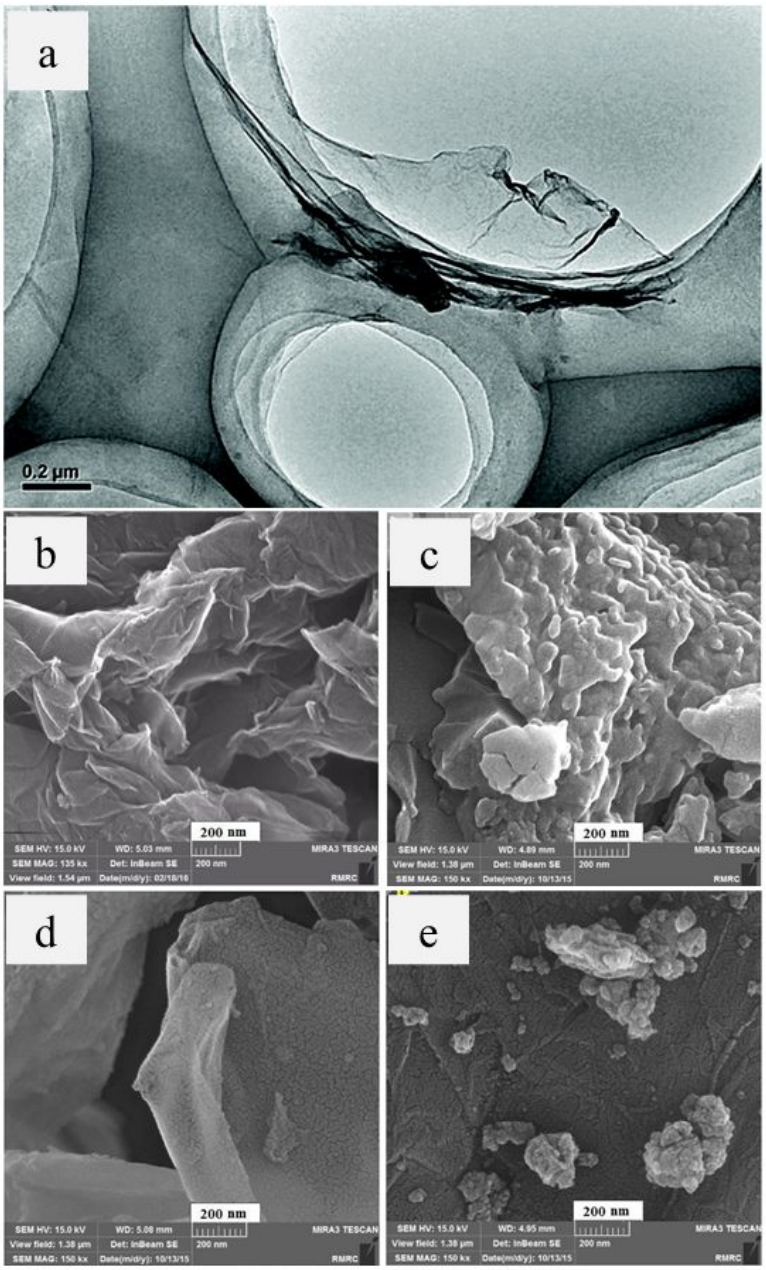

Figure 5. (a) TEM image of FLGO.[59] Reproduced with permission. Copyright 2011, American Chemical Society. SEM images of (b) GO, (c) sulfur-GO, (d) sulfur-GO/SiO_2, and (e) sulfur-GO/TiO_2.[63] Reproduced with permission. Copyright 2018, Elsevier.

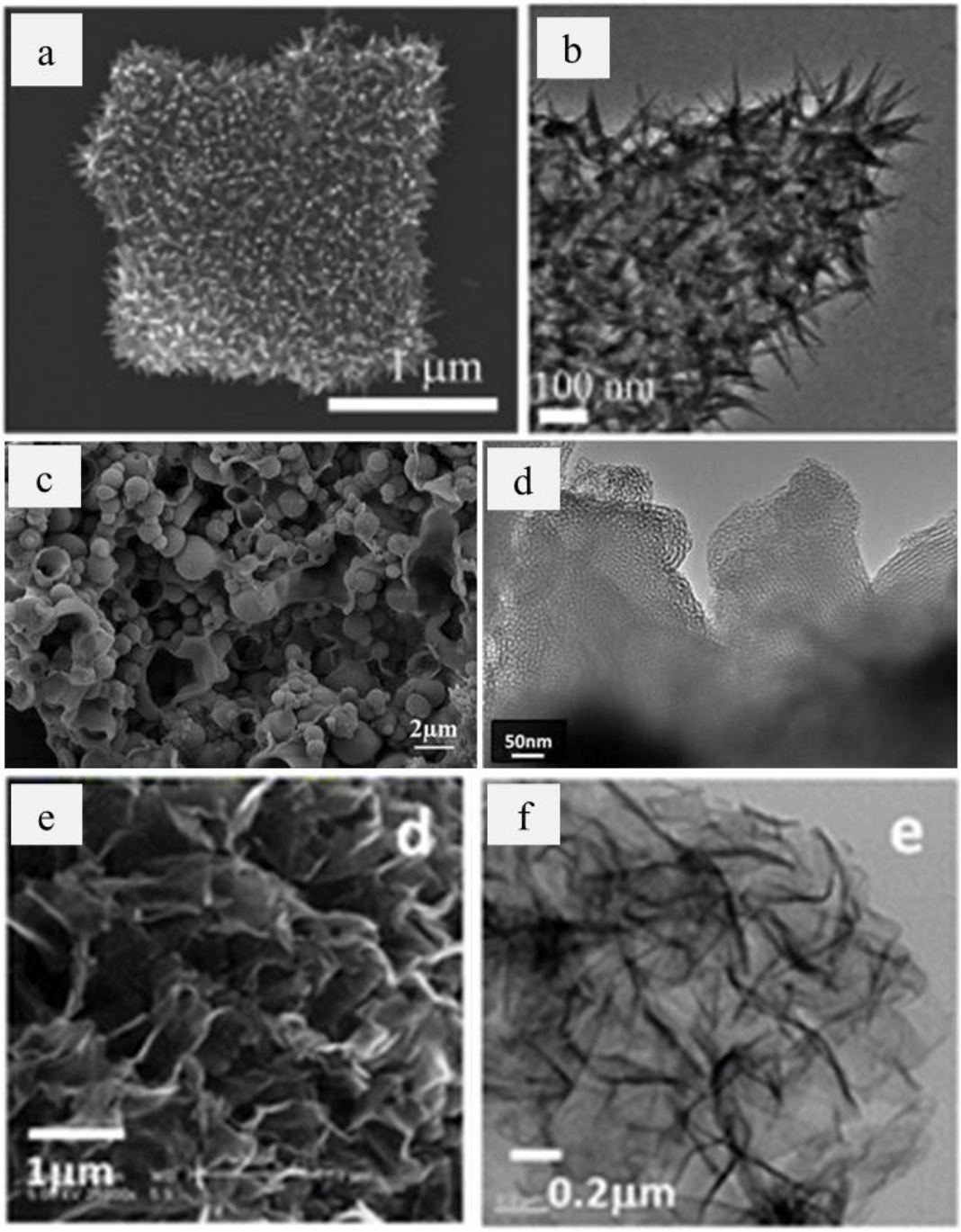

Figure 6. (a) SEM and (b) TEM images of IO/rGO.[64] Reproduced with permission. Copyright 2010, John Wiley and Sons. (c) SEM and (d) TEM images of SiO_2/graphene.[65] Reproduced with permission. Copyright 2014, Springer Nature. (e) SEM and (f) TEM images of PPy/rGO.[22] Reproduced with permission. Copyright 2011, Royal Society of Chemistry

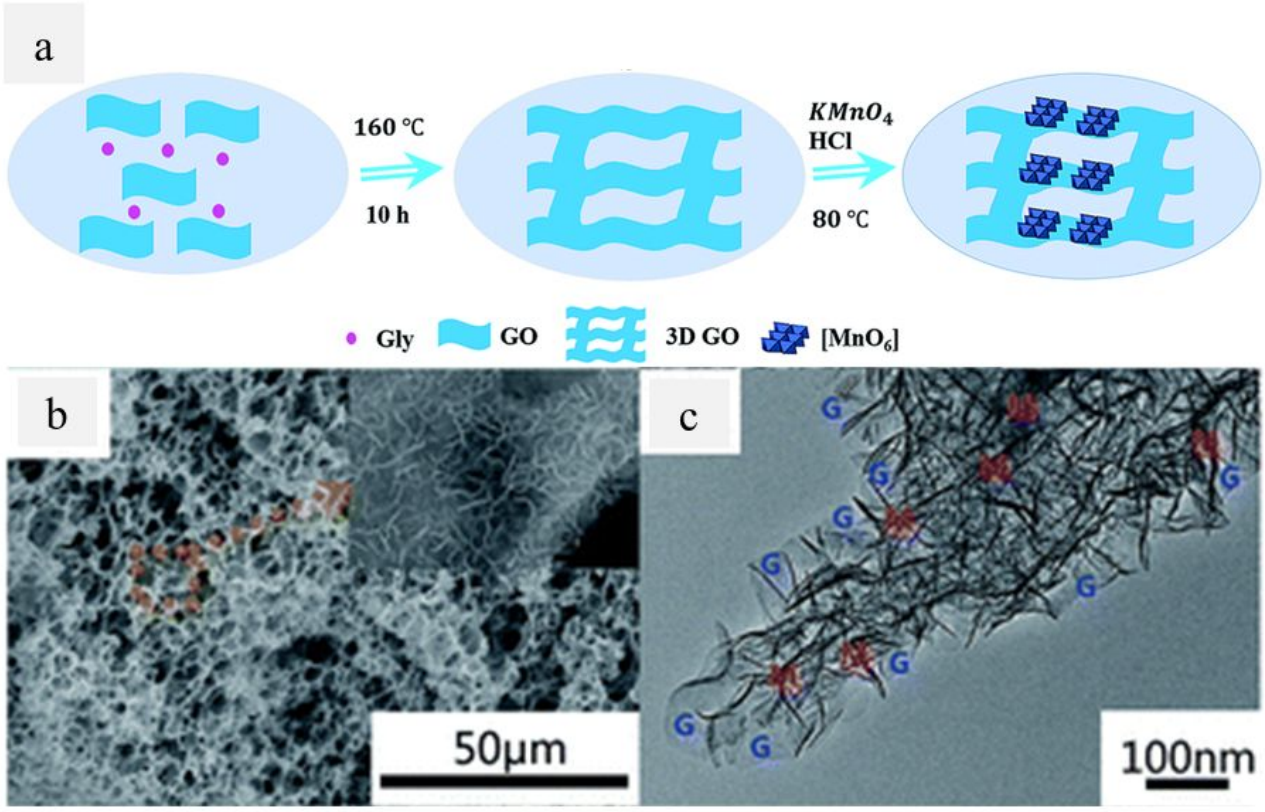

Figure 7. (a) Schematic illustration of the preparation process of 3DG/δ-MnO_2 aerogels; (b) SEM and (c) TEM images of 3DG/δ-MnO_2 aerogels.[73] Reproduced with permission. Copyright 2016, Royal Society of Chemistry.

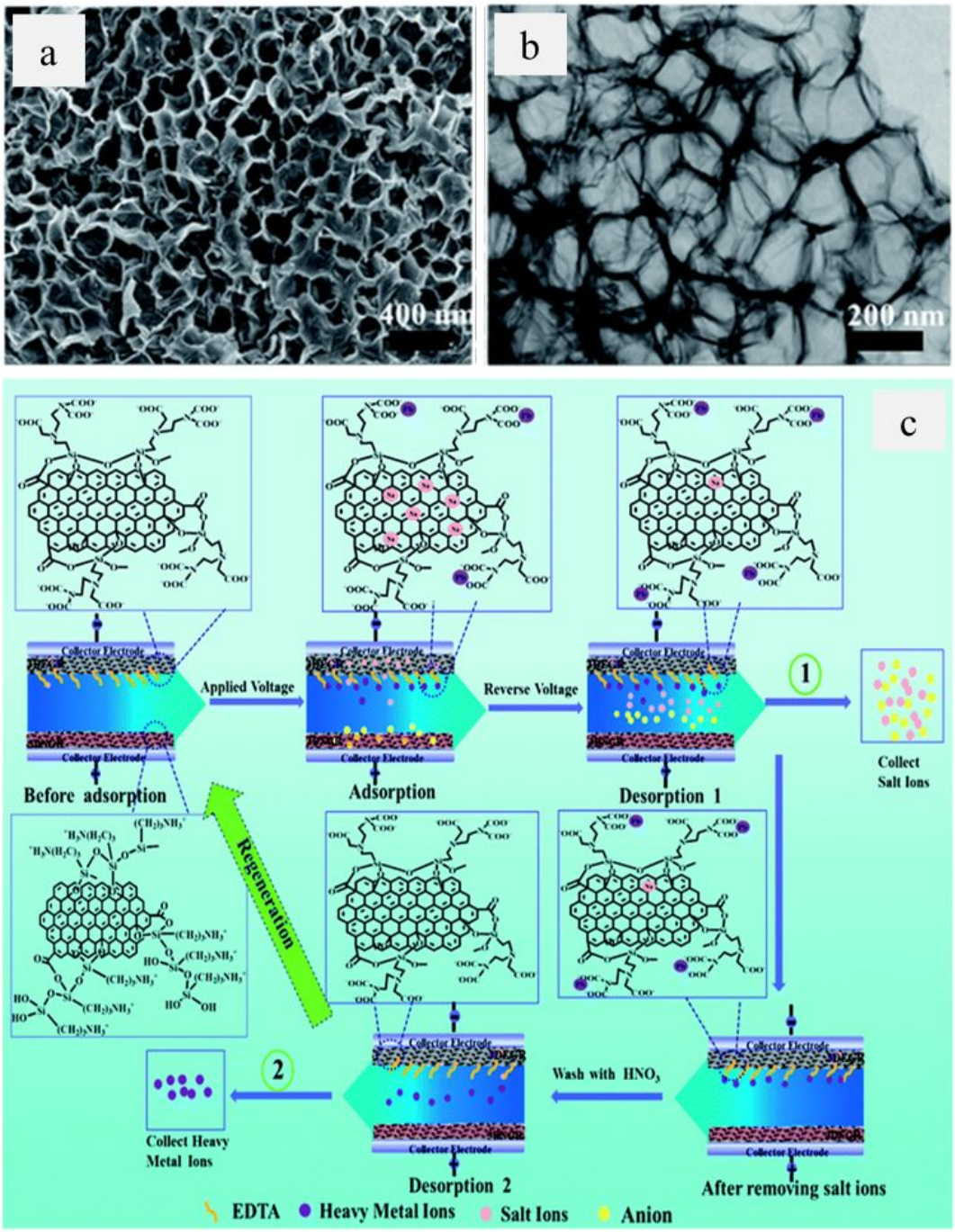

Figure 8. (a) SEM and (b) TEM images of 3DEGR; (c) Schematic illustration of the separation and recovery of heavy metal ions and salt ions from wastewater via CDI. The insets are the 3DEGR and 3DNGR structures.[82] Reproduced with permission. Copyright 2017, Royal Society of Chemistry.

Figure 9. Illustrated views of (a) monomers VIm-6 and VBIm-6; (b) supercritical CO_2 drying (SCD) of the polymers to obtain the hypercrosslinked PILs; and (c) Cr(VI) removal and regeneration process in water over the as-prepared PILs; (d) SEM image of hypercrosslinked PILs (the inset shows the TEM image).[117] Reproduced with permission. Copyright 2019, Elsevier.

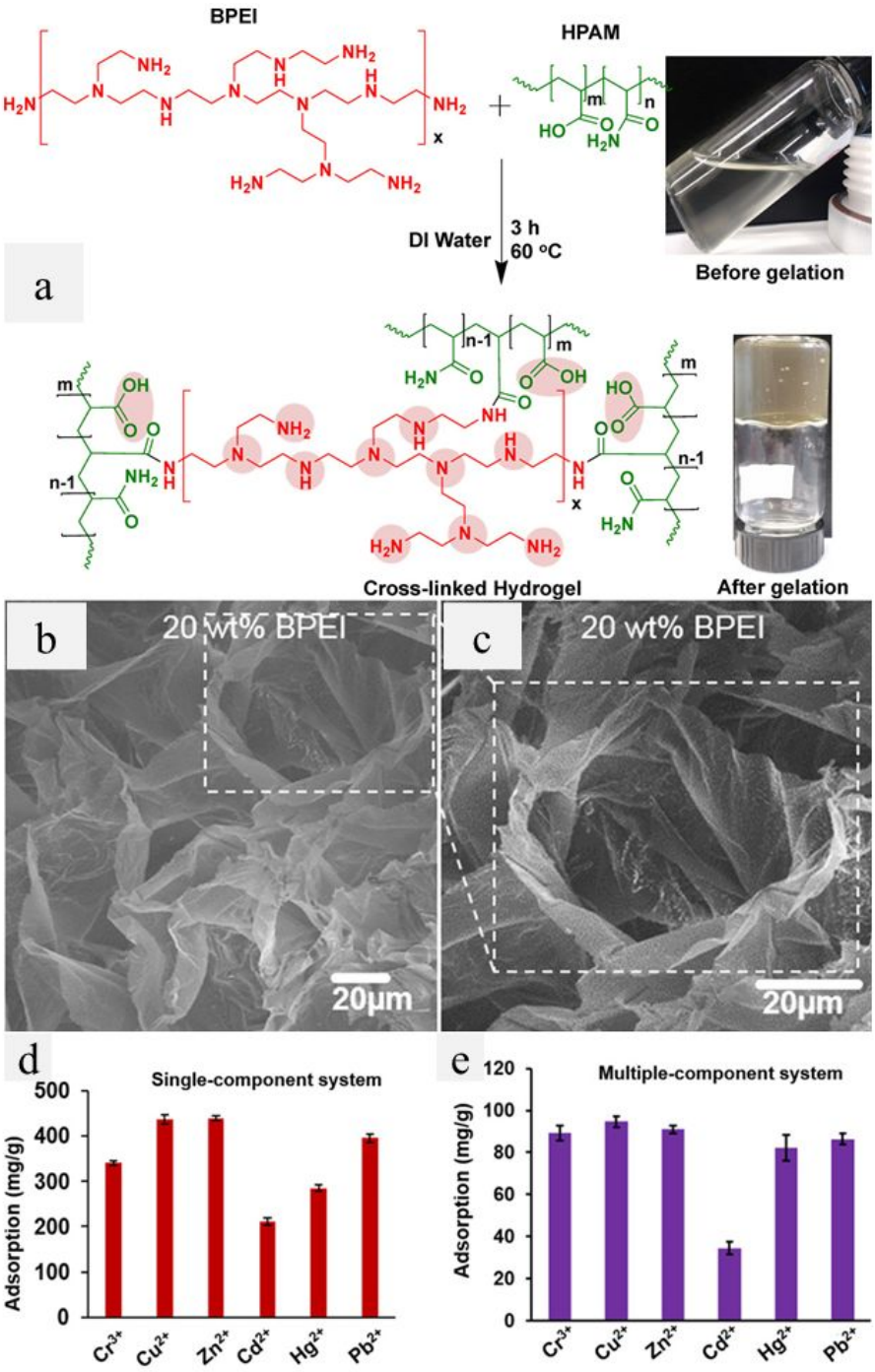

Figure 10. (a) Scheme for synthesis of EDTA-inspired polydentate hydrogels through the Transamidation reaction between partially HPAM and BPEI; the mixture of HPAM and BPEI before and after gelation are shown in the right panel. (b) SEM and (c) magnified SEM images of the hydrogel with 20 wt % cross-linker. Equilibrium adsorption capacities of metal ions tested in (d) a single-component system and (e) multiple-component systems over a period of 24 h at room temperature.[119] Reproduced with permission. Copyright 2020, American Chemical Society.

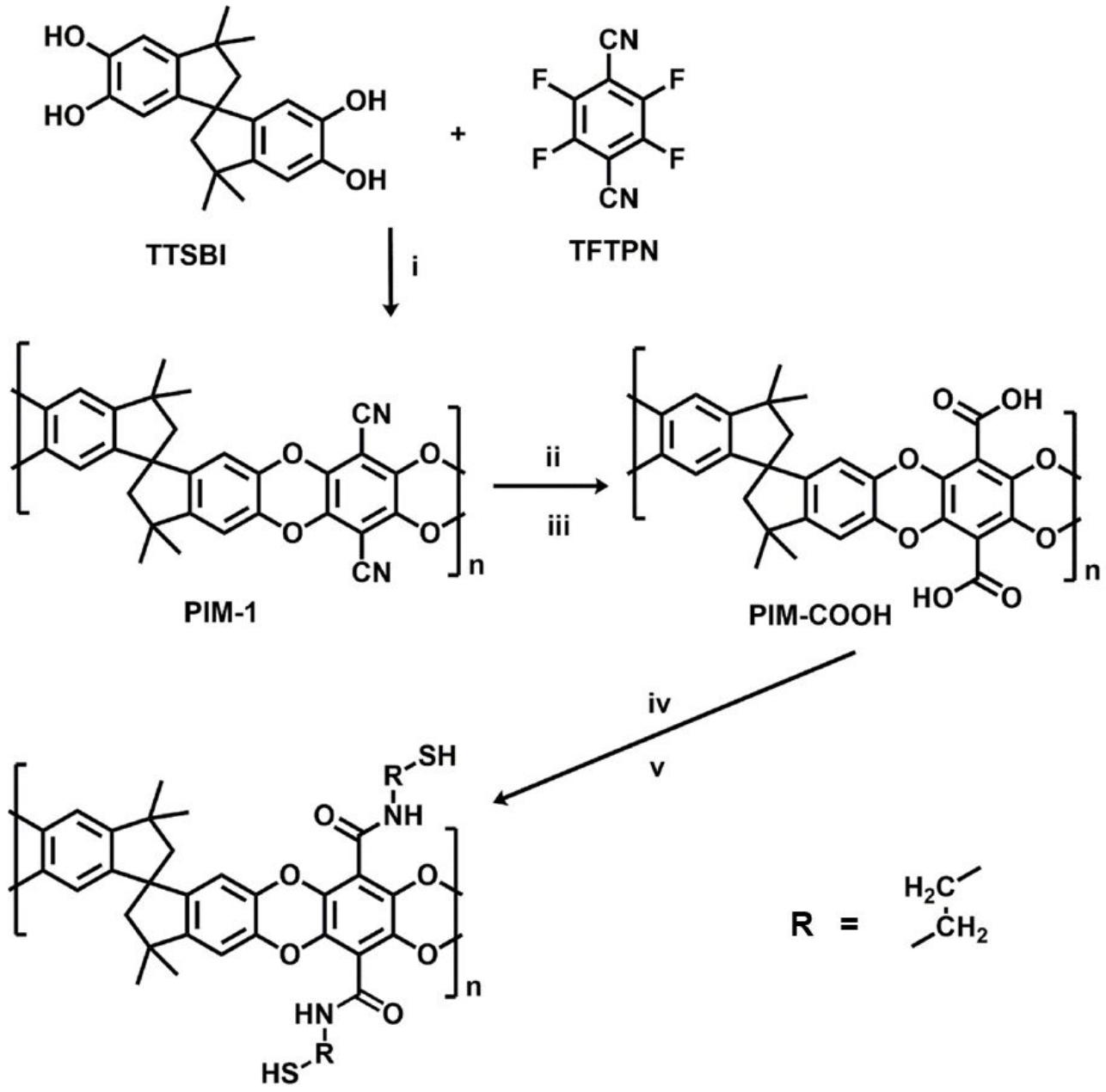

Figure 11. Scheme for thiol-functionalization of PIM-1. (i) K_2CO_3, DMF, 65°C, 48 h; (ii) 25 % KOH, H_2O and ethanol (1:1, v:v), reflux, 24 h; (iii) sulphuric acid, acetic acid, and H_2O (2:2:1, v:v:v), 120°C, 24 h; (iv) disulfide bond-containing diamines, $SOCl_2$, CH_2Cl_2, 60°C, 6 h; (v) dithiothreitol, DMF, 60°C, 12 h.[122] Reproduced with permission. Copyright 2020, Elsevier.

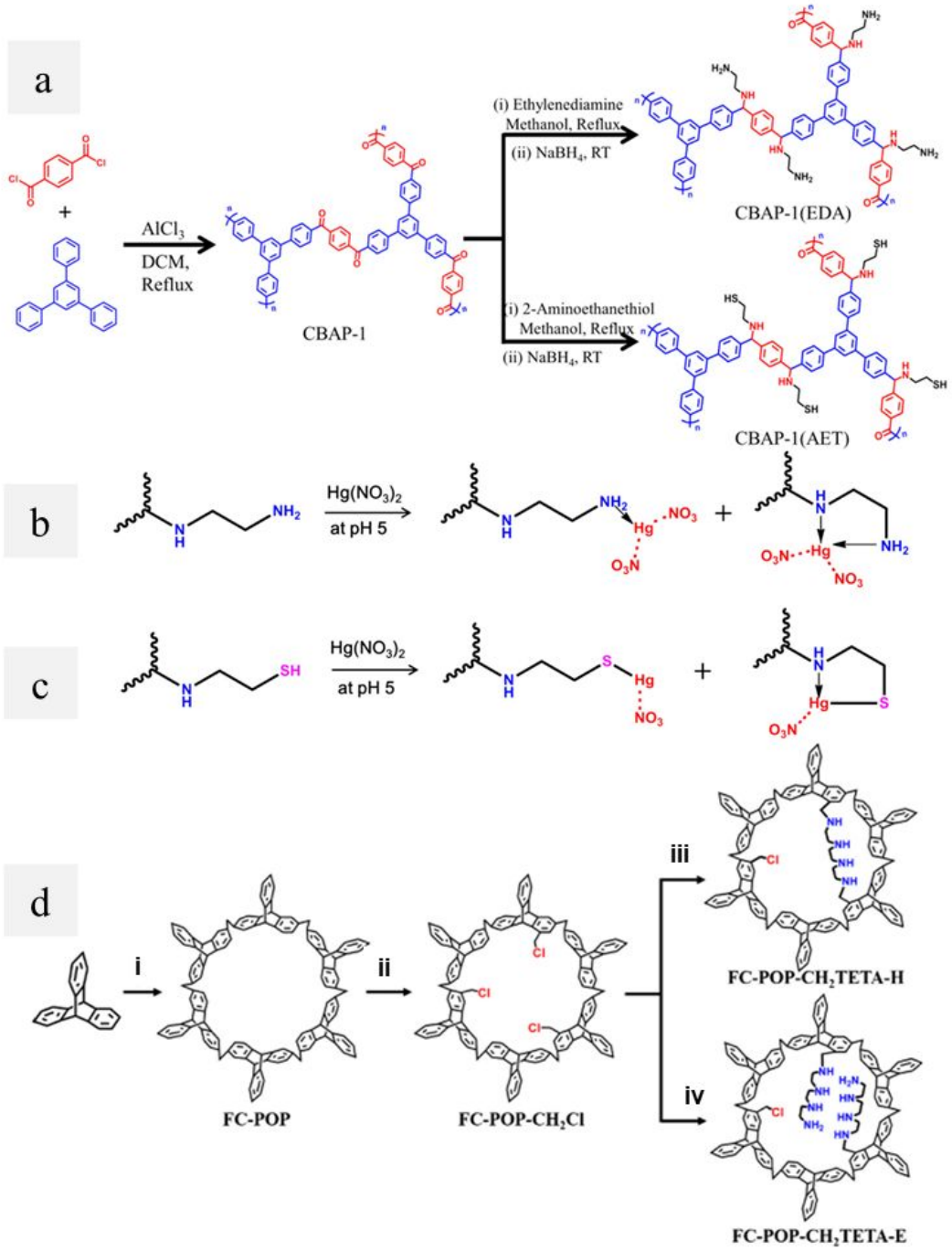

Figure 12. Schemes for (a) synthesis of CBAP-1(EDA) and CBAP-1(AET); host-guest interaction of Hg^{2+} and functionalized polymers (b) CBAP-1(EDA) and (c) CBAP-1(AET).[126] Reproduced with permission. Copyright 2017, American Chemical Society. (d) Synthesis procedures of FC-POP-CH_2TETAs. Reaction conditions in each step are: (i) formaldehyde dimethyl acetal, $FeCl_3$, dichloroethane, 45°C, 5 h; 80°C, 19 h; (ii) paraformaldehyde, H_3PO_4, HAc, HCl, 90°C, 72 h; (iii) THF, TETA, 0°C, 3 h; 15°C, 24 h; 48°C, 24 h; (iv) TETA, 90°C, 72 h.[130] Reproduced with permission. Copyright 2019, American Chemical Society.

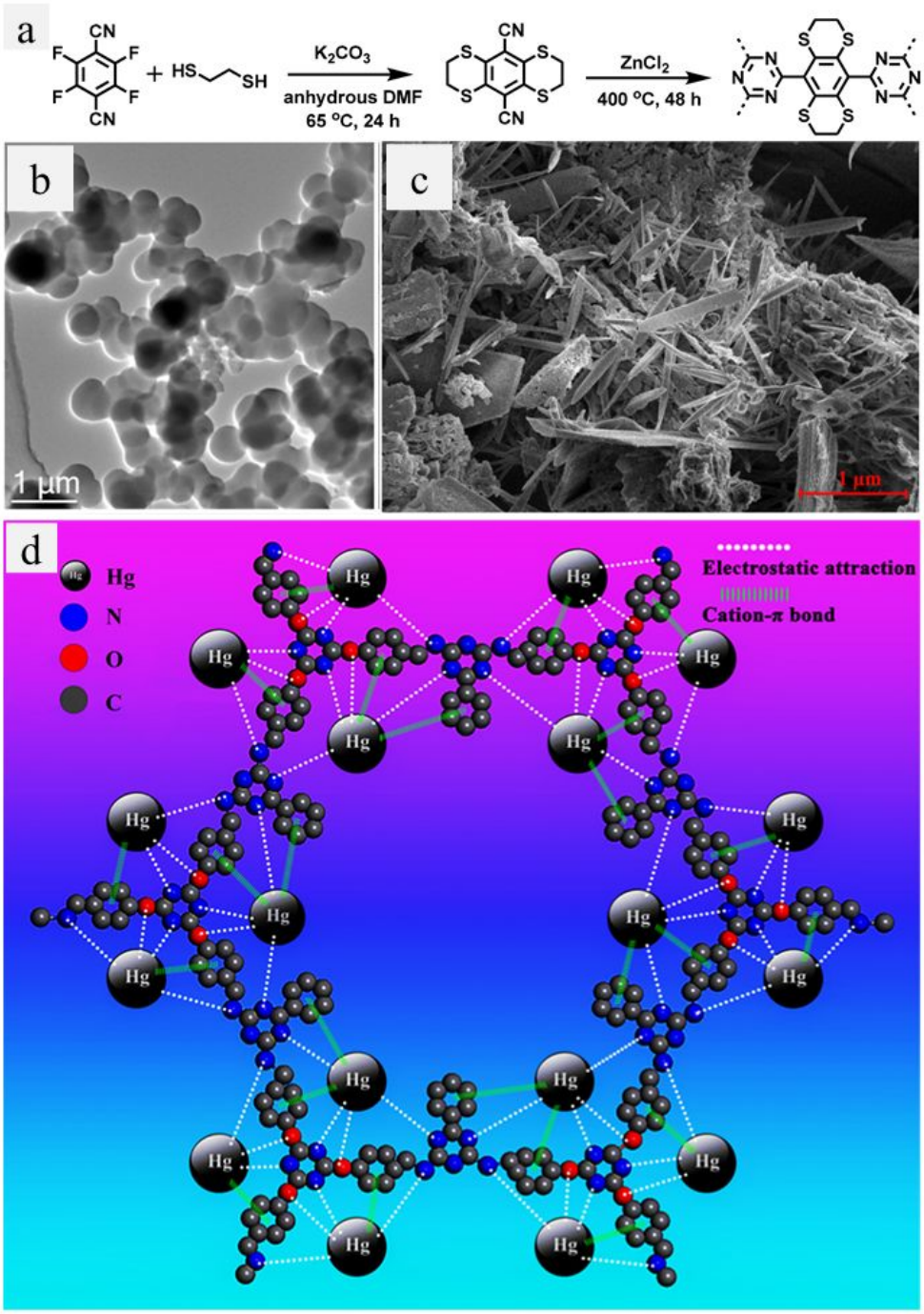

Figure 13. (a) Synthesis scheme and (b) HRTEM image of thioether-based CTF nanospheres.[136] Reproduced with permission. Copyright 2019, American Chemical Society. (c) FESEM image of CTF nanoneedles and (d) the possible illustration of the chelating interaction between Hg^{2+} and CTF.[137] Reproduced with permission. Copyright 2020, American Chemical Society.

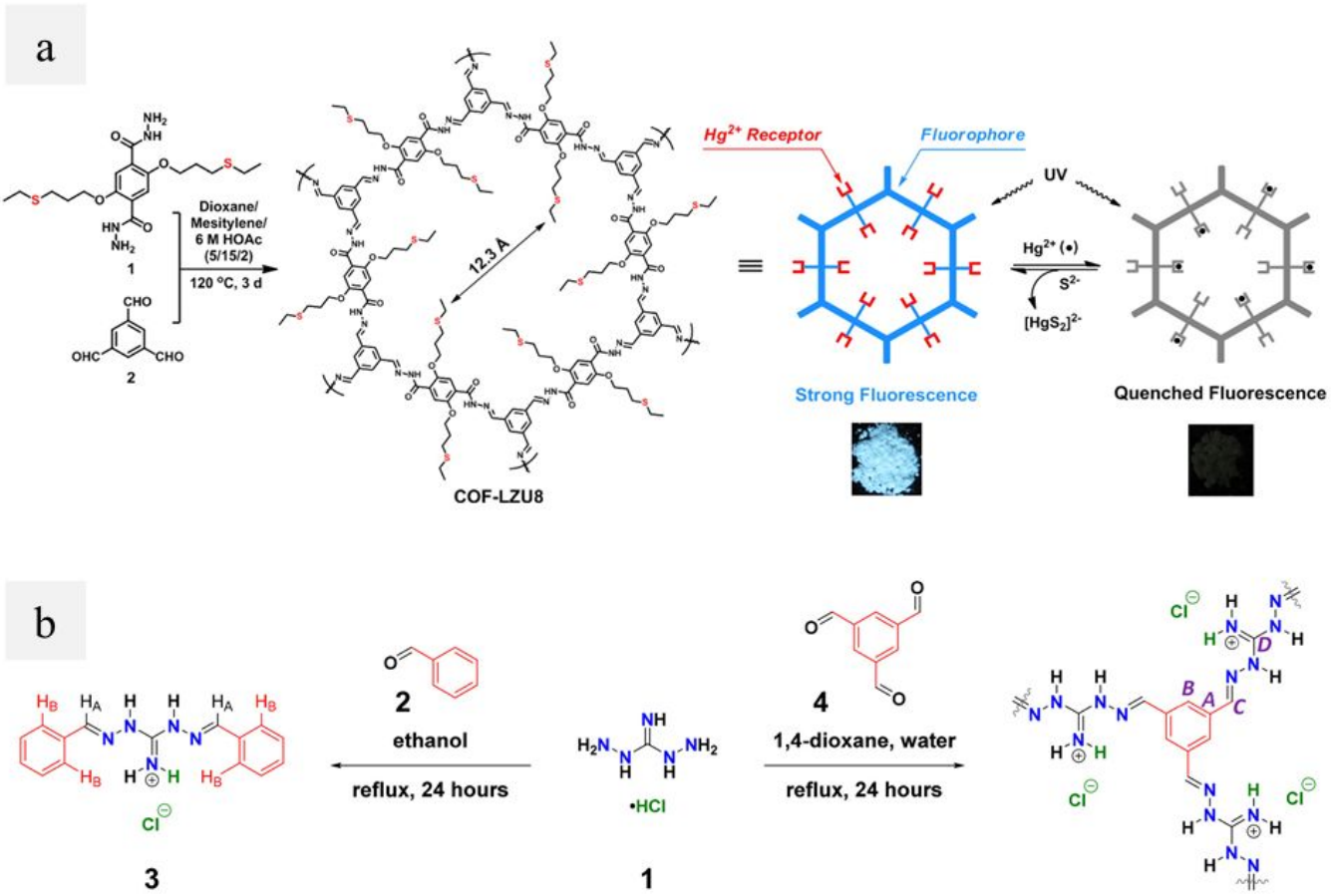

Figure 14. (a) Synthesis scheme of COF-LZU8 via the co-condensation of 1 and 2 under solvothermal conditions. With the π-conjugated framework as the fluorophore and the thioether groups as the Hg^{2+} receptor, the synthesized COF-LZU8 was applied for both detection and removal of Hg^{2+}. COF-LZU8 exhibited strong fluorescence upon excitation at 390 nm. Upon the addition of Hg^{2+}, the fluorescence of COF-LZU8 was effectively quenched. Photographs of COF-LZU8 under a UV lamp (λ_{ex} = 365 nm) visualize the significant change in the fluorescence emission before (left) and after (right) the adsorption of Hg^{2+}.[140] Reproduced with permission. Copyright 2016, American Chemical Society. (b) Synthesis scheme of a guanidinium-based ionic COF.[141] Reproduced with permission. Copyright 2019, American Chemical Society.

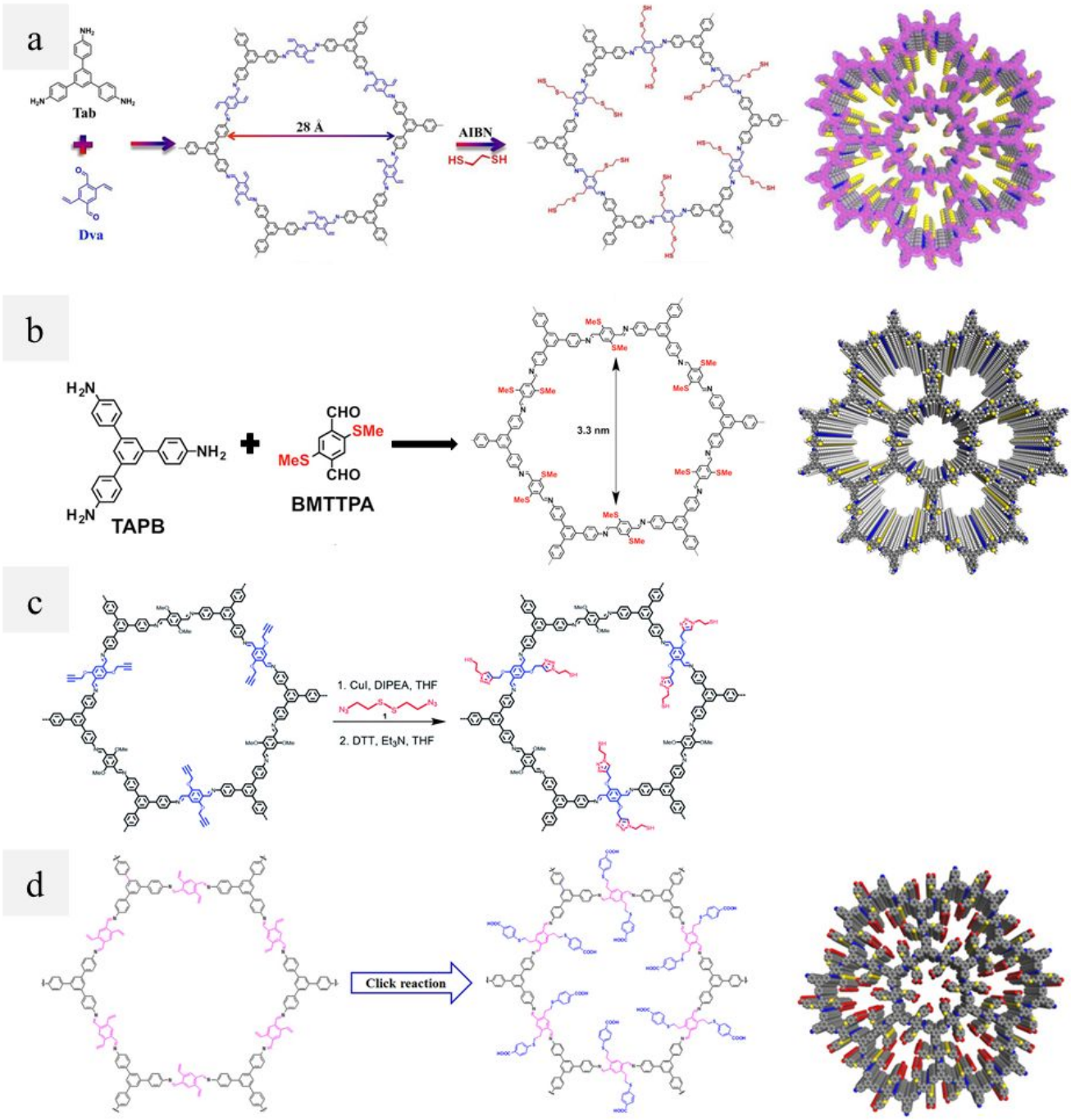

Figure 15. Synthesis schemes and extended structures (if given) of (a) COF-S-SH,[142] reproduced with permission. Copyright 2017, American Chemical Society. (b) TAPB-BMTTPA-COF,[143] reproduced with permission. Copyright 2017, American Chemical Society. (c) TPB-DMTP-COF-SH,[144] reproduced with permission. Copyright 2017, Royal Society of Chemistry. and (d) COF-COOH,[145] reproduced with permission. Copyright 2019, American Chemical Society.

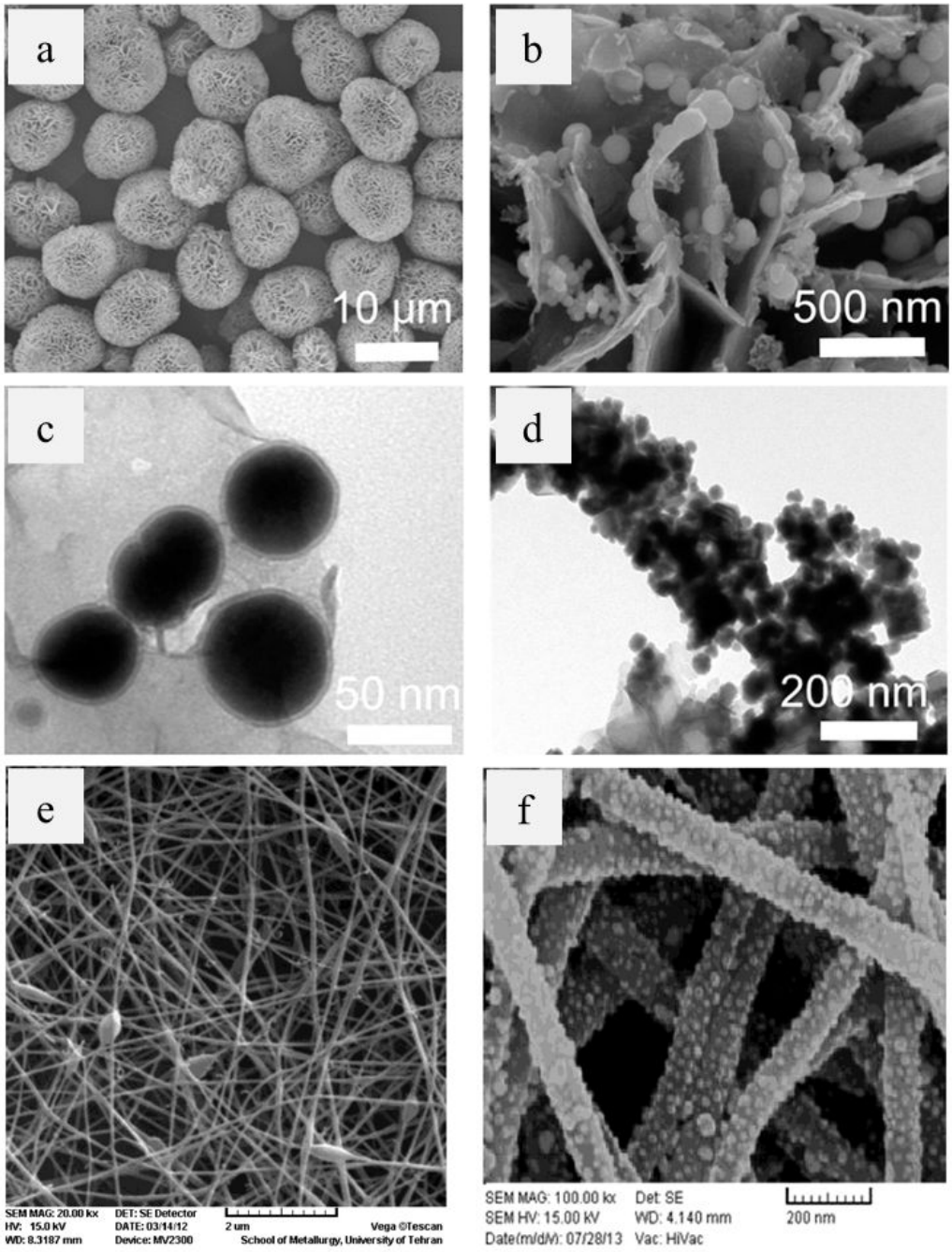

Figure 16. SEM images of (a) $Mg(OH)_2$ and (b) NZVI/$Mg(OH)_2$; and TEM images of (c) and (d) NZVI.[150] Reproduced with permission. Copyright 2015, American Chemical Society. SEM images of (e) TiO_2 embedded chitosan nanofibers and (f) TiO_2 coated chitosan nanofibers.[152] Reproduced with permission. Copyright 2016, Elsevier.

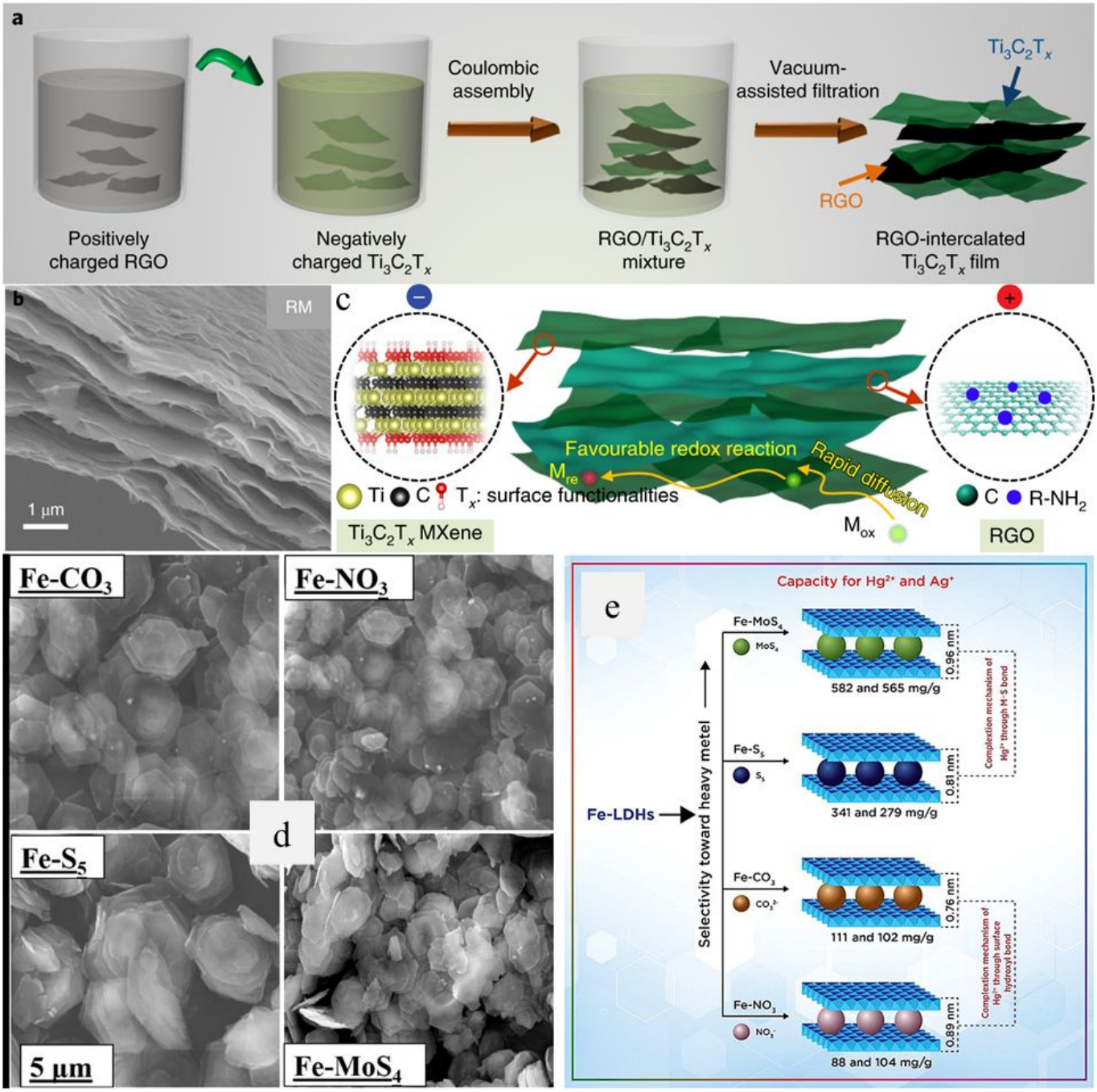

Figure 17. (a) Schematic preparation and (b) cross-section SEM image of rGO intercalated MXene; (c) schematic illustration of heavy metal removal from water by rGO intercalated MXene.[156] Reproduced with permission. Copyright 2019, Springer Nature. (d) SEM images and (e) heavy metal removal performance of $FeCO_3$, $FeNO_3$, FeS_5 and $FeMoS_4$.[157] Reproduced with permission. Copyright 2019, Elsevier.

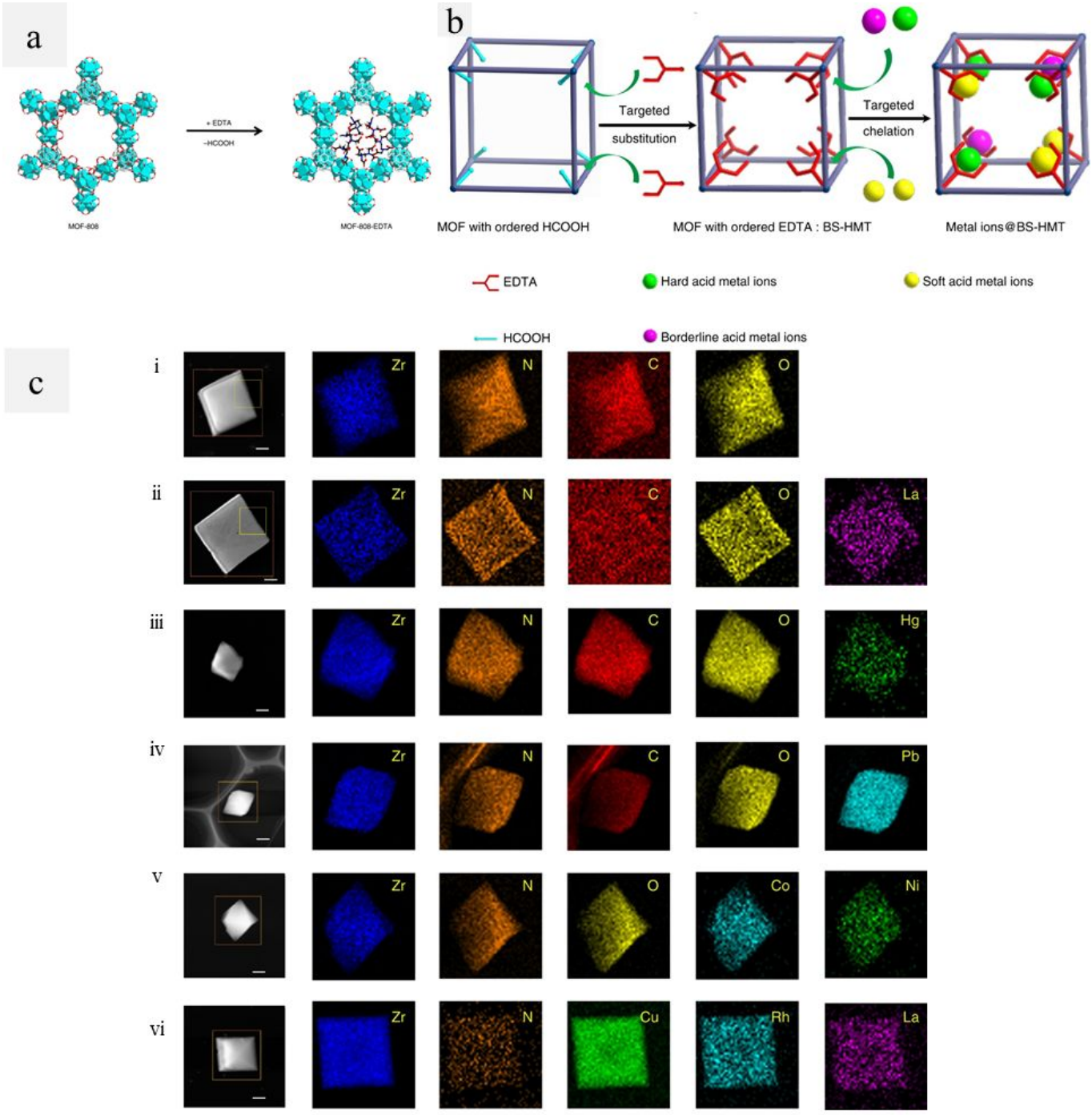

Figure 18. Schematic illustrations of (a) the structures of the two MOFs and (b) the heavy metal trap (HMT) concept; (c) Dispersity of metal ions in MOF-808-EDTA. STEM-HAADF images (scale bar, 100 nm) and the corresponding elemental maps for (i) MOF-808-EDTA, (ii)-(iv) single-metal systems (MOF-808-EDTA with loaded La^{3+}, Hg^{2+}, and Pb^{2+}, respectively), (v) binary system (MOF-808-EDTA with loaded Co^{2+} and Ni^{2+}), and (vi) ternary system (MOF-808-EDTA with loaded Cu^{2+}, Rh^{3+} and Ru^{3+}).[158] Reproduced with permission. Copyright 2018, The authors (Peng Yaguang et al.).

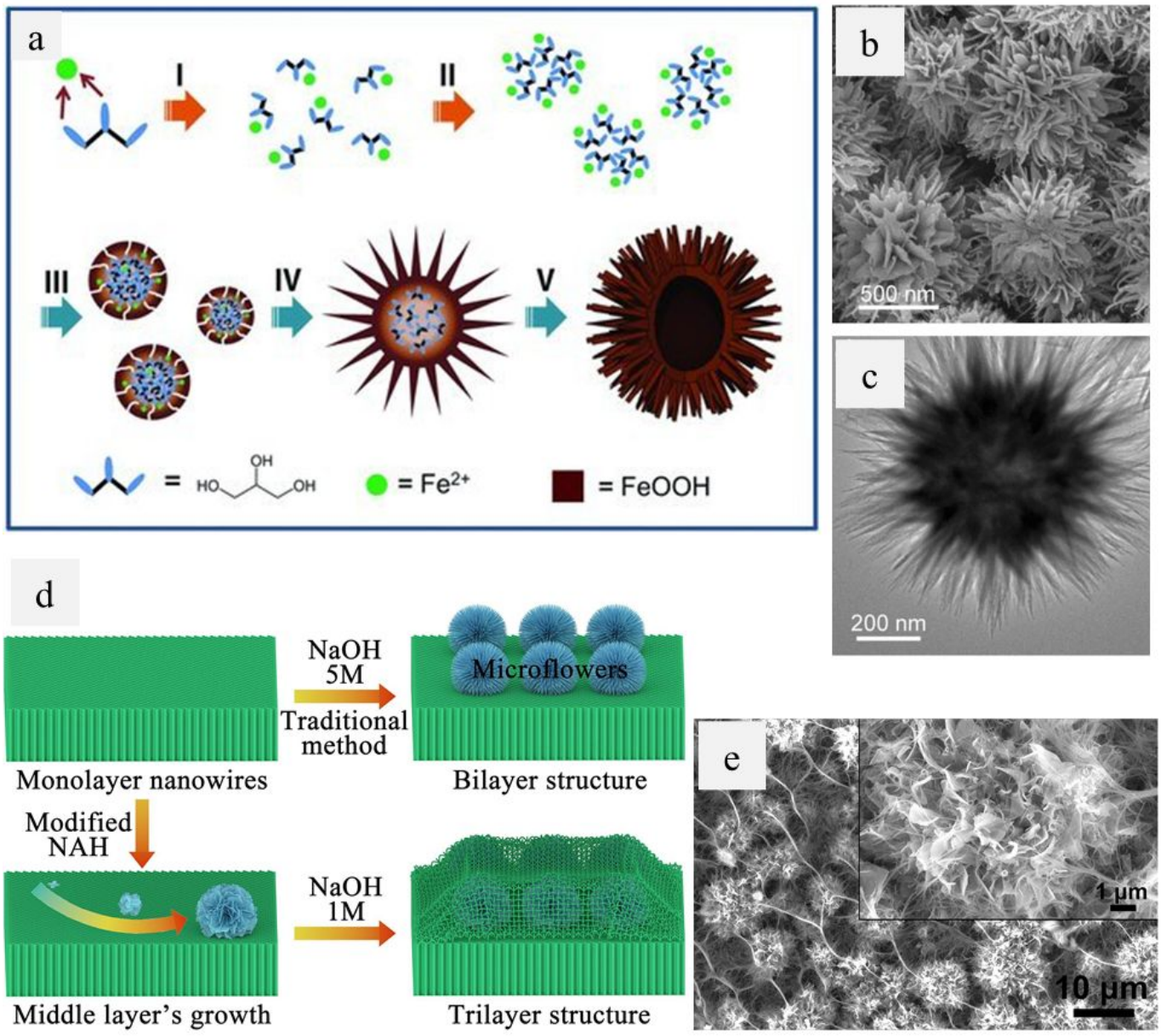

Figure 19. (a) Schematic illustration of the morphological evolution process of the urchin-like hierarchical α-FeOOH spheres: (I) formation of Fe(II)-glycerol complex, (II) formation of aggregate and quasi-emulsion,(III) hydrolysis and oxidation of Fe(II) to form initial FeOOH shell around the aggregates, (IV) further growth of nanorods on the shell, (V) formation of urchin-like hollow structures. (b) FESEM and (c) TEM images of the obtained hierarchical α-FeOOH spheres.[160] Reproduced with permission. Copyright 2012, John Wiley and Sons. (d) Synthesis scheme and (e) SEM images (including the SEM image with high resolution as the inset graph) of a stable trilayer titanate architecture.[161] Reproduced with permission. Copyright 2020, Elsevier.

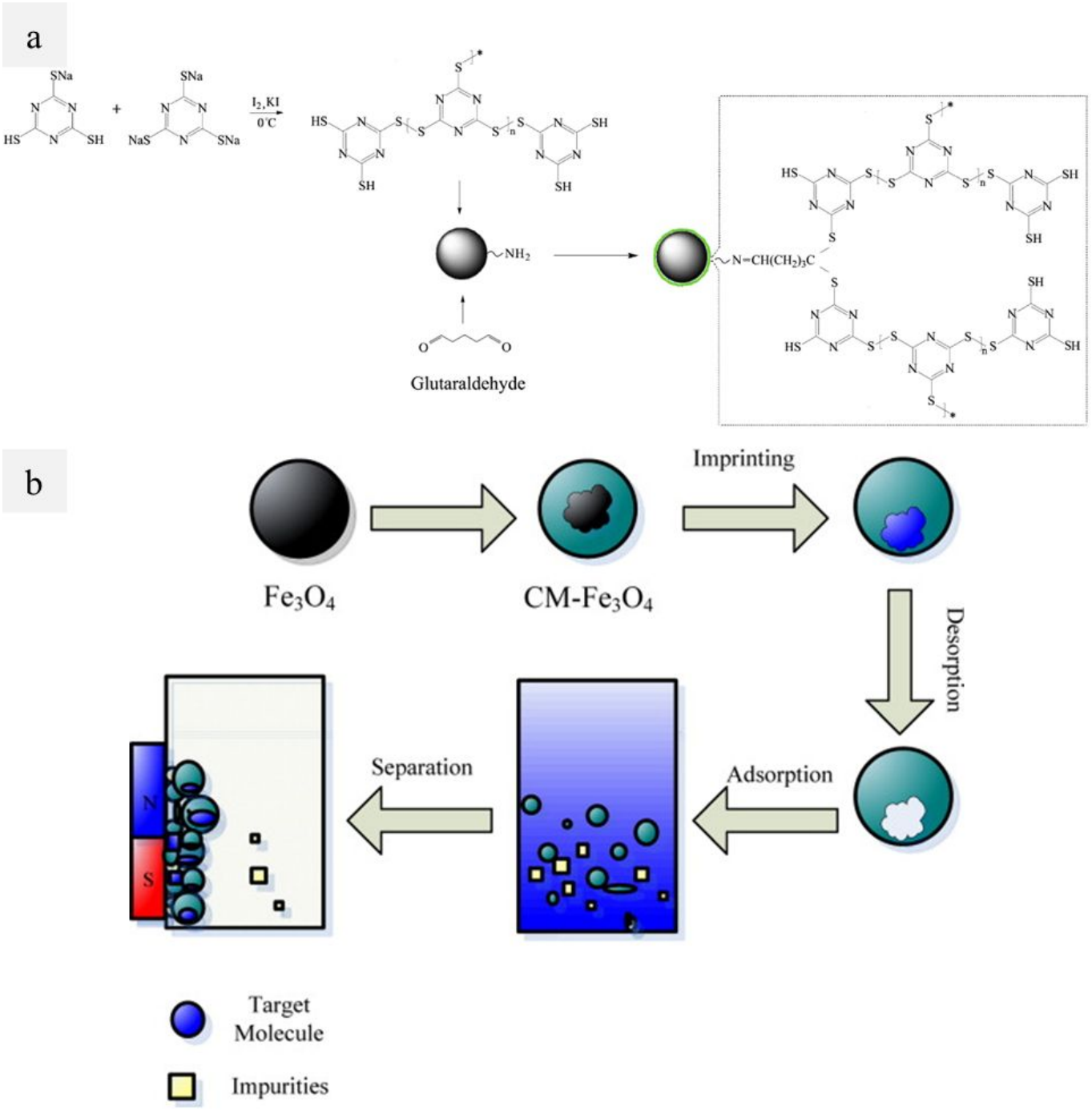

Figure 20. (a) Synthesis route of the organodisulfide polymer coated magnetite nanoparticles.[33] Reproduced with permission. Copyright 2018, Elsevier. (b) Synthesis scheme of the Fe_3O_4 nanoparticles coated with Ag^+-imprinted thiourea-chitosan polymer and their application for removal of Ag^+ with the help of an external magnetic field.[162] Reproduced with permission. Copyright 2011, Elsevier.

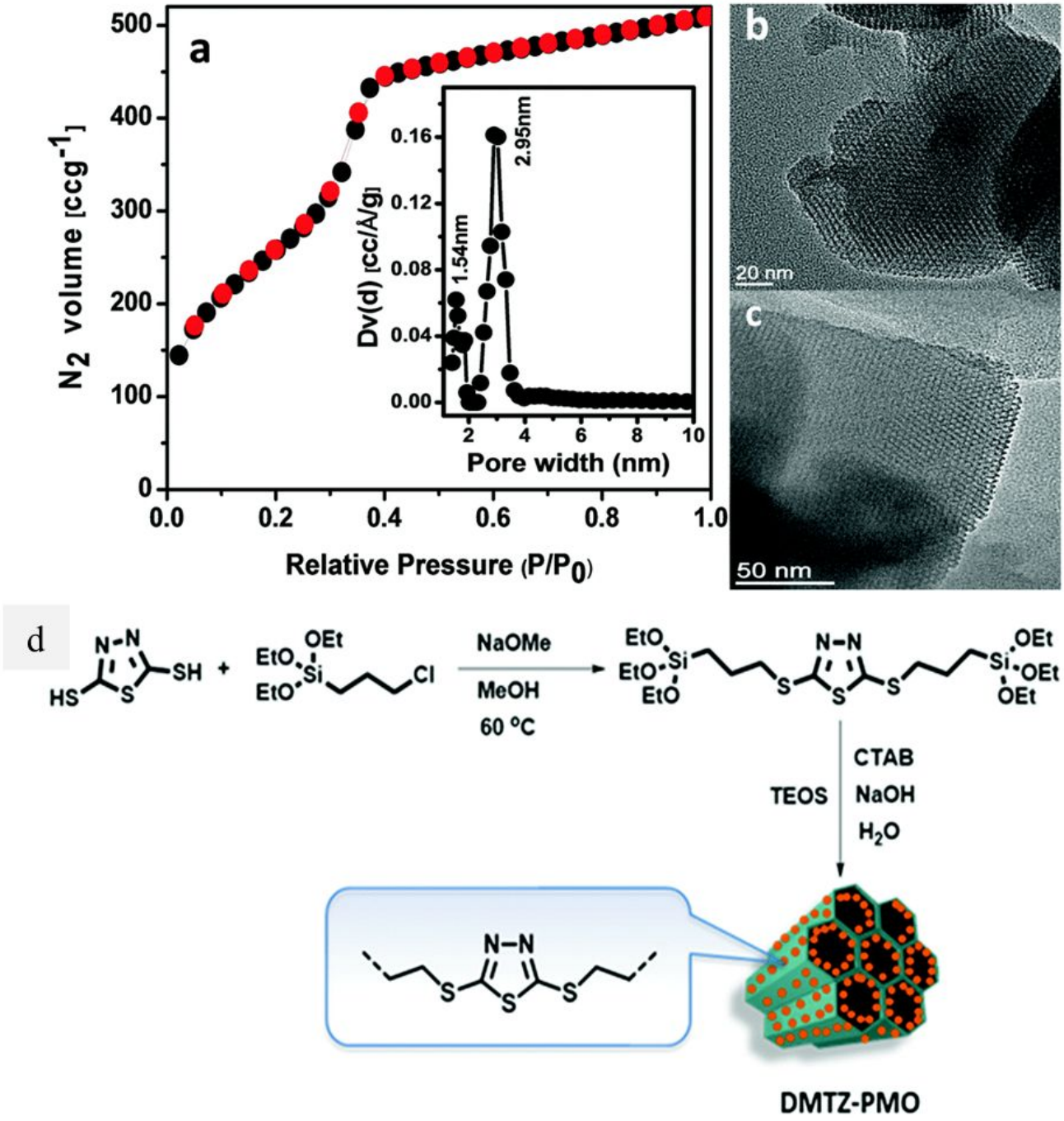

Figure 21. (a) N_2 adsorption/desorption isotherm of a highly ordered periodic mesoporous organosilica material (DMTZ-PMO) (adsorption points are black circles and those of desorption are red; PSD plot of the material employing the NLDFT model is shown in the inset). HRTEM images at different magnifications (b and c) of DMTZ-PMO. (d) Synthesis scheme of the organosilane precursor and DMTZ-PMO through the CTAB-assisted supramolecular-templating route.[209] Reproduced with permission. Copyright 2020, Royal Society of Chemistry.

Table 1. Removal of heavy metals by carbon adsorbents.

Adsorbent	Dose ($g\ L^{-1}$)	Heavy metal	Initial concentration ($mg\ L^{-1}$)	pH	T (K)	Time (min)	Adsorption capacity ($mg\ g^{-1}$)	Removal efficiency (%)	Ref.
Chemically activated carbon	0.2	Cd (II)	50.0	6.0	298	60	119.15	\	16
		Ni (II)	50.0	6.0	298	60	94.49	\	
Carbon foam	0.6	Pb (II)	120.0	7.0	298	600	491.36	\	40
		Cu (II)	120.0	5.0	298	1800	246.66	\	
Amine-nanoporous carbon	\	Pb (II)	10.0	7.0	298	\	161.41	\	41
		Cd (II)	10.0	7.0	298	\	85.64	\	
		Ni (II)	10.0	7.0	298	\	47.19	\	
		Cu (II)	10.0	7.0	298	\	46.88	\	
N-doped carbon	1.0	Pb (II)	40.0	5.0	298	120	94.00	\	43
		Cd (II)	40.0	5.0	298	120	43.50	\	
O_2-plasma oxidized MWCNTs	1.5	Pb (II)	17.0	5.0	293	40	35.08	\	48
Polyacrylic acid (PAA)/MWCNTs	1.0	Co (II)	10.0	6.8	303	1440	8.78	\	25
Polyaniline (PANI)/CNTs	\	Fe (II)	1.5	\	298	\	\	91.8	49
		Cu (II)	0.5	\	298	\	\	91.1	
		Zn (II)	16.0	\	298	\	\	93.6	
Polypyrrole (PPy)/CNTs	\	Fe (II)	1.5	\	298	\	\	95.4	
		Cu (II)	0.5	\	298	\	\	94.6	
		Zn (II)	16.0	\	298	\	\	95.7	
Polyhydroxylbutyrate (PHB)/CNTs	1.0	Cr (VI)	72.3	5.6	303	10	\	98.8	50
		As (III)	58.0	5.6	303	10	\	100.0	
		Cd (II)	3.0	5.6	303	10	\	98.8	
		Pb (II)	4.9	5.6	303	10	\	99.2	
		Ni (II)	106.1	5.6	303	10	\	89.7	
		Cu (II)	97.6	5.6	303	10	\	93.4	
		Zn (II)	167.6	5.6	303	10	\	86.2	
		Fe (III)	127.5	5.6	303	10	\	93.6	
Graphene oxide (GO)	0.5	Cu (II)	63.5	5.0	298	720	46.60	\	58
Few-layered graphene oxide (FLGO)	0.1	Cd (II)	20.0	6.0	303	1440	106.30	\	59
		Co (II)	30.0	6.0	303	1440	68.20	\	
GO	\	Cd (II)	200.0	2~7	298	1440	35.70	\	60
EDTA-GO	0.2	Pb (II)	100.0	6.8	298	20	479.00	\	61
2,2′-dipyridylamine (DPA)-GO	\	Pb (II)	20.0	5.0	298	4	369.75	\	62
		Cd (II)	20.0	5.0	298	4	257.20	\	
		Ni (II)	20.0	5.0	298	4	180.89	\	
		Cu (II)	20.0	5.0	298	4	358.82	\	
Sulfur-GO/TiO_2	\	Pb (II)	\	\	298	180	312.00	\	63
		Cd (II)	\	\	298	180	384.00	\	
		Ni (II)	\	\	298	180	344.00	\	
		Zn (II)	\	\	298	180	285.00	\	
Iron oxide/reduced graphene oxide (IO/rGO)	0.3	As (V)	71.9	\	298	60	218.00	97.0	64
		Cr (VI)	64.4	\	298	60	190.00	94.0	
GO/SiO_2	2.0	As (V)	100.0	\	298	1440	47.30	97.7	65
		Cd (II)	100.0	\	298	1440	48.00	96.9	
		Cr (II)	100.0	\	298	1440	45.50	96.0	
		Hg (II)	100.0	\	298	1440	49.00	98.5	
		Pb (II)	100.0	\	298	1440	39.50	78.7	
GO/chitosan	0.2	Pb (II)	20.0	3.0	298	960	216.90	\	66
		Au (III)	30.0	4.0	298	960	1076.60	\	

GO/alginate aerogel	\	Cu (II)	500.0	5.0	303	180	98.00	\	67
		Pb (II)	500.0	5.5	303	240	267.40	\	
GO/alginate gel beads	\	Cu (II)	635.0	\	298	90	60.20	\	68
GO/alginate/polyvinylalcohol (PVA) hydrogel microspheres	0.5	Cu (II)	100.0	6.0	298	360	247.16	\	21
GO/PPy	\	Hg (II)	50.0	3.0	293	180	980.0	92.3	22
3D graphene/δ-MnO_2 aerogels	0.04	Pb (II)	100.0	6.0	298	30	643.62	\	73
		Cd (II)	100.0	6.0	298	30	250.31	\	
		Cu (II)	100.0	6.0	298	30	228.46	\	
Rice and corn husk biochar	10.0	Cr (VI)	1.8	7.4	298	120	\	65.0	90
		Fe (III)	9.3	7.4	298	120	\	90.0	
		Pb (II)	1.6	7.4	298	120	\	90.0	
Sesame straw biochar	2.0	Pb (II)	320.0	7.0	298	1440	102.00	\	91
		Cd (II)	320.0	7.0	298	1440	86.00	\	
		Cr (VI)	320.0	7.0	298	1440	65.00	\	
		Cu (II)	320.0	7.0	298	1440	55.00	\	
		Zn (II)	320.0	7.0	298	1440	34.00	\	
Mg-loaded biochar	1.0	Cd (II)	1000.0	6.5	303	1440	333.33	\	92
		Cu (II)	1000.0	6.5	303	1440	370.37	\	
		Pb (II)	1000.0	6.5	303	1440	302.58	\	
MgO/N-biochar	1.0	Pb (II)	100.0	3~7	298	10	893.00	99.0	28

Table 2. Removal of heavy metals by capacitive deionization (CDI) with three-dimensional graphene-based electrodes.

Method	Electrode material	Contaminant	Concentration ($mg\ L^{-1}$)	Voltage (V)	Time (min)	Adsorption capacity ($mg\ g^{-1}$)	Removal efficiency (%)	Ref.
CDI	ACF//lamellar-structured graphene	Pb (II)	20.0	1.2	60	400.00	\	80
CDI	3DNGR//3DEGR	Pb (II)	20.0	1.4	60	134.40	99.8	82
CDI	SH-GO/AC	Pb (II)	1.0	1.2	60	\	99.0	35
CDI	Carbon cloth//pyrrolic-graphene	Pb (II)	\	1.2	180	481.50	\	83
CDI	Polypyrrole (PPy)//PPy/GO	Cu (II)	100.0	1.2	40	41.50	\	84
CDI	Fe-rGO/AC	As (V)	14.0	1.2	120	10.50	\	86
CDI	Fe_3O_4/porous graphene	Pb (II)	500.0	1.6	\	47.00	\	87
		Cu (II)	500.0	1.6	\	40.00	\	
		Cd (II)	500.0	1.6	\	49.00	\	
CDI	TiO_2 nanotubes/rGO	Cu (II)	80.0	1.2	120	253.25	\	88
		Pb (II)	80.0	1.2	120	241.65	\	
CDI	AC//MoS_2/graphene	Cu (II)	19.7	1.6	120	\	92.3	89
		Pb (II)	99.4	1.6	120	\	91.3	
MCDI	Porous N-graphene	Cd (II)	200.0	1.2	30	521.00	100.0	85
		Pb (II)	200.0	\	\	498.00	100.0	

Table 3. Removal of heavy metals by polymer adsorbents.

Adsorbent	Dose ($g\ L^{-1}$)	Heavy metal	Initial concentration ($mg\ L^{-1}$)	pH	T (K)	Time (min)	Adsorption capacity ($mg\ g^{-1}$)	Removal efficiency (%)	Ref.
Chitosan/bentonite	6.7	Pb (II)	200.0	4.0	298	240	28.00	\	210
		Cu (II)	200.0	4.0	298	240	20.00	\	
		Ni (II)	200.0	4.0	298	240	12.29	\	
EDTA-chitosan/SiO_2	2.0	Cd (II)	89.9	3.0	295	1440	67.45	96.5	98
		Pb (II)	165.7	3.0	295	1440	128.46	99.2	
		Co (II)	47.1	3.0	295	1440	37.12	93.5	
		Ni (II)	467.0	3.0	295	1440	35.80	95.2	
Chitosan/polyethylenimine (PEI)	1.5	Pb (II)	500.0	6.0	318	240	263.40	\	96
		Cu (II)	400.0	5.5	298	3840	145.92	94.7	
Chitosan/PAA/biochar	3.3	Cr (III)	400.0	3~7	298	180	312.50	\	97
		Pb (II)	400.0	3~7	298	180	476.19	\	
		Cu (II)	400.0	3~7	298	180	111.11	\	
		Cd (II)	400.0	3~7	298	180	370.37	\	
		Ni (II)	400.0	3~7	298	180	99.01	\	
		Zn (II)	400.0	3~7	298	180	114.94	\	
		Co (II)	400.0	3~7	298	180	135.14	\	
		Mn (II)	400.0	3~7	298	180	138.89	\	
Alginate	0.2	Pb (II)	800.0	4.5	295	10	435.30	\	99
		Cu (II)	900.0	4.5	295	10	167.10	\	
		Cd (II)	900.0	4.5	295	10	179.00	\	
Alginate/carboxymethyl cellulose (CMC) beads	8.0	Pb (II)	5.0	5.0	310	1080	\	99.6	100
Carboxymethyl cellulose/polyacrylamide (PAM) hydrogel	0.5	Cu (II)	500.0	5.5	298	1440	227.27	\	101
		Pb (II)	500.0	5.5	298	1440	312.50	\	
		Cd (II)	500.0	5.5	298	1440	256.41	\	
Surface-functionalized porous lignin	0.2	Pb (II)	20.0	5.0	298	30	188.00	99.0	102
NH_2-Starch/PAA hydrogel	1.0	Cd (II)	180.0	5.0	298	240	256.40	\	103
PEI/soy protein isolate hydrogels	0.5	Cu (II)	250.0	5.5	298	1200	136.2	\	104
Hollow gangue microspheres/geopolymer	6.0	Cu (II)	100.0	5.0	303	240	15.00	~90	105
	6.0	Cd (II)	100.0	5.0	303	240	14.60	~90	
	6.0	Zn (II)	100.0	5.0	303	240	11.60	~70	
	1.0	Pb (II)	100.0	5.0	303	240	90.90	~90	
Sulfonic acid-hypercrosslinked polymers (HCPs)	1.0	Cu (II)	80.0	5.5	303	30	51.45	\	114
Iminodiacetic acid-HCPs	0.4	Pb (II)	100.0	7~12	298	60	1138.00	99.6	115
Thiourea-HCPs	1.5	Pb (II)	1050.0	6.0	303	300	689.65	\	116
Hypercrosslinked poly(ionic liquid)s (PILs)	0.4	Cr (VI)	52.0	2~4	298	10	236.80	\	117
Pluronic F127-PAA hydrogels	1.0	Cu (II)	10.0	7.0	298	720	283.40	\	26
		Hg (II)	10.0	7.0	298	720	222.10	\	
Superabsorbent polymer hydrogels	2.0	Cd (II)	100.0	4.8	298	1440	\	84.0	118
		Ni (II)	100.0	4.8	298	1440	\	74.0	
		Cu (II)	100.0	4.8	298	1440	\	79.0	
		Co (II)	100.0	4.8	298	1440	\	76.0	
EDTA-inspired polydentate hydrogels	0.1	Cr (III)	50.0	\	298	1440	340.60	\	119
		Cu (II)	50.0	\	298	1440	436.50	\	
		Hg (II)	50.0	\	298	1440	285.10	\	
		Cd (II)	50.0	\	298	1440	210.70	\	
		Pb (II)	50.0	\	298	1440	395.10	\	
		Zn (II)	50.0	\	298	1440	439.30	\	
Hydrolyzed polymer of intrinsic microporosity PIM-1	\	Pb (II)	100.0	4~5	\	720	41.20	\	121

SH-PIM-1	0.25	Hg (II)	100.0	5.0	298	1	136.00	\	122
CBAP-1	1.0	Hg (II)	100.0	5.0	298	5	232.00	\	126
Melamine-based conjugated microporous polymer (MA-based CMP)	0.4	Hg (II)	100.0	\	298	120	372.00	\	127
Triazine-based CMP	\	Hg (II)	6.0	4.0	298	10	229.90	\	128
CMP	1.0	Ag (I)	52.0	\	298	2640	\	99.3	129
Mesoporous CMPs	5.0	Pb (II)	100.0	2~8	298	5	1134.00	\	130
Covalent triazine-based framework (CTF-1)	2.5	Cd (II)	262.00	7.0	298	50	29.3	\	135
Thioether-CTF	0.8	Hg (II)	5.0	\	298	5	1253.00	100.0	136
CTF nanoneedles	2.0	Hg (II)	500.0	5.0	298	480	1826.00	\	137
Covalent organic framework (COF)-LZU8	1.0	Hg (II)	10.0	\	298	\	\	98.0	140
Guanidinium-based ionic COF	5.0	Cr (VI)	1040.0	2~4	298	10	200.00	\	141
SH-S-COF	\	Hg (II)	5.0	\	298	30	1350.00	99.9	142
Thioether-COF	0.5	Hg (II)	10.0	7.0	298	15	734.00	100.0	143
SH-COF	0.5	Hg (II)	10.0	5~12	298	2	4395.00	100.0	144
COOH-COF	0.4	Pb (II)	100.0	6.0	298	20	123.80	\	145
Pb (II) ion-imprinted polymer [Pb (II)-IIP]	1.0	Pb (II)	500.0	6.0	298	60	27.95	\	31
Polystyrene-poly (N-isopropylmethacrylamide-acrylic acid) [PSt@p(NIPMAM-AA)] core/shell gel particles	0.01	Pb (II)	50.0	6.0	298	100	555.60	\	146
		Cu (II)	50.0	5.0	298	100	526.30	\	
		Cd (II)	50.0	6.0	298	100	476.20	\	
		Cr (III)	50.0	8.0	298	100	434.80	\	
Polyacrylonitrile (PAN) nanofibers	2.0	Cu (II)	100.0	7.5	298	120	33.44	\	29
		Pb (II)	100.0	7.0	298	120	1250.00	\	
		Zn (II)	100.0	7.2	298	120	769.23	\	
PVA/NaX/zeolite nanofibers	0.5	Ni (II)	50.0	5.0	318	60	342.80	\	106
		Cd (II)	50.0	5.0	318	60	837.80	\	

Table 4. Removal of heavy metals by metal-containing adsorbents.

Adsorbent	Dose ($g\ L^{-1}$)	Heavy metal	Initial concentration ($mg\ L^{-1}$)	pH	T (K)	Time (min)	Adsorption capacity ($mg\ g^{-1}$)	Removal efficiency (%)	Ref.
NZVI/RGO	0.4	As (III)	10.0	4~10	298	240	35.83	\	36
		As (V)	10.0	2.0	298	240	29.04	\	
Fe/Syzygium jambos Alston (SJA)	0.04	Cr (VI)	50.0	5.5	298	90	983.20	90.0	149
NZVI/$Mg(OH)_2$	0.5	Pb (II)	1000.0	6.9	298	120	1986.60	\	150
CuO	1.6	Cr (VI)	20.0	3.0	298	60	15.62	94.0	151
TiO_2/chitosan	0.5	Pb (II)	50.0	6.0	318	30	715.70	\	152
	0.5	Cu (II)	50.0	6.0	318	30	579.10	\	
ZnS nanocrystals	2.0	Hg (II)	200.6	5.5	298	5	\	99.9	153
		Cu (II)	63.6	5.5	298	5	\	99.9	
		Pb (II)	207.2	5.5	298	5	\	90.8	
		Cd (II)	112.4	5.5	298	5	\	66.3	
Activated $CaCO_3$	0.1	Cu (II)	63.6	6.2	298	100	\	99.3	154
		Zn (II)	65.4	6.6	298	100	\	53.4	
2D alk-MXene [$Ti_3C_2(OH/ONa)_xF_{2-x}$]	0.5	Pb (II)	51.8	6.0	323	2	140.00	80.8	155
2D titanium carbide MXene ($Ti_3C_2T_x$)	\	Ag (I)	200.0	\	298	360	1172.00	\	156
		Cr (VI)	20.0	5.1	298	120	84.00	\	
FeMgAl-layered double hydroxides (LDHs)	1.0	Ag (I)	200.0	3~8	303	180	565.00	100.0	157
		Hg (II)	200.0	3~8	303	180	582.00	100.0	
Metal-organic frameworks (MOFs)	1.0	Hg (II)	10.0	\	298	1440	592.00	100.0	158
Zeolite-imidazolate frameworks (ZIF-67)	0.1	Pb (II)	200.0	5.1	298	120	1348.42	\	159
	0.2	Cu (II)	200.0	5.2	298	120	617.51	\	
Urchin-like α-FeOOH hollow spheres	0.5	As (V)	1000.0	7.0	298	180	58.00	\	160
		Pb (II)	1500.0	7.0	298	180	80.00	\	
Titanate films/titanium foil	0.8	Pb (II)	207.2	5.0	293	1440	1013.21	\	161
Water-soluble Fe_3O_4 NPs	\	Pb (II)	10.0	7.0	293	2	\	90.0	19
Core-shell magnetic microspheres	0.4	Hg (II)	600.0	7.0	298	20	603.16	\	33
		Pb (II)	600.0	7.0	298	20	533.13	\	
		Cd (II)	600.0	7.0	298	20	216.59	\	
Ag-imprinted magnetic microspheres	5.0	Ag (I)	2157.4	5.0	303	50	531.79	90.0	162

Table 5. Removal of heavy metals by other adsorbents.

Adsorbent	Dose ($g\ L^{-1}$)	Heavy metal	Initial concentration ($mg\ L^{-1}$)	pH	T (K)	Time (min)	Adsorption capacity ($mg\ g^{-1}$)	Removal efficiency (%)	Ref.
NH_2-SiO_2 hollow nanospheres	3.0	Cd (II)	140.0	4.5	298	100	49.53	\	20
		Ni (II)	140.0	4.5	298	100	39.98	\	
		Pb (II)	140.0	4.5	298	100	143.30	\	
PAA-SiO_2	0.2	Cr (III)	120.0	5.0	298	240	178.60	\	147
Porous boron nitride (BN)	4.0	Cu (II)	1864.0	\	298	2880	373.00	\	172
Activated BN	\	Cr (III)	52.0	5.5	298	360	352.00	99.9	171
		Co (II)	52.0	6.0	298	360	215.00	\	
		Ni (II)	52.0	6.0	298	360	235.00	\	
		Pb (II)	52.0	6.0	298	360	225.00	\	
Hexagonal boron nitride (h-BN) nanosheets	1.2	Cu (II)	1000.0	4.0	298	600	807.60	\	173
		Fe (III)	1000.0	4.0	298	600	797.80	\	
		Cr (II)	1000.0	4.0	298	600	782.10	\	
		Ni (II)	1000.0	4.0	298	600	280.20	\	
Oxygen-doped bundle-like porous BN	0.2	Cu (II)	600.0	5.5	303	180	427.12	\	175
		Pb (II)	600.0	5.5	303	180	316.32	\	
		Zn (II)	600.0	5.5	303	180	215.78	\	
		Cr (III)	600.0	5.5	303	180	120.56	\	
Nanosheet-structured BN spheres	0.4	Pb (II)	200.0	5.5	298	720	678.70	100.0	174
		Cu (II)	200.0	5.5	298	720	536.70	100.0	
Graphitic carbon nitride (g-C_3N_4)	0.2	Pb (II)	10.0	5.0	298	420	65.50	\	176
2D-g-C_3N_4	0.3	Cd (II)	200.0	7.0	318	300	94.40	\	177
g-C_3N_4	0.2	Pb (II)	80.0	3.5	298	60	281.79	\	179
		Cu (II)	80.0	3.5	298	60	132.82	\	
		Cd (II)	80.0	3.5	298	60	112.41	\	
		Ni (II)	80.0	3.5	298	60	37.56	\	
g-C_3N_4 nanosheets	1.0	Cd (II)	100.0	8.0	298	60	123.20	\	180
		Pb (II)	100.0	6.0	298	60	136.57	\	
		Cr (VI)	100.0	2.0	298	60	684.45	\	
Activated non-metallic powder derived from electronic waste	1.0	Cd (II)	562.0	4.0	293	4320	236.07	\	189
Rice straw composites	\	Cu (II)	\	\	298	\	248.80	98.0	192
		Ni (II)	\	\	298	\	94.90	98.0	
		Pb (II)	\	\	298	\	662.90	98.0	
		Zn (II)	\	\	298	\	110.10	98.0	
Rice straw	\	Cd (II)	\	\	298	\	13.90	\	191
Bougainvillea spectabilis (citric acid modification)	\	Pb (II)	\	\	298	\	67.70	99.5	194
Bamboo charcoal (activated)	\	Ni (II)	\	\	298	\	52.90	\	195
		Zn (II)	\	\	298	\	40.50	\	
Almond shell biochar	\	Co (II)	\	\	298	\	28.10	\	196
Orange peel (copolymerization)	\	Cd (II)	\	\	298	\	293.30	\	193
		Ni (II)	\	\	298	\	162.60	\	
		Pb (II)	\	\	298	\	476.10	\	
Modified ordered mesoporous carbon	0.2	Pb (II)	97.3	5~6	298	30	724.50	\	207
Propyl-PEI-mesocellular silica foam	1.0	Cd (II)	400.0	5.0	295	\	625.00	\	208
Highly ordered periodic mesoporous organosilica	\	Hg (II)	2.0	1~8	298	5	2081.00	99.9	209